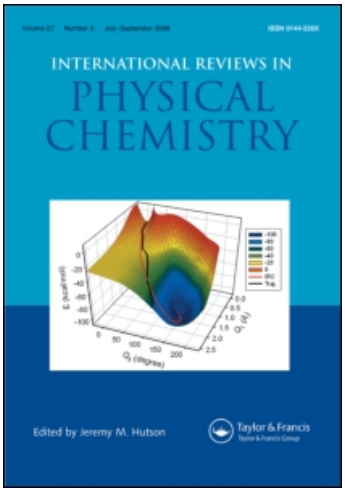

International Reviews in Physical Chemistry
Publication details, including instructions for authors and subscription information:
http://www.informaworld.com/smpp/title~content=t713724383

The $H+H_2$ reactive system. Progress in the study of the dynamics of the simplest reaction

F. J. Aoiz[a]; L. BaÑares[a]; V. J. Herrero[b]
[a] Departamento de Química Física, Facultad de Química, Universidad Complutense, 28040 Madrid, Spain [b] Instituto de Estructura de la Materia (CSIC), Serrano 123, 28006 Madrid, Spain

To cite this Article Aoiz, F. J. , BaÑares, L. and Herrero, V. J.(2005) 'The $H+H_2$ reactive system. Progress in the study of the dynamics of the simplest reaction', International Reviews in Physical Chemistry, 24: 1, 119 — 190
To link to this Article: DOI: 10.1080/01442350500195659
URL: http://dx.doi.org/10.1080/01442350500195659

International Reviews in Physical Chemistry,
Vol. 24, No. 1, January–March 2005, 119–190

Taylor & Francis
Taylor & Francis Group

The $H + H_2$ reactive system. Progress in the study of the dynamics of the simplest reaction

F. J. AOIZ*†, L. BAÑARES† and V. J. HERRERO‡

†Departamento de Química Física, Facultad de Química,
Universidad Complutense, 28040 Madrid, Spain
‡Instituto de Estructura de la Materia (CSIC), Serrano 123, 28006 Madrid, Spain

(*Received 31 January 2005; in final form 10 May 2005*)

Progress in the understanding of the $H + H_2$ reaction and its isotopic variants is reviewed with special attention to the achievements of the last decade. The detailed agreement between theory and experiment attained during this period is emphasized and major experimental and theoretical advances are highlighted. The excellent description of most experimental findings, from state-resolved cross sections to thermal rate constants, provided by the available quantum mechanical treatments, as well as the good overall behaviour of classical mechanics are underlined. Debated issues on short-lived complexes and delayed scattering, resonances and interferences, or geometric phase effects are extensively discussed. Finally, the state-of-the-art is summarized and prospects for future research on this prototypic system are presented.

Contents

*Corresponding author. Email: aoiz@quim.ucm.es

International Reviews in Physical Chemistry
ISSN 0144–235X print/ISSN 1366–591X online
http://www.tandf.co.uk/journals
DOI: 10.1080/01442350500195659

1. Introduction and scope

The simplest hydrogen-atom exchange reaction has been the prototype of all the theoretical and many experimental methods aimed to unravel the detailed mechanism of reactive collisions. Although dynamical studies on the system started in the late 1920s, the first accurate quantum mechanical (QM) calculations appeared in the mid 1970s and were restricted to the symmetric $H + H_2$ isotopic variant. The first *ab initio* potential energy surface was published a few years later and full dimensional and converged QM calculations for deuterated isotopic variants had to wait till the end of the 1980s. Given the lightness of the nuclei involved in this reaction, one would intuitively expect QM effects to be important. However, the nuclear dynamics turns out to be largely classical as demonstrated in many calculations since the mid 1960s. The overall good behaviour of classical mechanics, as well as its limitations close to threshold are discussed throughout the paper.

Experimental difficulties precluded the measurement of state resolved differential cross sections (DCS) till the mid 1990s. In spite of the efforts by many groups, the experimental results lagged behind the theoretical predictions for a long time, and this situation stimulated important experimental developments involving especially molecular beams and laser spectroscopic techniques.

Decisive progress, bridging finally the gap between calculations and measurements, has been achieved during the last ten years, and this is the period treated more extensively in the review. At present, a very good agreement between theory and experiment, and thus a sound understanding of the dynamics, exists from the level of internally state resolved DCSs to that of thermal rate constants in the 0.27–2.7 eV collision energy interval, whose limits correspond, respectively, to the threshold for reaction and to the conical intersection between the two first electronic states of H_3. In later times, investigations within this range of energies have concentrated on the search for subtle features like dynamical resonances or geometric phase effects, that do not play a significant role on the overall dynamics, but provide a strict test of the most precise theoretical treatments of reaction dynamics. As it will be seen, the identification of these effects and its actual physical origin remains in general controversial.

This review is organized as follows: In Section 2 a historical perspective of research till the beginning of the 1990s is given. Section 3 describes the convergence between detailed experimental and theoretical results achieved essentially since 1995. The next four sections are dedicated to specific issues that have been and, to a greater or lesser extent, still are debated subjects in the field. Section 4 focuses on the relation between features of the forward scattering and characteristic reaction times. Section 5 is centered on studies about the nature and likely experimental manifestations of resonances and interferences. Section 6 addresses the possible role of geometric phase effects on the dynamics, and Section 7 deals with recent measurements of rotational state distributions of reactive and inelastic scattering. The review closes with a section in which the present knowledge, including open issues, is summarized and some interesting aspects offering prospects for future research are outlined.

2. Historical perspective

All major theoretical advances in the field of gas-phase kinetics and reaction dynamics have used the hydrogen-atom exchange reaction as a benchmark. The concepts of potential energy surface [1] and transition state [2, 3], as well as the first methods for accurate dynamical calculations both classical [4] and quantum mechanical [5, 6] were developed using the $H + H_2$ reaction. Progress in the knowledge of this reaction from the twenties to the eighties is covered in detail in a series of good general reviews [7–11] and only a brief account of research prior to the 1990s will be given here.

The adequacy of the H_3 system, with just three nuclei and three electrons, for the performance of theoretical calculations was always evident. In addition, the first excited H_3 state lies at a sufficient high energy to justify an adiabatic treatment of the ground state. Dynamical calculations at the energies characteristic of chemical reactions (from fractions of a eV to several eV) are usually done by solving the nuclear motion problem on an adiabatic electronic potential energy surface (PES). The first systematic theoretical study was carried out in 1965 by Porter, Karplus and Sharma [4] using classical mechanics and a semiempirical PES of the London-Eyring-Polanyi-Sato (LEPS) type [12]. Although the method and the surface were only approximate, the main characteristics of the dynamics were already established in this pioneering work: the $H + H_2$ reaction takes place on a repulsive PES and proceeds basically via a direct interaction mechanism without formation of a long-lived complex. The lowest energy reaction path corresponds to a collinear nuclear geometry, but even for this orientation the threshold is high ($\approx$0.27 eV). The reaction cross section was found to rise monotonically from this threshold to an asymptotic value of about 1.2 Å^2 for collision energies higher than $\approx$1.5 eV. The thermal rate constants, $k(T)$, for reaction were consequently very small (of the order of $10^{-13}\,\text{cm}^{-3}\,\text{s}^{-1}$ at $T = 600$ K). These values have been later refined, but the essential picture has remained unchanged.

A number of approximate quantum mechanical (QM) methods were used for dynamical calculations during the 1970s and early 1980s. Approximations used in these approaches included the use of distorted waves, the uncoupling of certain rotational or bending motions, reduced dimensionality or a limitation in the value of the initial angular momentum (i.e. in the number of partial waves) considered. A discussion of these results is beyond the scope of this review. An extensive description of QM approximate methods can be found in [13].

The first fully *ab initio* PES, termed LSTH, was published in 1978 [14, 15]. Approximately a decade later, two refined versions of the H_3 potential surface, termed, respectively, DMBE [16] and BKMP [17], had been reported and accurate (i.e. three dimensional, 3D, and fully converged) QM calculations had been performed by several groups who had developed various approaches, including the use of hyperspherical coordinates or the application of variational principles, for the solution of the time-independent (TI) Schrödinger equation [18–25]. Progress in the quantum mechanical theory of reactive scattering until 1990 was reviewed by Miller [26]. The increase in the precision of the theoretical calculations stimulated a search for 'subtle' dynamical features, usually of a quantal nature, like tunnelling, resonances

or non-adiabatic effects. Much theoretical work was devoted to methodological issues and will not be discussed here. The comments in this review will be restricted mostly to theoretical results that can be directly compared with experiment.

From an experimental point of view the situation is much more problematic: the high barrier and a small effective reaction cross section, as well as the lack of dipole moment of hydrogen atoms or H_2 molecules and the fact that their electronic absorption spectra lie in the vacuum UV, complicate the state-specific preparation of the reagents and the detection of the products. In general, isotopic labelling, usually with deuterium, has been employed in the experiments to distinguish reagents from products. The most stringent test of theoretical predictions requires the measurement of differential cross sections (DCS) for selected quantum states of the reagents and resolved into the quantum states of the products. During the 1980s, many efforts were dedicated by different groups to the measurement of integral and differential cross sections with increasing angular and/or state resolution (see [10, 11] and comments below). However, these experiments did not allow, as a normal rule, the determination of absolute values of the cross sections. In this respect, conventional bulk measurements of thermal rate constants proved specially useful. Most of the experimental information about the energy barrier for reaction, the reactivity close to threshold or the actual reactive size were derived from this kind of measurements.

Kinetic studies on the reaction started in the 1920s and 1930s, and consistent values of the thermal rate constants were published in the 1960s and 1970s for the $D + H_2$ and $H + D_2$ reactions (see [11, 27, 28] and references therein). These thermal rate constants could be compared to the results of different theoretical calculations on the available *ab initio* PESs. A reasonable agreement with experiment was obtained in quasi-classical trajectory (QCT) calculations [29] performed on the LSTH PES for temperatures lower than 600 K. Good accordance with the measurements was also found using variational transition state theory (VTST) with tunnelling corrections [30–32]. Further experiments were carried out at low [33] and high [34, 35] temperatures. In 1990 the experimental $k(T)$ spanned a temperature range from $\approx$200 to 2000 K. In the $T \approx 200$–900 K interval, the measured values were in good agreement with the calculations of Park and Light [36], who used a full dimensionality QM method, and with the reduced dimensionality calculations of Bowman and co-workers [37], but the calculated rate constants deviated gradually toward lower values at higher temperatures, the deviation being surprisingly larger for the results of the more rigorous theoretical procedure.

At the lower end of the temperature range, the possible influence of tunnelling in the observed rate constants was an important issue during the 1980s [38]. Tunnelling corrections were applied by Mayne and Toennies [29] to their QCT results for the $H + H_2$ isotopic variant in order to improve the agreement with the measurements, but even without this correction the classical results were reasonable, especially for $D + H_2$ and $H + D_2$. This fact was attributed to a lucky cancellation of errors [38] in the QCT calculations: the lack of zero-point energy (ZPE) in the classical description was supposed to compensate the absence of a tunnelling contribution. An even lighter mass combination, especially adequate for the investigation of tunnelling and ZPE effects, was provided by the $Mu + H_2$ isotopic variant of the reaction (muonium, Mu, is nearly nine times lighter than H). The QCT rate constants [39] were larger by more than an order of magnitude than those from experiment [40], which were

in turn well reproduced by a coupled states (CS) QM treatment [41]. The failure of the standard QCT method to describe the $Mu + H_2$ reaction is mostly due to the high ZPE of the product molecule, MuH, and to a lesser extent to the neglect of the ZPE at the transition state. With the usual binning procedure applied for the assignment of the final product quantum states, the number of trajectories counted as reactive but leading to products' energies much lower than that of the ground state of MuH, is large. In this case, and in others with a comparatively high products' ZPE, the use of 'reverse' trajectories and the application of the microreversibility principle removes a significant part of the disagreement between the QCT and QM cross sections (see discussion in [39, 42]). With the exception of the $Mu + H_2$ isotopic variant, the QCT approach has been found to perform quite well for the study of the reaction dynamics of the H_3 system, as will be seen throughout this review.

Whereas the overall agreement between theory and experiment in the $k(T)$ was never too bad for ground state reagents, a noteworthy discrepancy was found in the reaction with vibrationally excited ($v = 1$) hydrogen molecules (see [10, 11] and references therein), where the rate constants measured at different laboratories were much higher than those from the calculations (both classical and quantum mechanical). The controversy was finally settled in favour of theory by new and more resolutive measurements [43, 44].

Differential reaction cross sections without internal state resolution were determined in a series of crossed molecular beam (CMB) experiments, using mostly mass spectrometric detectors. These experiments were gradually improved since the 1970s [44–49]. QCT calculations on the LSTH PES [29, 47] produced center-of-mass (CM) DCSs having maxima in the backward direction with respect to the incoming atom, that became gradually broader as the collision energy increased and more non-collinear atomic configurations contributed to the reaction (unless otherwise stated we will refer to HD scattering and keep this definition of the backward direction). The angular and, eventually, the velocity distributions of these experiments could be well reproduced with the mentioned QCT results [29, 47]. Towards the end of the 1980s, highly monoenergetic beams of hydrogen atoms were generated by laser photolysis of a precursor and this allowed the partial resolution of vibrational states in the time-of-flight distribution of the angle-selected product molecules [48, 49]. A brief description of the technical problems that had to be overcome during these years can be found for instance in [11, 50]. The simulation of the CMB measurements of Buntin *et al.* [48] with the accurate QM calculations of Zhang and Miller [21] and of Zhao *et al.* [51] showed some discrepancies that were attributed to deficiencies of the PES. Smaller differences were found between theory and the experiment of Lee and co-workers [26, 49].

State-specific integral cross sections and rate constants, as well as rovibrational distributions, $P(v', j')$, of the reaction products without angular resolution, were measured during the 1980s by different groups in bulk experiments (see, for instance [10, 11, 52–62] and the references therein). These experiments used a combination of laser techniques, including UV photolysis for the generation of the reacting atoms, Raman pumping for the selection of rovibrational states of the reagent molecule, and laser induced fluorescence (LIF) [52, 53], Coherent Antistokes Raman spectroscopy (CARS) [54–57], or resonance enhanced multiphoton ionization (REMPI) [58–62] for the state selective detection of the products. The delay between photolysis and probe

lasers was suitably chosen to guarantee single collision conditions. All these experiments used fast (translationally 'hot') atoms and the characteristic collision energies were well above the threshold for reaction. A global good agreement was found between these measurements and the results of QM [25, 51, 62–65] and, to a somewhat lesser extent QCT [66–70] calculations (the classical rotational distributions were always slightly hotter than those from QM and experiment). The small differences between theory and experiment were again mostly attributed to possible inaccuracies of the PES. However, sometimes noteworthy discrepancies, usually related to the possible experimental identification of QM effects, were found and gave rise to interesting debates stimulating further theoretical and experimental work. The two cases that have been of highest relevance for the studies of the reactive dynamics of $H + H_2$ over the last fifteen years will be briefly commented on here.

Some of the CARS experiments of the group of Valentini [54–57] on the $H + p\text{-}H_2 \rightarrow o, p\text{-}H_2(v', j') + H$ reaction led to sharp variations of the cross sections for the production of specific v', j' states as a function of collision energy. They were interpreted as a manifestation of Feshbach resonances by the authors. Scattering resonances for this system had been obtained in 3D QM calculations for low values of the total angular momentum [71], but accurate calculations by several groups [22, 24, 26, 72, 73] indicated that the resonance structure should not survive the partial wave summation needed to reproduce the experimental conditions. Ultimately, a REMPI experiment by the group of Zare [59] demonstrated the absence of sharp structures in the cross section. It was then generally accepted that scattering resonances would not show up in the energy dependence of the integral cross section. However the search for other manifestation of resonances, that would be experimentally observable, continued. Miller and co-workers [74, 75] showed that a structure, possibly due to a broad resonance (i.e. with contributions from several values of the total angular momentum) was indeed observable in the energy dependence of the v', j' state-resolved DCSs at low j' values. This structure is manifest in a 3D representation of the DCS *vs*. total energy, E, and CM scattering angle, θ, where it takes the form of a ridge moving from backward to forward scattering over the $\approx$0.3–1.4 eV collision energy range (see, for instance figure 7 of [75]). A detailed QCT study [76] led also to a similar ridge structure, albeit less marked, showing that the effect was not purely quantum mechanical. The nature of the short-lived classical complexes and its relation to the analogous QM structures gave rise to a series of theoretical and experimental works that will be discussed in detail in Section 4.

Another interesting discrepancy was found between the product rotational state distribution measured by Zare and co-workers [60] for the $D + H_2(v = 1,\ j = 1) \rightarrow HD(v' = 1, j') + H$ reaction at a collision energy, E_{col}, of 1.0 eV, and the theoretical results. The observed $P(j')$ for $HD(v' = 1, j')$ had a peak at significantly lower j' than those from QCT and QM theoretical calculations [24, 64, 65]. This situation was particularly upsetting since, as commented on above, good agreement was found in general between the products' rotational distributions from experiment and theory for the different isotopic variants, over a wide range of collision energies and internal states of the reagents. In a first moment, experimental problems associated with the use of DBr as photolytic precursor of the D atoms, were deemed responsible for the discrepancy. The DBr was substituted by DI, the pump/probe experimental scheme was improved,

and new measurements, including one at a similar (but not exactly the same) energy as that of the dubious experiment, were carried out and were found to be in good agreement with QM wave packet calculations [61, 62]. However, the polemical experiment just mentioned [60] was to be reinterpreted, in the light of new theoretical results, as an effect of the geometric phase (GP) in the dynamics [77, 78]. This interpretation has also led to a long controversy that will be discussed more thoroughly in Section 6.

3. Towards a detailed agreement between theory and experiment

In 1991, Welge and co-workers [79] measured the D atom reactive scattering of the $H + D_2 \rightarrow HD + D$ reaction using a novel technique developed at the University of Bielefeld [80] in which lasers were used both for the production of the H reactive atoms and for the detection of the D product. In particular, the H atoms were generated by laser photolysis of HI. This procedure provided a group of 'slow' H atoms, associated with the production of $I(^2P_{1/2})$, and a group of 'fast' H atoms, corresponding to the production of $I(^2P_{3/2})$. A suitable choice of the laser polarization allowed the selection of slow or fast atoms for reaction. By using the fourth harmonic (266 nm) of a Nd:YAG laser, the respective collision energies were 0.54 and 1.29 eV. For the analysis of the products, the nascent D atoms were promoted to an excited metastable Rydberg state (Rydberg 'tagging') by two photon (VUV plus UV) absorption in the reaction zone. The Rydberg atoms were then allowed to fly until a rotatable detector, where they were field ionized. A scheme of the experimental set-up is shown in figure 1. From the angle-selected time-of-flight spectra of the scattered D atoms, the internal state distribution of the corresponding HD molecules could be derived. In this first version of the experiment only vibrational state resolution was possible.

In 1993, Kitsopoulos *et al.* [81] performed a pioneering experiment on the same reaction using a similar photolysis scheme, and thus the same collision energies, but a different detection procedure, based on the REMPI technique. The product D atoms were ionized by $2 + 1$ REMPI, extracted and projected onto a microchannel plate (MCP) detector coupled to a phosphor screen. The phosphorescence was then imaged onto a CCD camera, yielding an angle-velocity polar map of the reaction in a direct way. This reaction product imaging (RPI) technique provided a global picture of the reactive scattering in a nearly straightforward manner, but had a relatively low resolution since the images were blurred by the use of grids in the extraction and acceleration plates of the Wiley-McClaren time-of-flight (TOF) type spectrometer. This was the imaging setup used before the introduction of the velocity mapping technique by Eppink and Parker in 1997 [82] and the slicing imaging technique by Kitsopoulos and co-workers [83], Liu and co-workers [84] and Suits and co-workers [85]. In fact HD, internal states could not be resolved in this experiment. Besides, the angular distribution had to be recovered by an Abel transformation from a two dimensional projection of a three dimensional reactive sphere.

The data of the two experiments were simulated with the results of QCT and accurate QM calculations [86, 87]. Additional comparisons between QM, QCT and experiment at the same collision energies were reported in [88, 89]. In general, good accord with small differences was found between QM and QCT total and vibrationally state

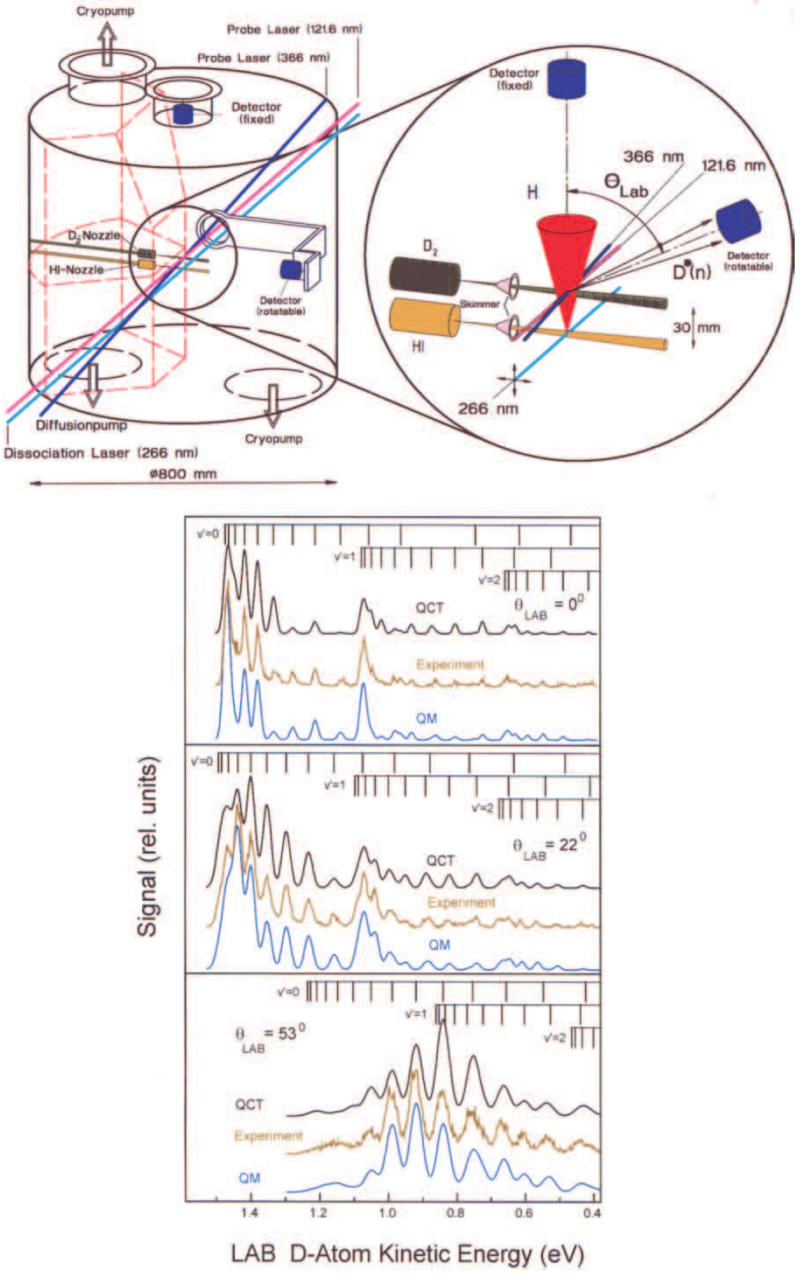

Figure 1. Upper part: Scheme of the experimental set up used by the group of Bielefeld [91, 92]. Lower part: Kinetic energy spectra of the D atoms scattered in the $H + D_2(v = 0, j = 0) \rightarrow HD(v', j') + D$ reaction at $E_{col} = 1.28$ eV. The three panels correspond to three laboratory scattering angles. The middle trace corresponds to the experimental measurements, the lower trace to the QM simulations (at $E_{col} = 1.30$ eV) on the LSTH surface and the upper trace to QCT simulations on the same PES [91]. The energies of the various rovibrational levels of HD accessible in the experiment are also indicated. Reprinted with permission from [91]. Copyright 1995 American Association for the Advancement of Science.

resolved DCSs. The comparison of both theoretical approaches with the lower resolution ion imaging experiment [81] showed only qualitative agreement with appreciable discrepancies, in particular, the velocity distributions derived from the measurements were broader with maxima at lower velocities than the theoretical ones, and the CM DCSs presented a marked peak, especially at $E_{col} = 1.29\,eV$, that was not reproduced in the theoretical calculations. In contrast, the agreement between experiment and theory was very good in the case of the vibrationally resolved Rydberg atom TOF spectra [79–87]. Again in this case, the polemical peak in the lower resolution experiment was later attributed to an effect of the geometric phase in the reactivity [90], but this interpretation has also been questioned (see Section 6).

The Rydberg atom 'tagging' technique was further improved and in 1995, angle-selected fully state-resolved TOF spectra of the D atoms produced in the $H + D_2(v = 0,\ j = 0) \rightarrow HD(v', j') + D$ reaction at a collision energy of 1.29 eV were published by Schnieder *et al.* [91]. These measurements represent, to the present day, the state-of-the-art experimental resolution in dynamical studies not only of the hydrogen-atom exchange reaction, but also of other elementary reactions yielding hydrogen atoms. In the same article, the measurements were simulated with the results of QCT and accurate QM calculations performed on the LSTH surface. As shown in figure 1, the QM simulations could reproduce very well the measured TOF spectra and the QCT simulations were only slightly worse. The extraordinary quality of the measured data allowed the determination of experimental fully v', j' resolved DCSs in the CM system [92] and made possible a direct comparison with the predictions of theoretical calculations [92, 93]. Within the angular range sampled by the experiment (corresponding to $\theta \approx 180 - 40^{\circ}$) the agreement between the experimental and the QM DCSs was excellent; furthermore essentially all the details of the v', j' DCSs were also found in the QCT calculation with minor quantitative discrepancies.

The very good accordance obtained in these rigorous comparisons increased the confidence, both in the quality of the PES and in the theoretical approaches used for the solution of the dynamical problem. The good behaviour of the QCT method, at least for this relatively high collision energy, was encouraging given its computational advantages and its great interpretative power. In addition, classical results are necessary for the identification of possible QM effects in the dynamics. The limitations of the quasiclassical treatment when threshold or ZPE effects are relevant were discussed in the previous section. A detailed appraisal of the QCT method based on an extensive comparison of QCT calculations (from state-resolved cross sections to thermal rate constants) with QM and experimental results for various elementary reactions can be found in [93, 94].

By changing the energy of photolysis of the HI precursor, the group at Bielefeld used the Rydberg 'tagging' technique during the second half of the 1990s for the measurement of v', j' resolved DCSs for the $H + D_2(v = 0,\ j = 0)$ reaction at selected collision energies between 0.52 and 2.67 eV [95–99]. In all cases the measurements were in good agreement with the results of QCT and accurate QM calculations and in some instances they were decisive to clarify existing discrepancies as will be shown later. Figure 2 illustrates the almost quantitative agreement observed between experiment and QM calculations on the BKMP2 PES [100] at a collision energy of 2.2 eV and the good performance of the QCT approach. Figure 3 shows the impressive comparison

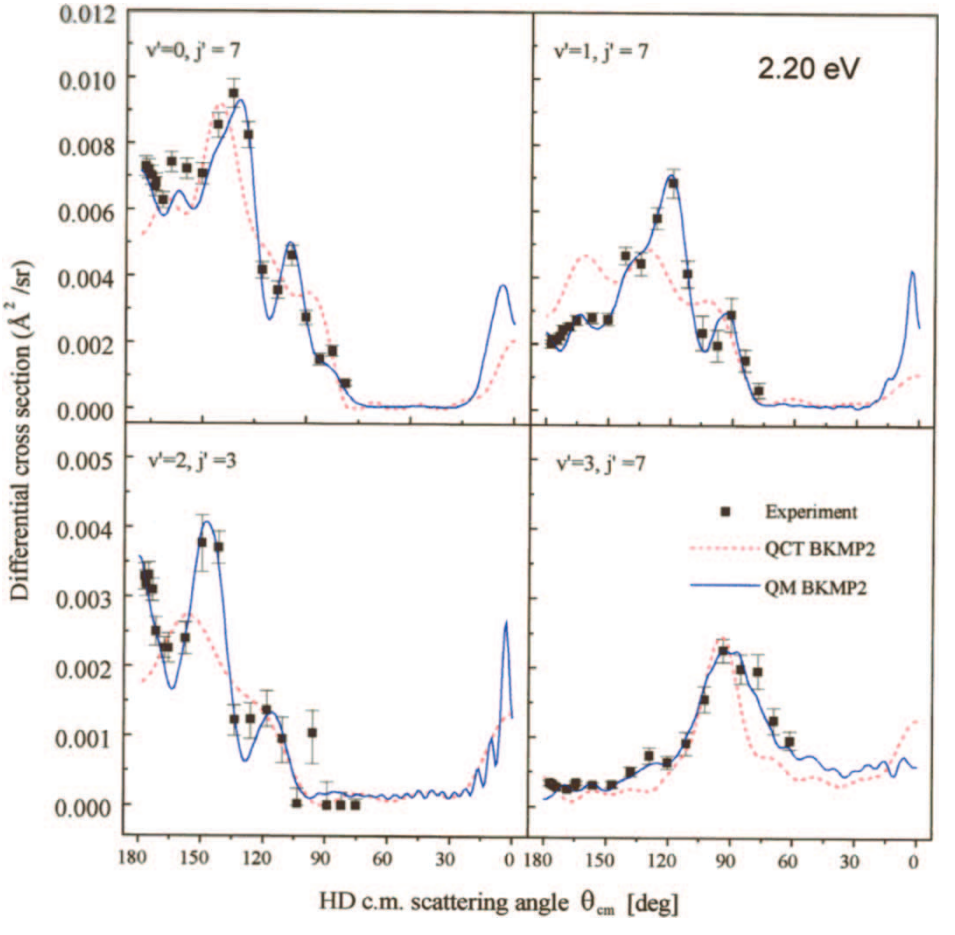

Figure 2. Centre-of-mass differential cross sections for reactive scattering into selected rovibrational states of the HD molecules generated in the $H + D_2(v = 0, j = 0) \rightarrow HD(v', j') + D$ reaction at $E_{col} = 2.2$ eV [99]. Solid squares with error bars: experimental data. Solid lines: QM calculation on the BKMP2 PES. Dashed lines: QCT calculation on the same surface.

of experimental and QM state-resolved angle-velocity polar map, summarizing the global dynamical information about the reaction at this energy. Note again that the CM angular range accessible to the experiment is limited to $\theta \gtrsim 40^\circ$. The various *ab initio* PESs available in the literature [14–17, 100] were of sufficient accuracy to account for the results at the higher collision energies (> 1 eV) sampled in the molecular beam experiments. However, very careful measurements around $E_{col} = 0.5$ eV [98] allowed a detailed appraisal of the quality of the different PESs, as discussed later. Further experiments using the Rydberg 'tagging' technique have been performed more recently by Yang and co-workers [101–104] on the $H + HD$ and $H + D_2$ isotopic variants of the reaction. In contrast with the experimental set-up at Bielefeld, these new measurements could access very low CM angles and provided a most valuable information about the forward scattering of the product molecules.

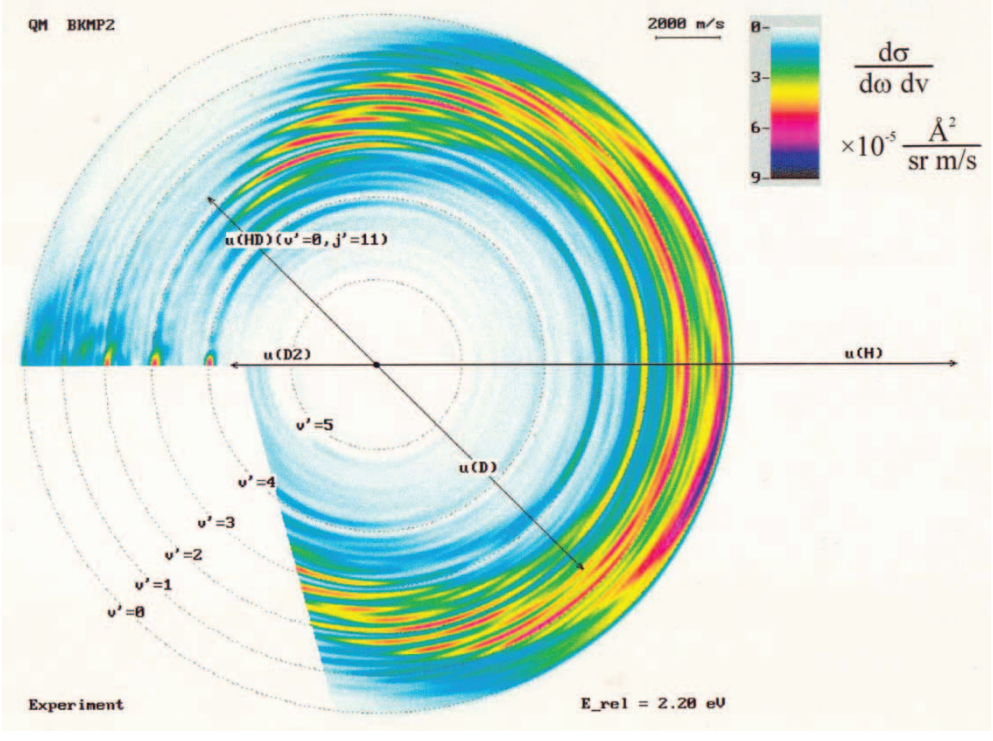

Figure 3. Centre-of-mass angle-velocity polar map corresponding to the scattering of D atoms from the $H + D_2(v = 0, j = 0) \rightarrow HD(v', j') + D$ reaction at $E_{col} = 2.2$ eV [99]. The polar map is symmetric with respect to the CM collision direction (horizontal axis). In the upper half, the results of a QM calculation on the BKMP2 surface are represented. The lower half shows the experimental data. The experimentally inaccessible angular range is also indicated in the figure. Reprinted with permission from [99]. Copyright 1999 American Institute of Physics.

Since 1999, state-resolved DCSs for the $H + D_2 \rightarrow HD(v', j') + D$ reaction were also derived by Zare and co-workers [105–113] with a different experimental technique [114, 115] termed *photoloc*. The name of this technique is a synthesis of its two main elements: the reaction is initiated by laser *photolysis* in a free jet co-expansion of a suitable H atom precursor, like HBr or HI, and reagent molecules, D_2, and then the *law of cosines* is used to relate the product laboratory velocity distribution to the CM differential cross section. The REMPI-TOF technique with core extraction [116] is used for the detection of the $HD(v', j')$ product molecules. The method is experimentally less demanding than the Rydberg atom 'tagging' TOF technique and provides reliable rovibrational states distributions, but the DCSs are inferred in a more indirect way and the angular resolution is comparatively poor.

During the 1990s, progress in the methodology of quantum reactive scattering continued [117] and higher collision energies were gradually accessed. After 1995, most time-independent dynamical calculations for $H + H_2$ have used hyperspherical-coordinate methods [90, 99, 101–104, 108, 112, 113, 118–129] for which a general and very efficient code has been released [130]. Important methodological advances in wave

packet time-dependent approaches have taken place over the last ten years [131] and these methods have been also employed for extensive dynamical studies of the H_3 system [109, 112, 113, 131–136]. For a recent review on quantum reactive scattering calculations see [137].

In general, the agreement between experimental data and accurate QM calculations was found to be virtually quantitative in the case of the Rydberg 'tagging' measurements [87, 91, 98, 99, 101–104]. In lower resolution hot-atom experiments a quite good accordance with theory has also been found, with only eventual discrepancies [113, 124] that will be discussed later. In some of the experimental results, peculiar features were identified in the measured DCSs, whose interpretation has given rise to interesting theoretical discussions as will be seen in the next sections.

Whereas a very good agreement between theory and the hot-atom dynamical experiments was found since 1995, significant discrepancies persisted throughout the 1990s in the case of the thermal rate constants, which sample mainly lower energy regions of the PES. (Note that at 2000 K the average collision energy, $\approx$0.26 eV, is still below the classical threshold for reaction.) In 1994, Mielke *et al.* [138] reported converged QM thermal rate constants for $D + H_2(v = 0)$ over the 167–900 K temperature range and rate constants extrapolated or calculated within the separable rotation approximation (SRA) up to 1500 K. The authors employed the outgoing wave variational principle to calculate reaction probabilities, which were then integrated with Boltzmann weighting to yield $k(T)$. The calculations were performed on the LSTH [14, 15], DMBE [16] and BKMP [17] *ab initio* PESs existing at the time. A good agreement with the measured rate constants was obtained on the LSTH and DMBE surfaces for $T < 900$ K, but the low temperature calculations on the BKMP PES led to higher $k(T)$ than those from experiment. This was surprising since the BKMP surface was in principle the most accurate one, with the highest number of calculated *ab initio* data and the smallest root-mean-square deviation from these *ab initio* points. For temperatures higher than 900 K, the theoretical estimates of the rate constants deviated gradually from the measurements toward lower values, so that for $T = 1500$ K the calculated $k(T)$ were $\approx$30–40% smaller than the experimental value. This deviation was smaller than that previously obtained by Park and Light [36] (a factor of two), but still unsatisfactory. From a comparison of rate constants for different values of the initial total angular momentum, J, Mielke *et al.* [138] concluded that the $k(T)$ of Park and Light [36] were not fully converged. Accurate QM cross sections and rate constants for the reactions of Mu with H_2,D_2 and HD were published by Nakamura and co-workers [139, 140]. The calculations used the LSTH PES and the results were in good agreement with the experimental rate constants [40] and with the $k(T)$ from approximate CS calculations of Schatz [41].

QCT thermal rate constants on the LSTH, DMBE and BKMP surfaces were calculated by Aoiz and co-workers for the $D + H_2$ [141] and $H + D_2$ [142] reactions for temperatures between 200 and 1500 K. In the lower temperature range, the $k(T)$ for $D + H_2$ were smaller than those from experiment and from the accurate QM calculations of Mielke *et al.* [138], probably due to the neglect of tunnelling in the classical treatment. At high temperature the QCT rate constants were somewhat lower than the QM ones, and thus lower than the measurements. Interestingly, the values of the low temperature classical $k(T)$ on the different PESs showed the same trend than their

QM counterparts, i.e. they were very similar on the LSTH and DMBE surfaces and were higher on the BKMP PES. For the $H + D_2$ isotopic variant [142], the agreement of the classical results with the measurements was good between 250 and 800 K, but as in the previous case, the QCT rate constants became lower than the experimental values for higher temperatures. Also for this isotopic variant, the low temperature $k(T)$ on the BKMP surface were higher than those on the LSTH and DMBE PESs.

Two issues were specially addressed in the just mentioned QCT investigations: the influence of rotation on reactivity and the intermolecular isotope effect on the available PESs. The important role of rotation on the reactivity of the $H + H_2$ system has been analysed in a number of QCT works (see for instance [4, 141–148] and the references cited therein). For $D + H_2$ and, to a lesser extent, for $H + H_2$ the calculations show that the rotational excitation of the molecule up to $j = 4$–6 leads to a decrease in the cross section for collision energies lower than 0.6–0.8 eV. For higher collision energies or rotational quantum numbers, rotational excitation increases the cross section for reaction. For $H + D_2$, rotational excitation has always a beneficial influence on the reactivity, as can be seen in the top panel of figure 4, in which the QCT excitation functions for the $H + D_2(v = 0, j = 0$–$4)$ reaction calculated on the LSTH PES are depicted. A similar effect of rotation has been found in QM calculations [51, 133, 140, 149, 150], and, in particular in those performed within the multi-configuration time-dependent hartree (MCTDH) wavepacket approach carried out by Meyer and co-workers [133] and shown in the bottom panel of figure 4.

The analysis of the classical trajectories provides an explanation for the observed behaviour. The potential surface for the H_3 system has a marked collinear character and at low energies rotation is expected to perturb the atom-diatom orientations favourable for reaction. This disorienting effect is more pronounced in the post threshold region, where the steric hindrances of the potential are more strict and the possible reacting geometries of the three nuclei are more constrained. The negative influence of rotation is expected to be more marked for quick rotation and slow translation, consequently, the disorienting effects should decrease along the sequence $D + H_2$, $H + H_2$, $H + D_2$ in accordance with the QCT results [142]. The concrete magnitude of the dynamical disorientation depends on the features of the different surfaces. For the H_3 system, the effects are somewhat more marked on the DMBE PES. As far as we know, direct experimental studies of the effect of rotation on reactivity have not been reported, but it might play a role in the different threshold reactivity of $D + H_2$ and $H + D_2$ [142]. A QCT investigation of the $(D + H_2)/(H + D_2)$ intermolecular isotope effect showed that the larger reaction cross section of $D + H_2$ as compared with $H + D_2$ is caused by the more efficient transfer of collision energy from the heavier D atom to the molecular bond of the lighter H_2 molecule [142].

By the mid 1990s, there was still no agreement between the experimental and theoretical thermal rate constants for $T > 900$ K and the low temperature accurate QM $k(T)$ calculations on the BKMP PES, expected to be the accurate one, were in worse agreement with experiment than those on the LSTH and DMBE surfaces.

More work was then invested in the improvement of the PES. Partridge *et al.* [151] calculated new *ab initio* points, and Diedrich and Anderson [152, 153] made a very precise estimate of the classical barrier height using a quantum Monte Carlo procedure; new ways of fitting *ab initio* data [154] were also proposed. In 1996 using

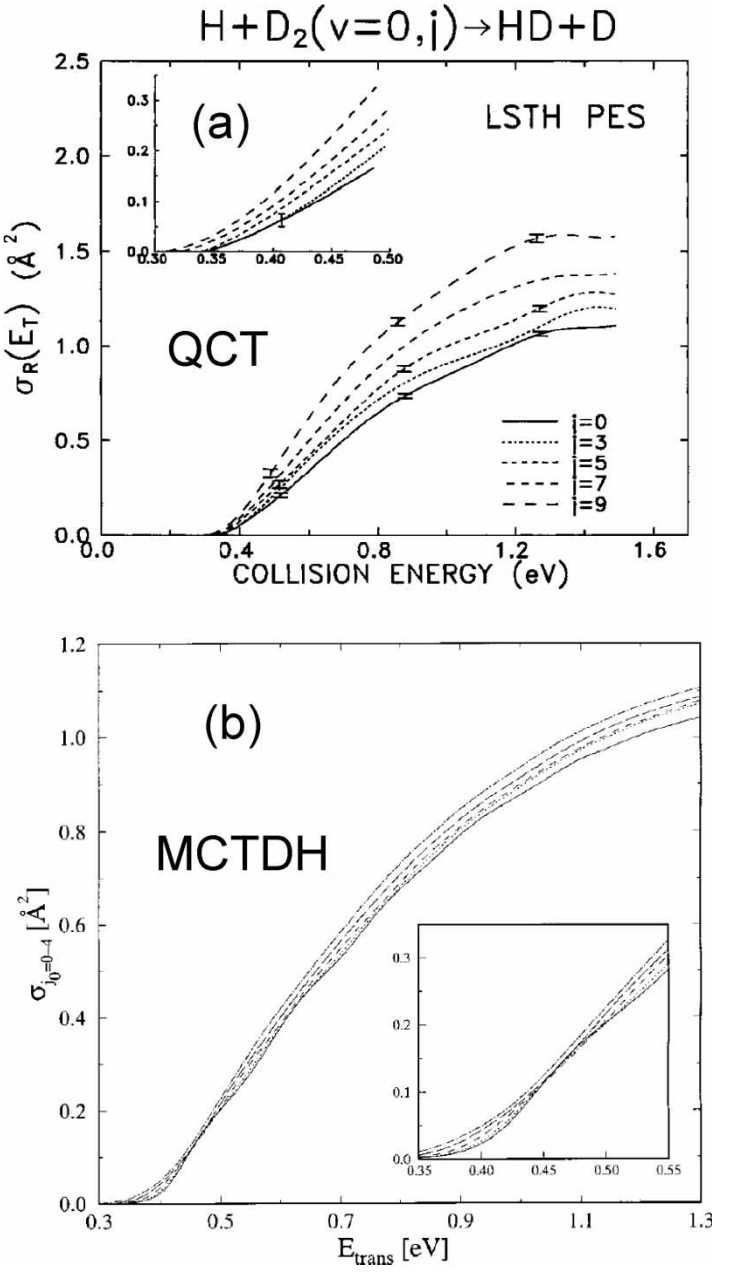

Figure 4. (a): QCT reaction cross sections as a function of collision energy (excitation functions) for the $H + D_2(v = 0, j = 0–4) \rightarrow HD + D$ reaction at the indicated reagent rotational quantum number j calculated on the LSTH PES. The error bars indicate one standard deviation of the calculations [142]. Bottom panel: (b) exact calculations for reagent rotational quantum numbers $j = 0–4$ carried out on the LSTH PES [133]. Solid line, $j = 0$; dotted line, $j = 1$; dashed line, $j = 2$; long-dashed line, $j = 3$; dot-dashed line, $j = 4$. The insets in both panels display the cross section near the reactive threshold. Reprinted with permission from [142] and [133]. Copyright 1997, 2001 American Chemical Society.

all this information and adding new *ab initio* points and further refinements to the fitting method, Boothroyd *et al*. released a new version of their PES termed BKMP2 [100]. The new surface was based on a set of 8701 *ab initio* data (as compared with the 772 of the previous BKMP one) and the fit matched the points with an overall rms error of 7.4 meV. QM thermal rate constants, based on calculations of converged reaction probabilities on this surface, were reported by Bañares and D'Mello [155] for the $D + H_2 \rightarrow HD + H$ reaction. The new low temperature $k(T)$ were only slightly lower (8%) than those on the BKMP PES and thus still too large as compared with the measurements and with the rate constants calculated on the other *ab initio* potential surfaces. Interestingly, similar calculations for the $H + D_2$ reaction, presented in this review for the first time, lead to a much better agreement with the experiment (see figure 5).

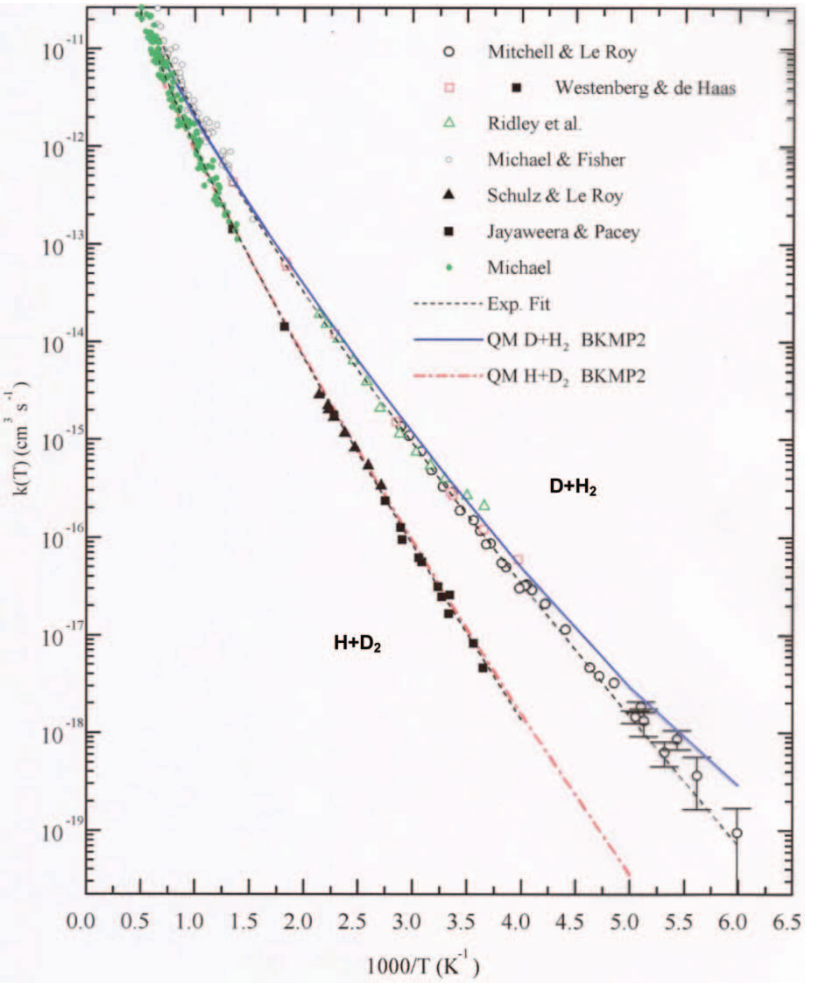

Figure 5. Experimental and QM thermal rate constants for the $D + H_2 \rightarrow HD + H$ [155] and $H + D_2 \rightarrow HD + D$ (present work) reactions. The calculations were carried out on the BKMP2 potential energy surface.

The high temperature disagreement with experiment found for all the previous PESs [138] persisted also with this new one.

An assessment of the four *ab initio* PESs mentioned in the previous paragraphs, based on the comparison of accurate QM calculations with state-to-state molecular beam experiments, was presented by Bañares *et al*. in 1998 [98]. The study was carried out for the $H + D_2(v=0,\ j=0) \rightarrow HD(v'=0,j') + D$ reaction at collision energies between 0.52 and 0.54 eV. This is close to the lowest energy accessed in the Rydberg 'tagging' experiments, but is still above the energies relevant for the thermal rate constants. The variation of the experimental collision energy within this small energy interval was achieved by slightly changing the angle of intersection of the molecular beams. The very high resolution of the measurements allowed a clear distinction between the various *ab initio* PESs as illustrated in figure 6, where the theoretical and experimental rotationally resolved DCSs and the rotational state distribution, $P(j')$, of the HD molecules are shown. The BKMP2 surface, which leads to an excellent agreement with the measured data, is definitely favoured in this comparison.

The very good behaviour of the BKMP2 PES for the description of the detailed dynamical results and its inability to accurately reproduce the low and high temperature thermal rate constants remained a puzzle. Work on the surface continued. In 1999, Wu *et al*. [156] published a new H_3 surface consisting of spline fits of extensive quantum Monte Carlo (EQMC) calculations, similar to the earlier work of Diedrich and Anderson [152, 153]. Mielke *et al*. [157, 158] identified some inaccuracies in the EQMC calculations and constructed in turn a hierarchical family of global analytic Born–Oppenheimer (BO) PESs based on an extensive set of accurate multireference configuration interaction (MRCI) data. The most precise of this surfaces, termed CCI, was fitted to *ab initio* energies calculated in the complete basis set (CBS) limit and its mean deviation from the true BO PES is expected to be less than 0.45 meV. In their work [158], the authors performed an extensive comparison of their PES to the earlier analytic H_3 surfaces (LSTH, DMBE, BKMP and BKMP2) and concluded that the long range anisotropy, which should be important for the precise description of low energy scattering processes, is better represented by the latest CCI PES. Mielke *et al*. [158] also noted, that for accurate work one should include a correction to the BO approximation due to the nuclear motion on the electronic ground state PES (see [159] and the references therein). They estimated that this Born–Oppenheimer diagonal (BOD) correction would raise the barrier height by ≈6 meV for the $D + H_2$ reaction.

In 2003, a combined theoretical and experimental study of the thermal rate constants for the $D + H_2$ and $H + D_2$ reactions was reported by Mielke *et al*. [160]. In the experimental part of the work, Michael and co-workers [160, 161] used the shock tube technique with D- and H-atomic resonance absorption spectroscopy (ARAS) detection for the measurement of $k(T)$. The reactant H and D atoms were generated from the thermal decomposition of molecular precursors (C_2H_5I and C_2D_5I). This limited the experimental accessible range to the high temperature region (≈1150–2100 K), but avoided many of the complications associated with secondary reactions found in earlier experiments in which the atomic reagents had been generated by flash photolysis [34, 37]. An Arrhenius fit of the new high T data led to values of $k(T)$ significantly lower (≈35% for $H + D_2$ and 28% for $D + H_2$) than those of the previous

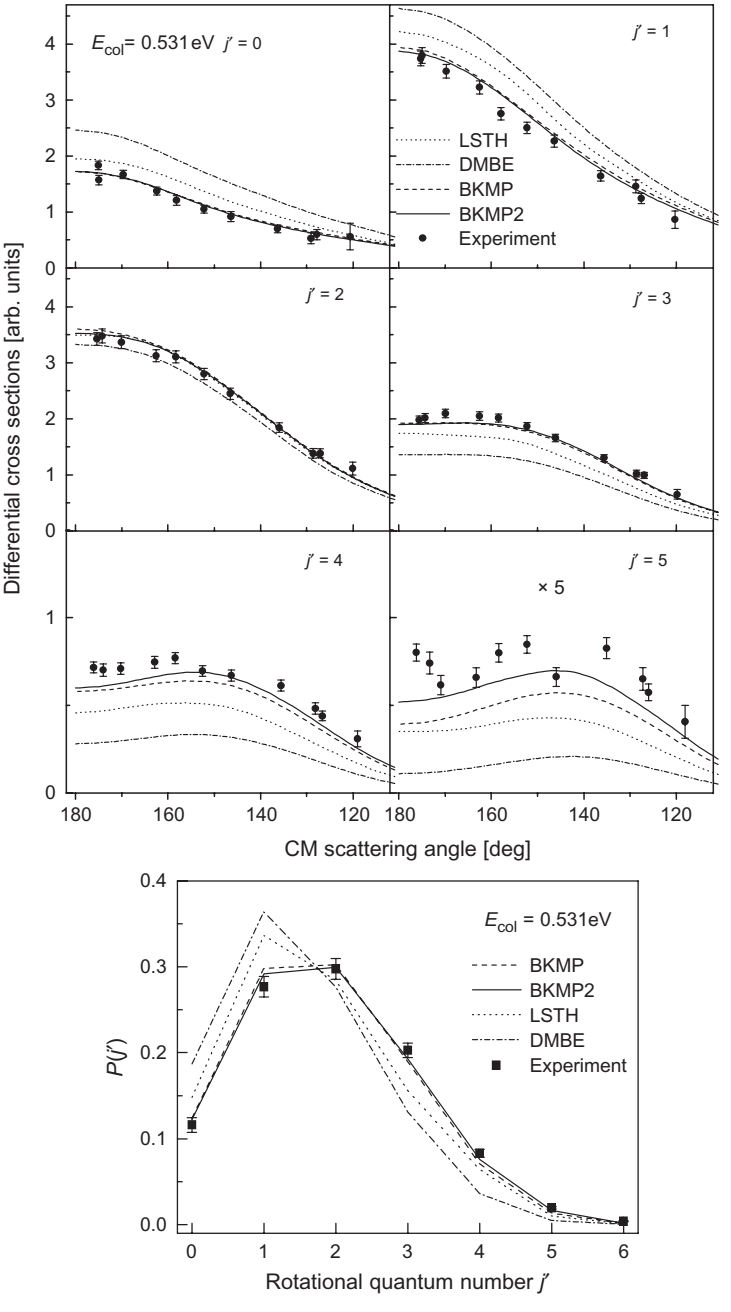

Figure 6. Upper part (six panels): QM differential cross sections for the $H + D_2(v = 0, j = 0) \rightarrow HD(v' = 0, j') + D$ reaction at a collision energy of 0.531 eV [98]. Lower part: rotational state distribution for $HD(v' = 0)$ molecules of this reaction. Solid circles with error bars: experimental data. The different lines correspond to calculations performed on the LSTH [14, 15], DMBE [16], BKMP [17] and BKMP2 [100] potential surfaces. Reprinted with permission from [98]. Copyright 1998 American Institute of Physics.

publications [26, 37]. The dynamical calculations carried out on the CCI PES used a method similar to that of [138]. The effect of the BOD correction on this surface, which depends on the particular isotopomer considered, was determined by means of MRCI calculations employing extended reference spaces and large basis sets. This correction raises the barrier height by 6.03 meV and 3.90 meV for $D + H_2$ and $H + D_2$, respectively. The $k(T)$ calculations were performed on the adiabatic CCI surface. The authors observed that the BOD correction affected mostly the barrier height and applied a Boltzmann factor of the type $\exp(-\Delta E_b/kT)$, where ΔE_b is the increase in the barrier height, to the $k(T)$ calculated on the Born–Oppenheimer CCI PES [160]. With the experimental and theoretical improvements described, there is at last agreement, within the experimental uncertainty, between the calculated and measured thermal rate constants for the two isotopic variants over the whole temperature range investigated thus far (see figure 7). It should be noted here that the Born–Oppenheimer barrier height is practically the same for the BKMP2 and CCI PESs (0.4169 eV and 0.4164 eV, respectively, with respect to the ground state minimum of the isolated H_2 molecule); thus, if the BOD corrections were of the same order for the two surfaces, which is plausible, a similar good agreement with experiment would be obtained on the BKMP2 PES by applying the corresponding correction factor. Note also that the correction should be negligible even for the lowest collision energies of the molecular beam experiments, for which the high accuracy of the BKMP2 PES had been established with molecular beam experiments and QM calculations [98].

4. Forward scattering and delayed scattering

As mentioned above, Zhang and Miller [21, 22] carried out one of the first fully converged extensive QM calculations on the $H + H_2(v=0,\ j=0)$ and $D + H_2(v=0,\ j=0)$ reactions using the LSTH PES at a series of collision energies ranging from the vicinity of the threshold up to 1.1 eV. State resolved integral and differential cross sections were determined at all these E_{col}. At collision energies above 0.8 eV the calculations predicted the existence of forward scattering in the DCS resolved in final vibrational states. This forward scattering seemed to increase with increasing collision energy and, at energies above 1.0 eV, the existence of a relative maximum in the DCS at $\theta = 0^\circ$ was clear.

In a subsequent article, Miller and Zhang [75] showed that when the state resolved DCS are plotted in 3-D representations as a function of the scattering angle and the collision energy a ridge appears in the energy-angle plane moving from backward to forward scattering over the ≈0.3–1.4 eV collision energy range (see, for instance, figures 8 and 9 of [75]). Forward scattering into $HD(v' = 0, 1)$ was found to be confined to the lowest rotational states ($j' = 0$–3). This was attributed to a 'broad resonance' involving a narrow range of total angular momenta and short lived collision complexes. The effect was ascribed to an interference of several partial waves with different J values. The ridges on the θ–E plane have also a counterpart when the state resolved reaction probability is represented as a function of the total energy and total angular momentum, $P(E; J)$. Actually, the representation of $P(E; J)$ for various Js gives rise

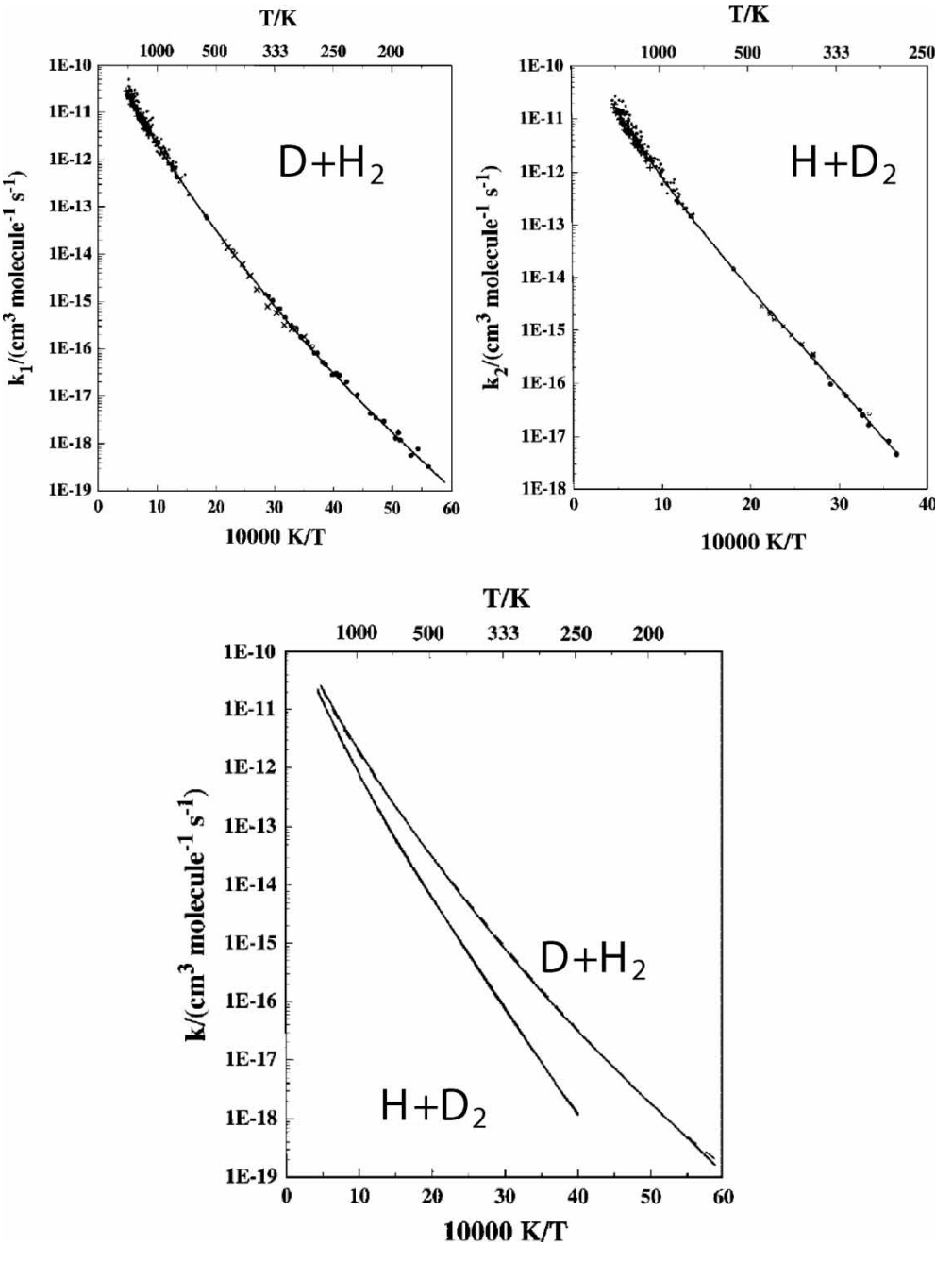

Figure 7. Comparison of experimental and quantum mechanical thermal rate constants for the $D + H_2 \rightarrow HD + H$ and $H + D_2 \rightarrow HD + D$ reactions [160]. In the upper panels the dots correspond to different experimental measurements and the solid lines are Arrhenius fits of the data. In the lower panel the QM calculations (dashed lines) are compared with Arrhenius plots of the experimental data (solid lines). Reprinted with permission from [160]. Copyright 2003 American Institute of Physics.

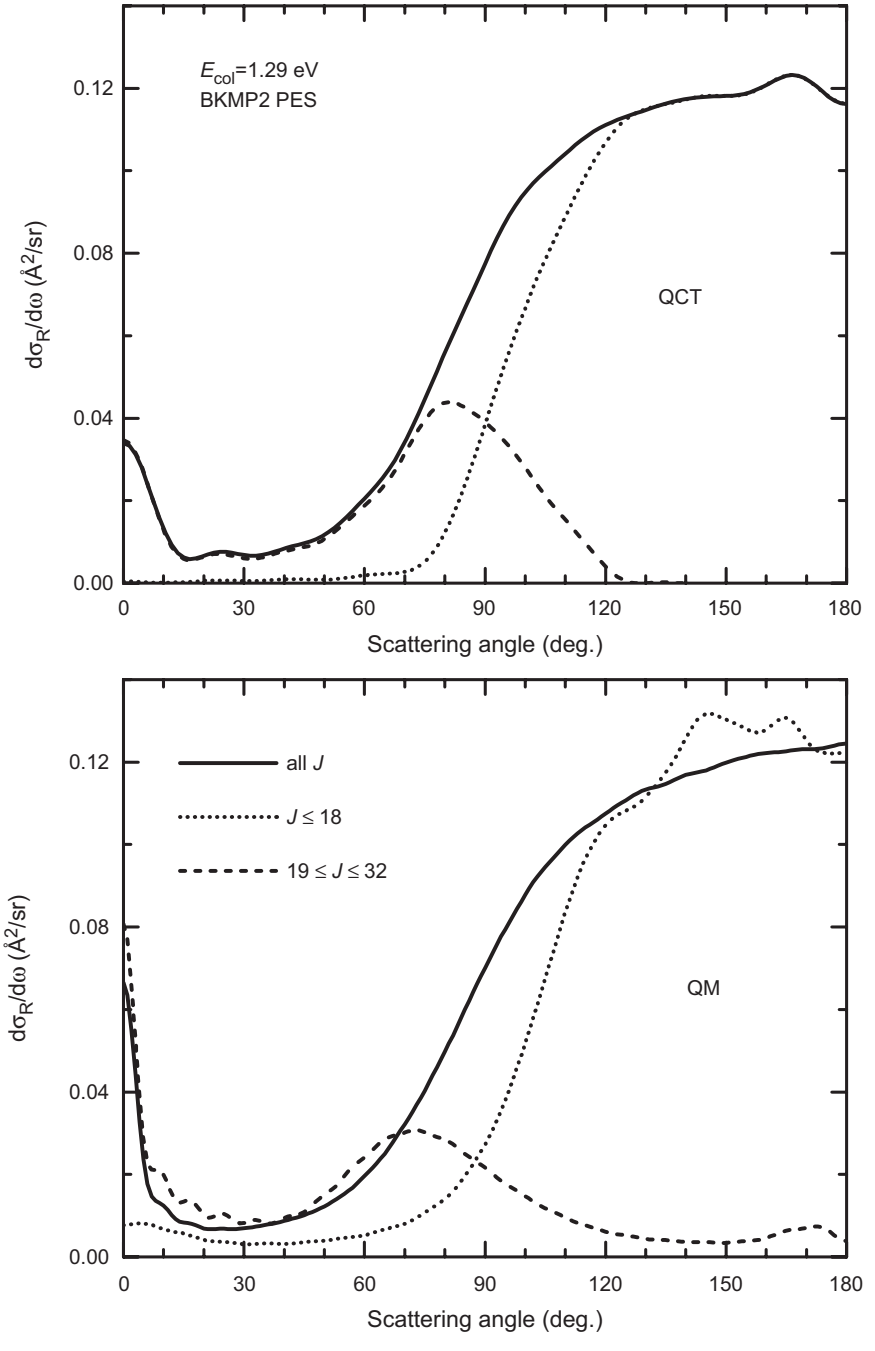

Figure 8. Vibrationally resolved DCS at collision energy 1.29 eV for the $H + D_2(v = 0, j = 0) \rightarrow HD(v' = 0) + D$ reaction showing the contributions of low and high values of the total angular momentum quantum number J. (Top) QCT results. (Bottom) QM calculations. Solid line: all J values. Long-dashed line: contribution from $19 \leq J \leq 28$. Short-dashed line: contribution from $J \leq 18$. Both sets of calculations performed on the BKMP2 PES [100].

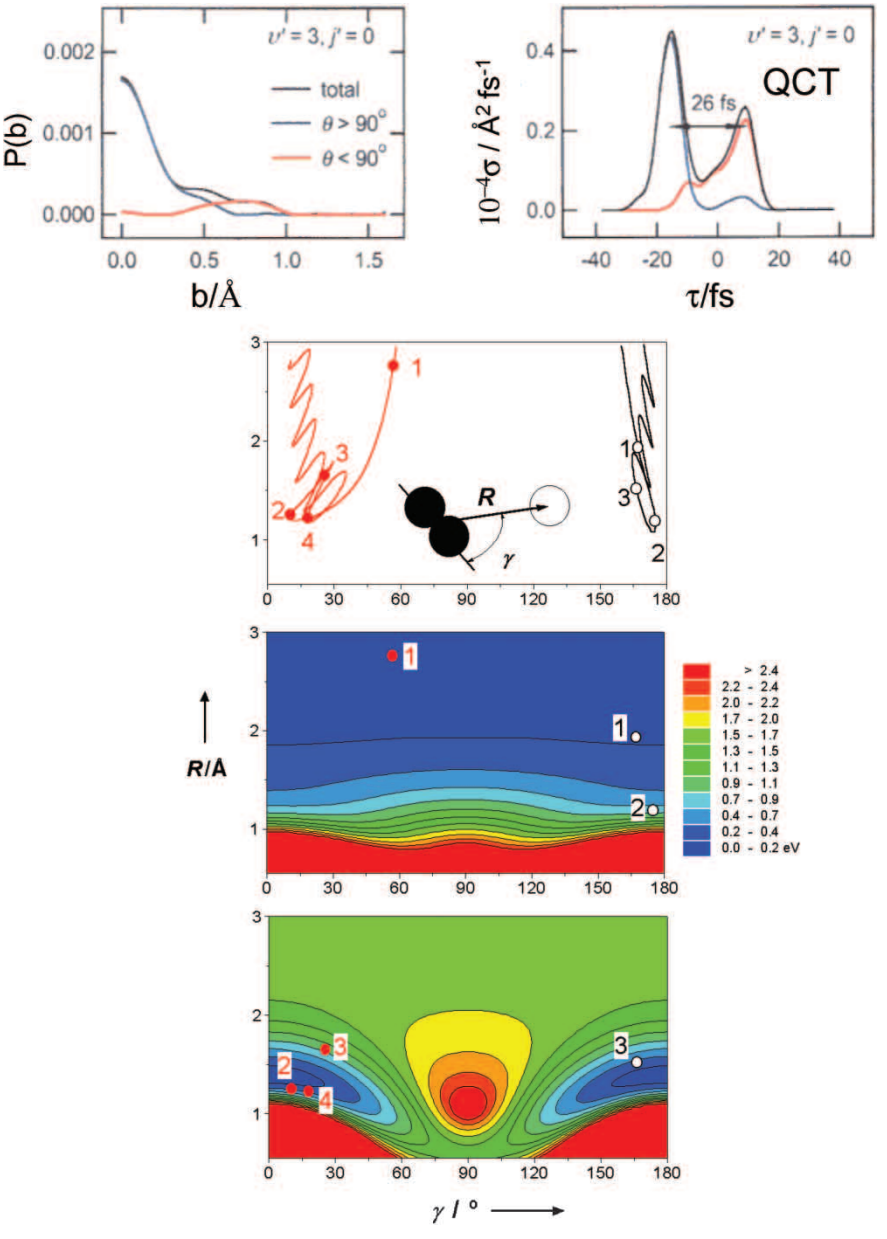

Figure 9. Top panels: QCT reaction probability $P(b)$ as a function of impact parameter b for all, backward and forward reactive trajectories for the $H + D_2(v = 0, j = 0) \rightarrow HD(v' = 3, j' = 0) + D$ reaction at 1.64 eV collision energy. The plot on the right shows the QCT reactive cross section as a function of time delay, τ, for all, backward and forward trajectories. Bottom: R–γ plots of typical indirect (red line on the left) and direct (black line on the right) trajectories. Middle and bottom panels correspond to potential energy contour plots of the BKMP2 PES with D_2 bond length fixed at 0.74 Å (middle plot) and 1.21 Å (bottom plot). The trajectory dots have been overlaid on the potential energy contours corresponding to the instantaneous D_2 bond length. The color scale shown applies to both the middle and bottom contour plots. Reprinted with permission from [106]. Copyright 2000 Wiley-VCH Verlag GmbH.

to a maximum that shifts to higher J values as the total energy increases. No rigorous time delay analysis was carried out in this work, but from the analysis of the reaction probabilities as a function of the total angular momentum and total energy, and assuming a Lorenztian function, it was estimated that the lifetime of the collision complexes would be of the order of 5–8 fs. In any case, this effect was considered to be of quantal nature.

However, shortly afterwards, it was shown that similar ridges were also obtained in QCT calculations [76]. A forward scattering peak was also present in the quasiclassical DCS at $E_{\mathrm{col}} \geq 0.9$ eV, although smaller in magnitude than the corresponding QM one, and also restricted to the lowest rotational states of the HD products. An analysis in terms of the collision time was carried out and it was found that forward scattering, or more generally, the scattering pertaining to the ridge, corresponded to trajectories which were longer lived than those yielding backward scattering. The collision time was defined as the time during which the radial energy, $1/2\mu\dot{\boldsymbol{R}}^2$, where $\mathbf{R}$ is the Jacobi vector joining the centre-of-mass of the diatom and the incoming atom, is lower than the potential energy [76]. While the three atoms stay together, the potential energy is perturbed with respect to that of the separate atom-diatom, and, for this particular reaction, it becomes larger than the radial energy. Specifically, the difference in collision time between forward and backward scattering at $E_{\mathrm{col}} = 1.0$ eV was of the order of 20 fs. This is substantially less than the rotational period of the triatom, but more than the collision time of the direct trajectories ($\approx$8 fs). In spite of the attractive quantal interpretation of the ridge scattering, and thus of the forward peak commented on above, it seemed that classical mechanics could account, at least partially, for this effect.

The possible formation of classical collision complexes for this system was considered by Muga and Levine [162], who demonstrated the existence of relatively long-lived complexes with positive time delays. However, the authors did not comment on the influence of these 'trapped' trajectories in the value of the cross section. Miller argued that if these trajectories affected the integral cross section, they should be also present in the QM calculations [26]. The difference between the 'trapped' trajectories just mentioned and those causing the ridge should be stressed. The former, with collision times above 40 fs, were also found in the QCT study commented on above [76]. However, these trajectories are not frequent enough to have a noticeable effect on the collision observables. Moreover, they are spread over the whole range of impact parameters and scattering angles. The ridge trajectories, on the contrary, span a well defined range of impact parameters and, at a high enough collision energies, they are the cause of the forward scattering for defined final rovibrational states.

The analysis of further calculations for the $H + D_2(v = 0,\ j = 0)$ reaction at $E_{\mathrm{col}} \geq 1.29$ eV [87] revealed that the classical forward scattering was also caused by the largest impact parameters (0.9–1.3 Å), which in terms of total angular momentum correspond to $J = 19$–28. The results shown in figure 8 using the BKMP2 PES are very similar to those obtained originally on the LSTH PES [87]. The analysis of the QM data yields similar results: forward scattering proceeds mainly from partial waves with $J > 18$. Partial waves from lower J also contribute to forward scattering via interferences with higher J values, but this contribution is relatively small and in part of negative nature. The net peak obtained in the QM calculations for $v' = 0$,

summed on all rotational states, is about twice in magnitude than that found in the classical calculations and more confined at angles near 0° [87].

Unfortunately, the high resolution Rydberg 'tagging' experiments carried out in Bielefeld [91, 92, 96] for this reaction at the same collision energy could not verify experimentally the appearance of this forward peak. Instrumental constraints in the molecular beam apparatus prevented the measurement of scattering at the LAB angles corresponding to $\theta \leq 40°$ in the CM frame. The first experimental evidence of the forward scattering for this and for any other isotopic variant of the H_3 reactive system had to wait until 2000, when Zare and co-workers, using state and velocity resolved REMPI with the *photoloc* technique [106], inferred the state resolved DCSs from a careful analysis of the TOF profiles of ions from the $HD(v' = 3, j')$ products of the $H + D_2$ reaction at 1.64 eV collision energy. Although the angular resolution of these experiments is significantly lower than that achieved in the Rydberg 'tagging' technique with cross molecular beams, the analysis of the TOF profiles can provide also the DCSs. In spite of the fact that the sensitivity for forward scattering is less than for backward scattering, peaks at the corresponding arrival time of forward products were clearly identified. The analysis showed that these features corresponded to large forward peaks in the CM DCS for the lowest j' states of the $HD(v' = 3)$ product and, most prominently, for $j' = 0$.

In this same work, QCT calculations carried out at the same collision energy [106] also predicted the existence of forward scattering for that particular state, although its magnitude was significantly smaller than that found experimentally. The analysis based on the time delays of the trajectories revealed that forward scattered trajectories had positive time delays, whereas those corresponding to backward scattering exhibited negative time delays. The classical time delay is defined as the time difference for collisions with and without the presence of a potential. For direct processes, the time delay is, in general, negative for direct collisions involving repulsive potentials. Positive values of the time delay are associated with longer lived trajectories in which the three atoms spend some time together before evolving to separate products. Strictly speaking, the time delay so defined is only meaningful for specific initial and final states and care should be exercised when the time delays of trajectories ending in different final states are compared [76]. In particular, for the reaction yielding $HD(v' = 3,\ j' = 0)$, the difference found between the most probable time delays for forward and backward scattering was $\approx$26 fs, as shown if figure 9. This time difference is considerably smaller than the time corresponding to the rotational period of the H–D–D complex, and cannot be attributed to a true 'long lived complex', whose lifetime is larger than the rotational period. The analysis of the motion of the trajectories giving rise to forward scattering indicated that the initial attack is mainly L-shaped, as shown schematically in the bottom panel of figure 9. As the atom continues to approach the molecule, the angle of attack changes towards collinearity. This is essentially due to the centrifugal energy associated with large impact parameters rather than to an orientational effect of the PES. This large conversion of radial energy into angular energy of the three atom system slows down the relative motion and causes the three atoms to spend together more time than for direct trajectories. During this period, the D_2 molecule has time to elongate its internuclear distance, and as a result of that, a well appears in the PES for the collinear configuration, further trapping

the trajectory. In this scenario, the formation of quasi-bound states giving rise to scattering resonances becomes plausible. It was argued that the difference in the magnitude of the forward peak between QCT and experiment could be caused by such resonances [106]. In contrast, in a typical back-scattered trajectory, characterized by small impact parameters, the atom approaches the diatom collinearly and hits it at a relatively small R value, without the D_2 molecules adjusting its internuclear distance. After the break of the D_2 bond, the HD molecule is formed and rebounds in the backward direction.

Subsequently, Althorpe, Zare and co-workers presented a combined theoretical and experimental study of DCSs for the $H + D_2 \rightarrow HD(v' = 3, j' = 0) + D$ reaction at collision energies in the range 1.39–1.85 eV [109]. QM calculations were carried out using a novel time dependent (TD) method developed by Althorpe, which allows the determination of final state resolved integral and differential cross sections [135]. The simulation of the experimental results using the calculated DCSs led to an excellent agreement with the measured TOF ion profiles. Shortly afterwards, TI QM calculations carried out by using the ABC code of [130] for a dense grid of energies spanning those reported in [109] were published [123]. The simulation of the experimental results, shown in figure 10 was practically identical to that obtained with the TD DCS (figure 1 of [109]), as expected considering the excellent agreement between the QM results obtained with the two different methodologies. The QCT simulation is also presented in figure 10 at the collision energy of 1.64 eV using the same scaling as the QM one. Forward scattering is also predicted by this calculation, but, as mentioned above, its magnitude is notably smaller. The agreement between the experimental TOF profiles and the TI QM simulations is also excellent for the various $HD(v' = 3, j')$ rotational states at 1.64 eV collision energy, as shown in figure 11.

The $HD(v' = 3, j' = 0) + D$ channel becomes open at a collision energy of $\approx$1.30 eV. Near this threshold, the DCS is backward. As the collision energy increases to the range 1.40–1.54 eV, the DCS becomes essentially sideways, as shown in figure 12. However, quite abruptly, at higher E_{col}, a sharp forward peak, which grows up with collision energy until $E_{col} = 1.9$ eV, dominates the DCS. Beyond this collision energy, the forward peak decreases. The oscillatory structure of the DCS at small scattering angles is also interesting. Other views of the collision energy dependence of the DCS can be found in the 3D representation shown in figure 13(a) and in figure 2 of [109] (in the latter, the DCS was multiplied by $\sin\theta$). In essence, what is observed is the evolution of a ridge, similar to those presented in [75, 76] and discussed above, for a particular rovibrational product state. Figure 10 clearly shows the appearance of the forward scattered wings at 1.54 eV, that become more prominent at 1.64 eV collision energy. The fact that its relative magnitude with respect to the central peak of the profiles decreases with collision energy between 1.64 eV and 1.85 eV is due to a reduction in the experimental sensitivity to forward scattering features [108], which, in any case, is perfectly reproduced in the theoretical simulations. Thus the progressive appearance and evolution of the outermost peaks in the TOF profiles constituted the first experimental evidence of the forward scattering for the H_3 reactive system, and by comparison with the theoretical results, of the ridge structure in the θ–E plane for the production of $HD(v' = 3, j' = 0)$.

Two important aspects must be considered in the quantal interpretation of the forward scattering. On the one hand, the analysis of forward scattering in terms of

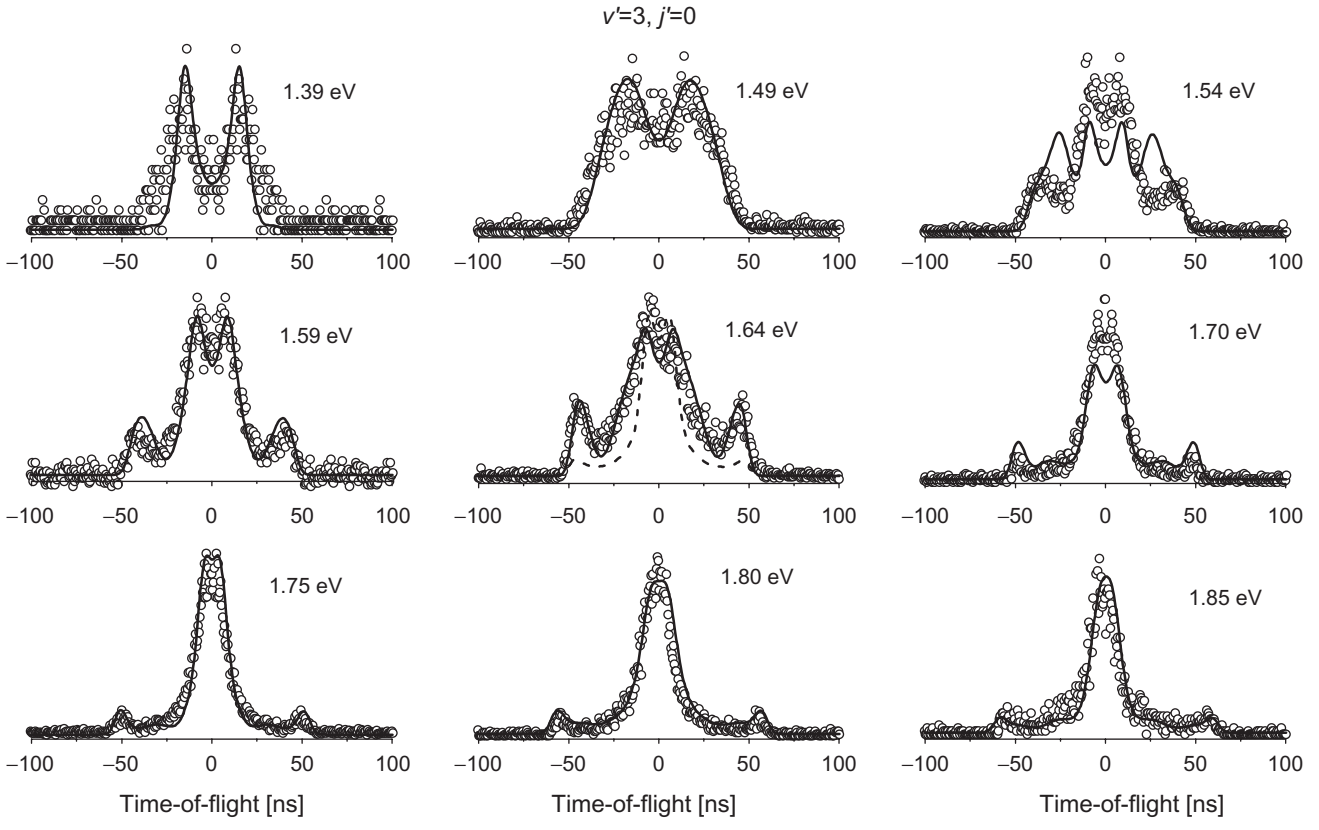

Figure 10. Experimental TOF profiles (open circles) and theoretical simulations (solid curves) based on the state-resolved QM DCSs shown in figure 12 for the $H + D_2(v = 0, j = 0) \rightarrow HD(v' = 3, j' = 0) + D$ reaction at the indicated collision energies. The data at 1.64 eV collision energy include the simulation based on the QCT DCS (dashed curve). The experimental and theoretical data are scaled to have the same area. Reprinted with permission from [123]. Copyright 2002 American Institute of Physics.

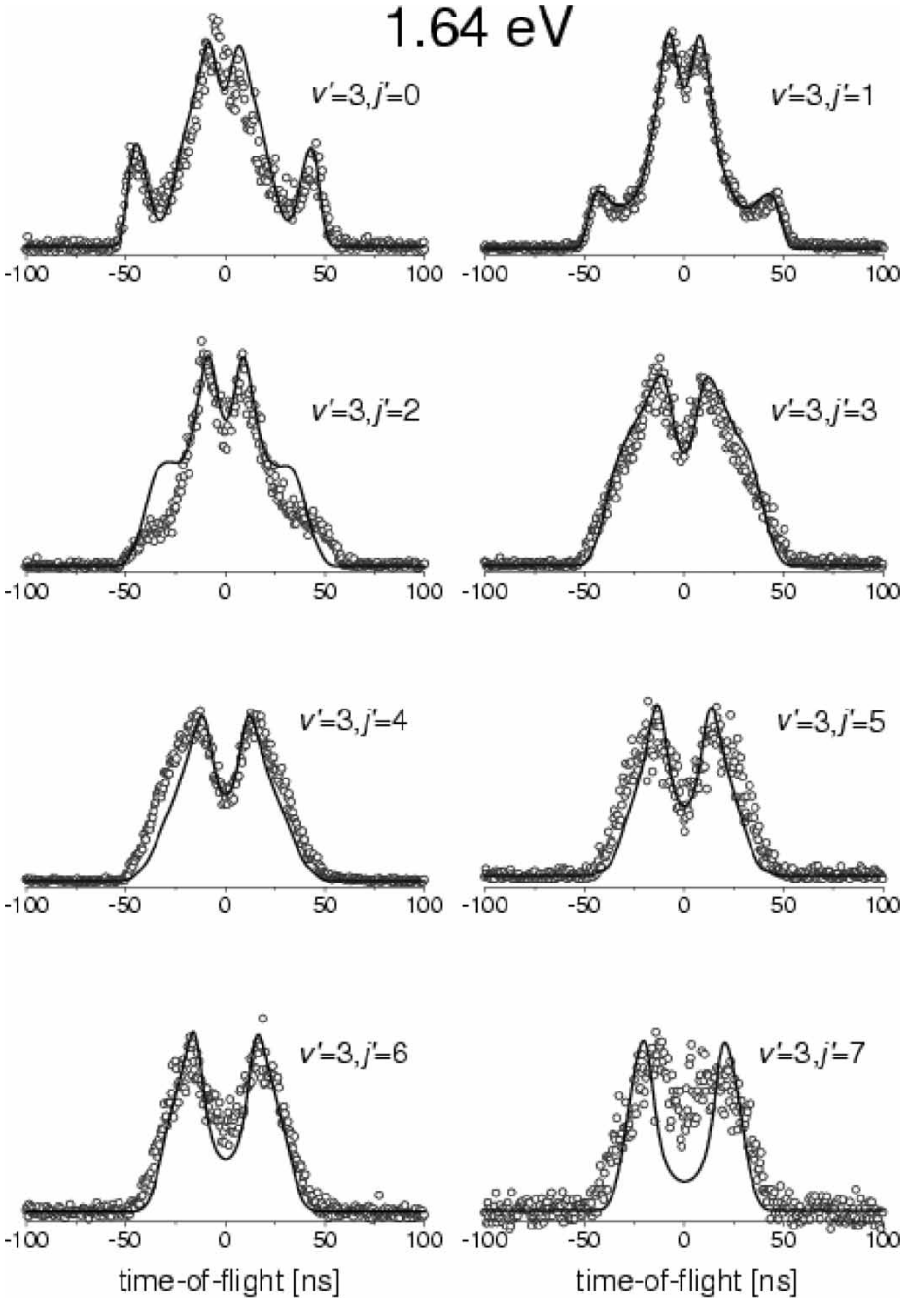

Figure 11. Experimental TOF profiles (open circles) and theoretical simulations (solid curves) based on the state-resolved QM DCSs for the $H + D_2(v = 0, j = 0) \rightarrow HD(v' = 3, j' = 0\text{–}7) + D$ reaction at 1.64 eV collision energy on the BKMP2 PES.

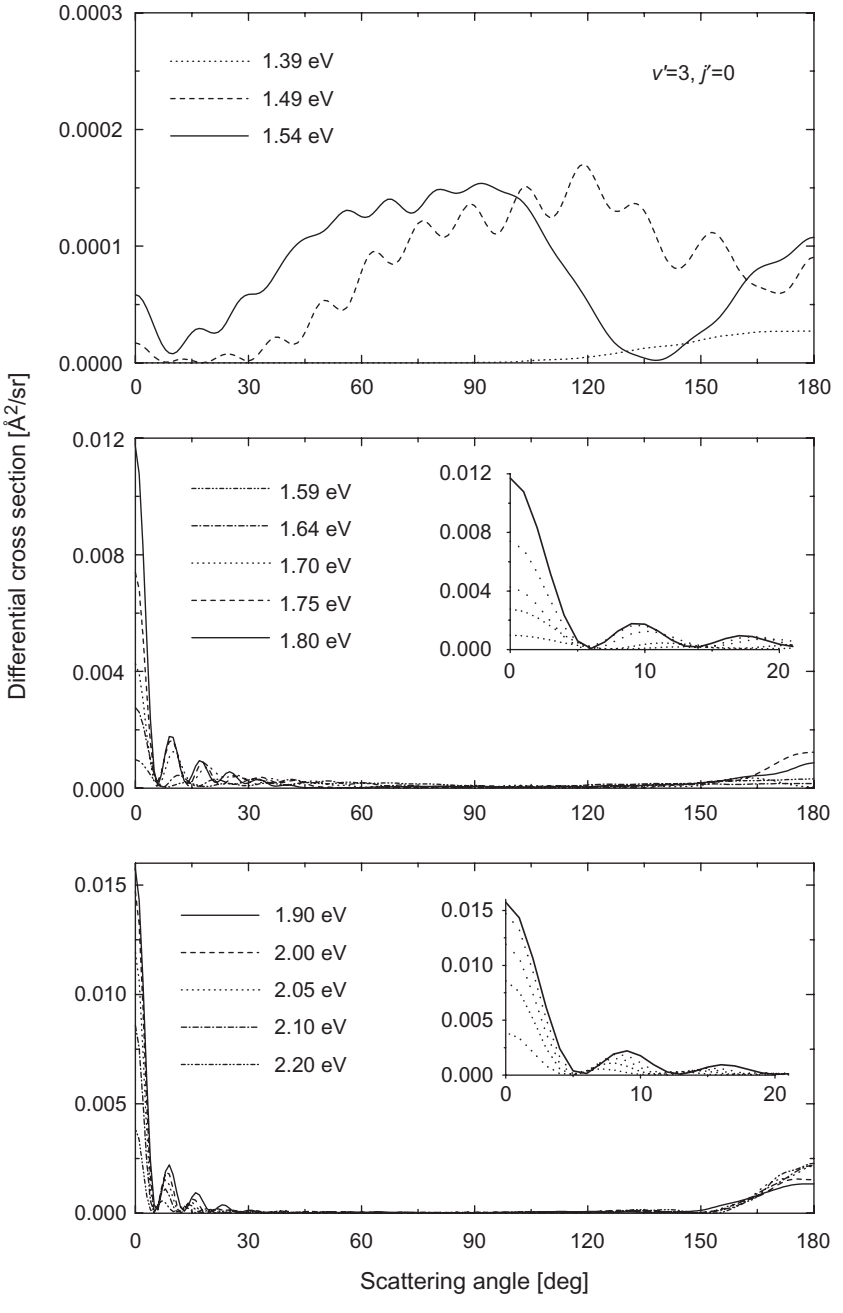

Figure 12. QM DCSs for the $H + D_2(v = 0, j = 0) \rightarrow HD(v' = 3, j' = 0) + D$ reaction as a function of collision energy in the range 1.39–2.20 eV calculated on the BKMP2 PES. Reprinted with permission from [123]. Copyright 2002 American Institute of Physics.

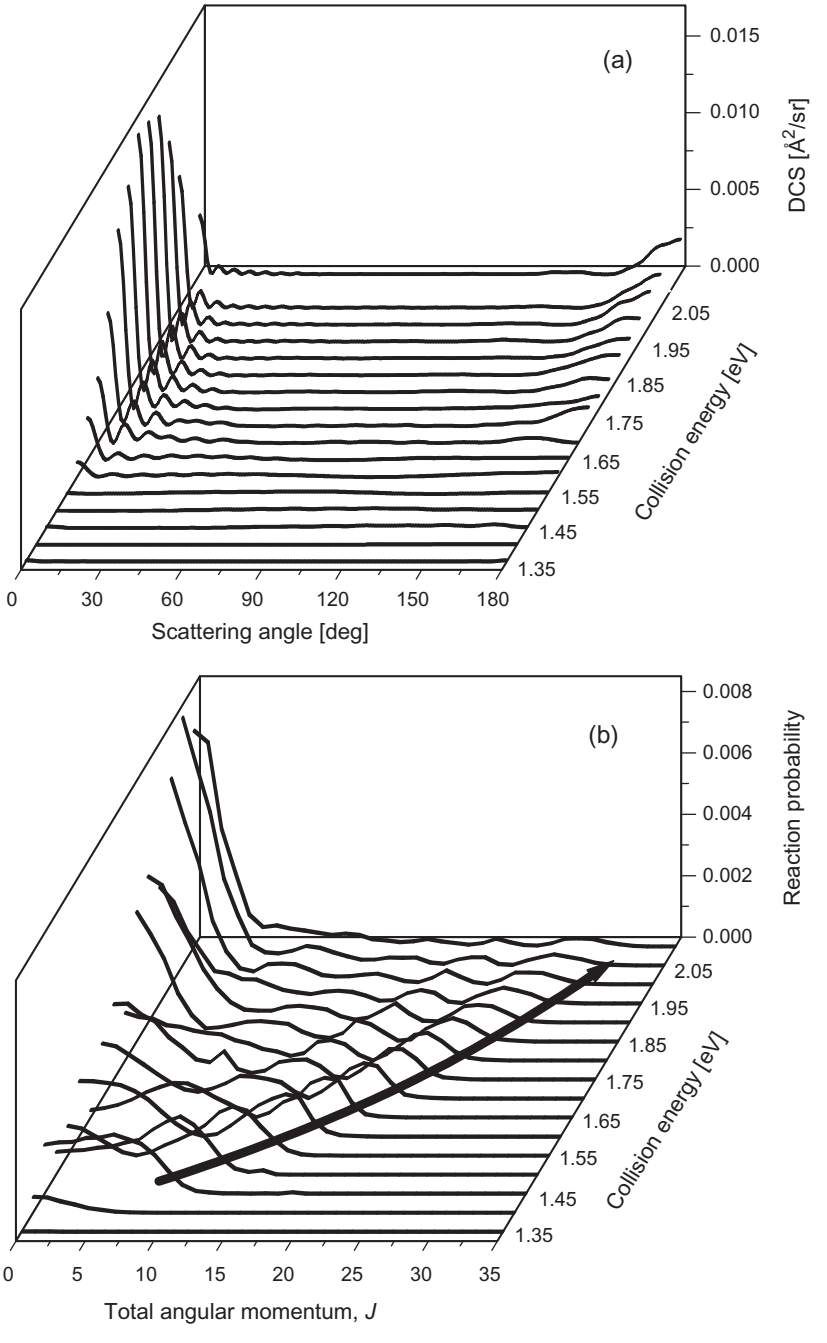

Figure 13. (a) Three dimensional perspective of the QM DCSs for the $H + D_2(v = 0, j = 0) \rightarrow HD(v' = 3, j' = 0) + D$ reaction as a function of collision energy in the range 1.35–2.20 eV calculated on the BKMP2 PES. (b) QM reaction probabilities as a function of total angular momentum J for the same reaction. The curve arrow indicates the outermost $E_{col} - J$ ridge. Reprinted with permission from [123]. Copyright 2002 American Institute of Physics.

the contribution of partial waves with different total angular momenta is supposed to contain valuable information. On the other hand, it is necessary to determine if forward scattering is associated with longer delay times as predicted by the QCT calculations [123].

The evolution of the state specific reaction probability into $v' = 3, j' = 0$ as a function of the total angular momentum and collision energy is shown in figure 13(b). The state-to-state reaction probabilities, $P_{v,j\to v',j'}(J;E)$, are calculated from the S matrix elements by the standard equation:

$$P_{v,j\to v',j'}(J;E) = \frac{1}{2\min(J,j)+1}\sum_{\alpha'\neq\alpha}\sum_{P}\sum_{K,K'}\left|S^{J,P}_{\alpha',v',j',K',\alpha,v,j,K}\right|^2, \tag{1}$$

where the sums run over the possible values of the reagent and products helicity quantum numbers, K, K', parities, and the reactive arrangement channels, α'. Representing the $P_{0,0\to v'=3,j'=0}(J;E_{\mathrm{col}})$, one can observe a series of ridges in the J–E_{col} plane (see figure 13(b)) which are the counterpart of those observed in the DCS. At $E_{\mathrm{col}} = 1.50$ eV the maximum in the $P_r(J)$ is not at $J = 0$, but shifted towards a value of $J \approx 9$, as shown in the lower panels of figure 14. With increasing collision energy, this maximum shifts further towards higher J, as indicated in figure 13(b) by a curved arrow. In addition, new subsidiary maxima appear at lower J values forming a nested ridge structure. The two panels of figure 14 show the evolution of the reaction probability with total energy, $P_r(E;J)$, and with total angular momentum, $P_r(J;E)$, respectively. Comparison with the corresponding QCT $P_r(J)$, shown in figure 14 for E_{col}=1.64 eV and 2.2 eV, reveals that in all cases the classical $P_r(J)$ peaks at $J = 0$ and no sharp maxima are found at higher J values. Interestingly, only at those collision energies above 2.0 eV, in which the forward peak in $v' = 3$ has declined, the shapes of the classical and quantal $P_r(J)$ become more similar. Thus, the existence of a sharp maximum in the opacity function is predominantly quantum mechanical in nature [123].

The analysis of the evolution of the state resolved DCS with the contribution of successive partial waves is shown in figure 15(a) at $E_{\mathrm{col}} = 1.64$ eV. Forward scattering only appears when the contributions of $J \geq 15$ are included. Actually, the magnitude of the scattering at $\theta = 0^\circ$, shown in figure 15(b), grows with J up to $J \approx 20$. The addition of larger Js does not contribute to the overall reactivity. At this collision energy, the main contributions to the forward peak are from $J = 18$–19. Clearly, the forward peak in the DCS and its magnitude is closely related to the existence of the peak observed in the specific reaction probability at the highest J, as it can be concluded by comparison of figure 15(b) and the reaction probability at this collision energy, shown in figure 14. Analogous behaviour has been found at the rest of collision energies investigated; namely, the forward peak is invariably due to the largest partial waves contributing to reaction [123].

These results are not limited to this particular ro-vibrational state or isotopic variant of the reaction. Kendrick carried out a comprehensive computational study [126] of the $H + D_2(v = 0\text{–}2, j) \to HD(v', j') + D$ on the BKMP2 PES. He found the same effect for HD formation into $v' = 0$–3 and $j' = 0$. Chao *et al.* [102] found the same behaviour for the $H + HD(v = 0, j = 0) \to H_2(v' = 0, 1,\ j' = 0, 1) + D$ reaction

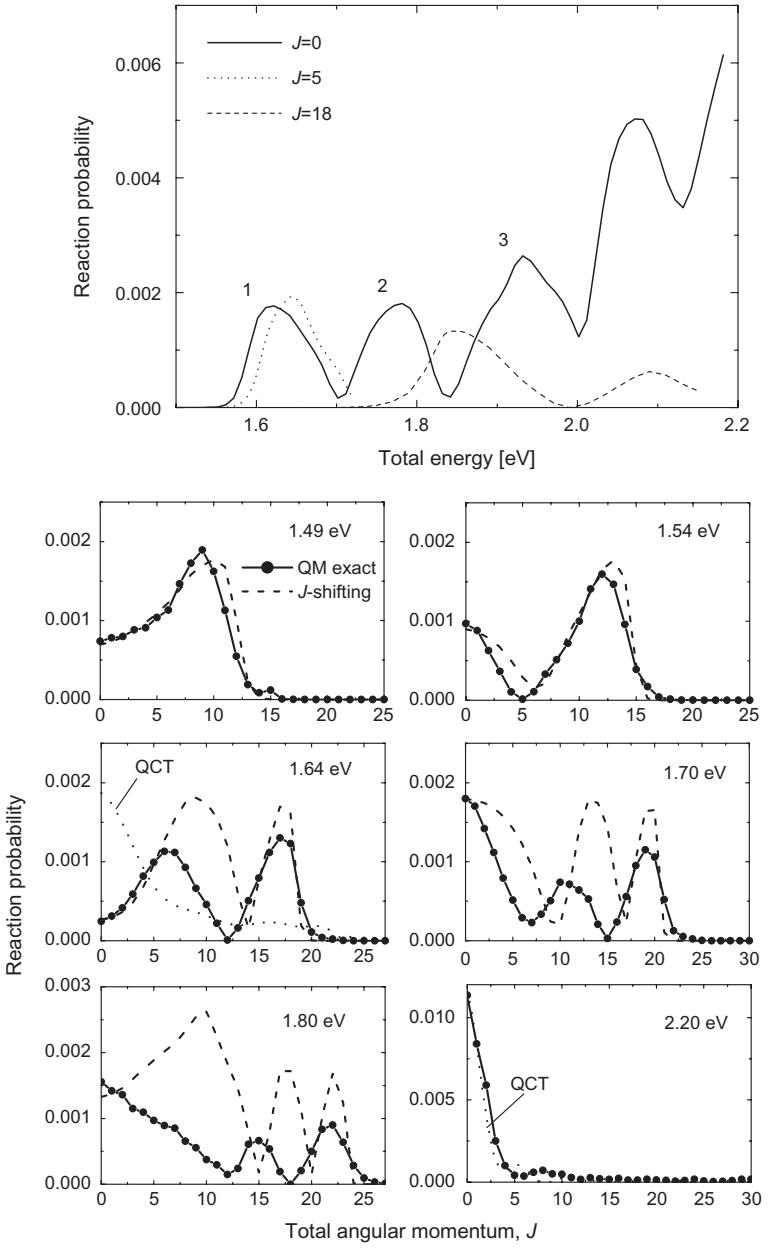

Figure 14. Top panel: QM reaction probability as a function of total energy at total angular momenta $J=0$, $J=5$ and $J=18$ for the $H+D_2(v=0, j=0) \rightarrow HD(v'=3, j'=0)+D$ reaction calculated on the BKMP2 PES. The labels correspond to the first three peaks in the reaction probability for $J=0$. Bottom panels: Reaction probability as a function of total angular momentum J at the indicated collision energies for the same reaction. Solid line with solid circles: exact QM calculation. Dashed line: results obtained by applying the J-shifting approximation to the data shown in the top panel of this figure. Dotted line in panels corresponding to 1.64 eV and 2.20 eV collision energies: QCT calculation. Reprinted with permission from [123]. Copyright 2002 American Institute of Physics.

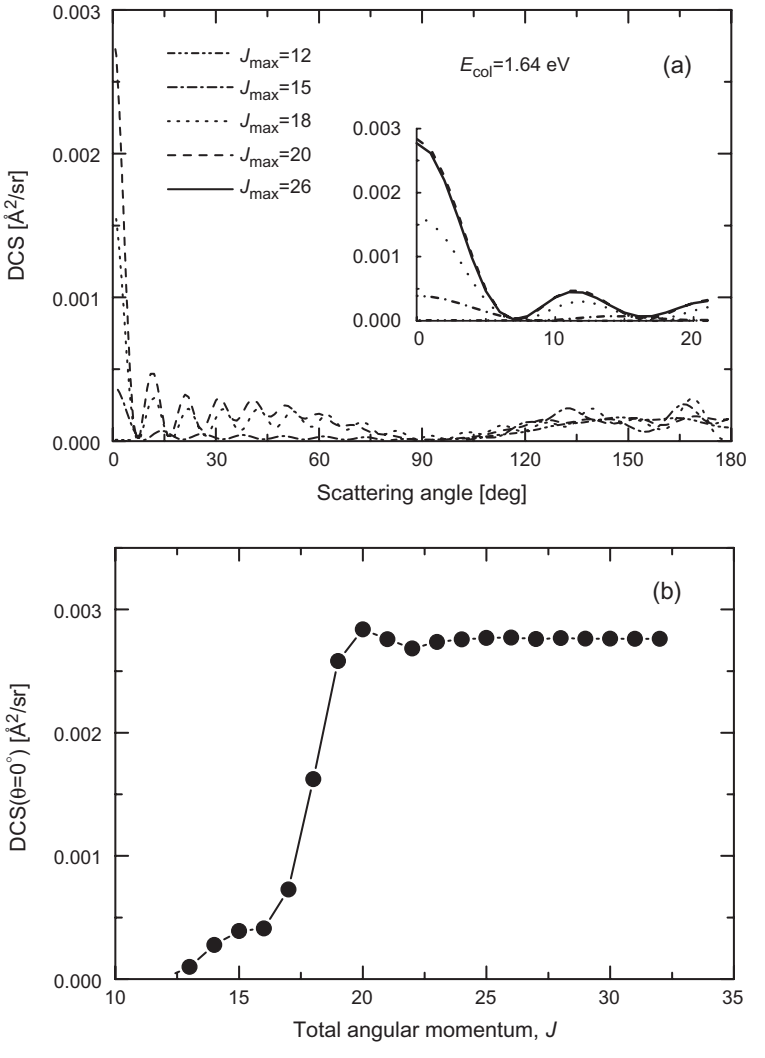

Figure 15. (a) QM DCSs for different values of J_{max}, the number of partial waves included in the calculation, for the $H + D_2(v = 0, j = 0) \rightarrow HD(v' = 3, j' = 0) + D$ reaction at 1.64 eV collision energy. (b) Evolution of the DCS at with J_{max} at 1.64 eV collision energy. Reprinted with permission from [123]. Copyright 2002 American Institute of Physics.

at $E_{col} = 1.20$ eV, as will be discussed in more detail afterwards. The fact that forward scattering is mainly caused by collisions implying the largest J (or largest impact parameters) is part of the common wisdom in reaction dynamics, and it is expected for direct abstraction reactions. For other types of reactions, as those proceeding by an insertion mechanism with a deep well, this is not the case, at least to the same extent.

The reaction probability into $v' = 3$, $j' = 0$ as a function of the total energy, $E = E_{col} + E_{int}^{v,j}$, for $J = 0$ has a remarkable oscillatory structure presenting a series of

successive maxima as shown in the upper panel of figure 14. The corresponding reaction probabilities, $P_r(E,J)$, for $J=5$ and 18 are also represented in this figure. The peak labelled as '1' in the $P_r(E,J=0)$ shifts to higher values of the total energy and broadens as J increases. A similar result was presented by Miller and Zhang for the $H+H_2$ reaction yielding products into $v'=0$ and $j'=1$ [75]. If these peaks in the reaction probability were due to a resonance, one can expect that their energies would vary with J as [75]

$$E_{\text{peak}}(J) \approx E_0 + B^{\ddagger}J(J+1), \tag{2}$$

where $B^{\ddagger}$ represents the 'rotational constant' of the activated complex, assumed to be a linear rotor, and E_0 is the energy of the peak at $J=0$. Consequently, the $P_r(J)$ at a given collision energy could be predicted within the J-shifting approximation using the $P_r(E;J=0)$ and the rotational constant obtained from the fit of the peak position of the $P_r(J)$ with the total energy for a given final state (actually, it was found that the best fit for the E_{peak} with J was a second degree polynomial in $J(J+1)$). With this approximation, the J-shifted $P_r(J;E)$ are given by

$$P_{v',j'}(J;E) = P_{v',j'}(J=0;E_J^{\ddagger}), \tag{3}$$

where $E_J^{\ddagger} = B^{\ddagger}J(J+1)$. The reconstructed $P_r(J)$ are shown in the bottom panels of figure 14, and compared with the exact reaction probabilities. In general terms, the J-shifted $P_r(J)$ reproduce quite well the magnitude and position of the peak at the highest J value, especially for the lowest energies shown. Nevertheless, at energies above 1.60 eV, the overall resemblance deteriorates rapidly and at 1.80–1.90 eV, where the forward peak is maximum, the agreement is rather poor [123].

Chao and Skodje carried out a similar analysis for several $v=0$, $j=0 \rightarrow v'=0$, j' transitions of the $H+D_2$ reaction at lower collision energies [129]. Pronounced oscillations were also found in the $P(E;J=0)$ for $v'=0,1$, $j'=0$. They fitted the position of the peaks found in the $P(E;J)$ as a function of J to equation (2). In general, they found that the peaks were poorly fitted by that equation, and moreover, that the value of $B^{\ddagger}$ changed substantially with the different transitions. In particular, for $v'=0$, $j'=0$ the rotational constant was found to be almost twice than that based on a harmonic analysis around the adiabatic barrier maximum for the transition state symmetric stretch and bending quantum numbers $v_{\text{ss}}=0$, $v_{\text{bend}}=0$ or with the rotational constant of 6.9 cm^{-1} that would characterize the collinear activated complex.

A very ingenious formulation of the TD QM methodology giving the time dependence of the differential cross section and thus providing a rigorous quantal description of the motion of the atoms during the reaction was presented in [109]. The plane wave packet (PWP) approach developed by Althorpe has been thoroughly reviewed recently [131] and only a brief comment will be included here. The basic idea is to describe the reagents by a plane wave, which contains a finite spread of energies, a situation analogous to that of a femtochemistry experiment. The initial separation of the reagents is also finite, chosen in such way that the interaction potential is negligible. The products are 'detected' at the equivalent distance, by projecting the time evolving wave packet

onto a fixed plane wave packet, which acts as a 'probe' packet. In contrast, in conventional scattering theory, the equivalent wave packet would have a fixed and well defined energy, and the initial wave packet would be prepared with the reagents separated by an asymptotically large distance. In this respect, the plane wave packet method is analogous to the classical trajectory calculations, except that all possible quantum effects (tunnelling, interferences, resonances, etc.) are naturally included. The PWP is a method of interpretation rather than a numerical method to solve the Schrödinger equation and as such complements standard TI and TD methods of analysis of the DCS. This methodology allows the investigation of the scattering of a wave packet into space following a two body collision and, thus, the determination of the DCS directly from the time evolution of a plane wave packet. Consequently, it becomes possible to establish not only at which angles the collision products are scattered, but also when are they scattered. In this way, a most valuable information about the mechanism of the collision process can be extracted.

The PWP method was first applied to the investigation of the $H + D_2 \rightarrow HD(v' = 3, j' = 0) + D$ reaction. One of the most salient results is presented in figure 16, as a series of successive snapshots that represent the spatial evolution of scattered products at different times [109, 136]. The spatial part of the initial wavefunction at time $t = 0$ is a PWP which describes the approach of the H atom to the D_2 molecule and consists of a superposition of time independent functions covering a range of collision energies from 1.33 to 2.2 eV with a flat distribution. In figure 16, the horizontal axis represents the H–DD relative distance, and R and θ correspond to the HD–D relative distance and the scattering angle, respectively. The contour lines represent the HD density. The propagation of the wavepacket is carried out using a recent methodology developed by Althorpe [135]. The DCSs are obtained at each time by projecting the wavepacket onto the 'probe' function that describes the $v' = 3$, $j' = 0$ state and are represented multiplied by $\sin\theta$ to account for the total (in and out of plane scattering) at each angle. For more details, the reader is referred to [131, 136].

At the earliest stages of the reaction, the scattering is purely backward, with the HD molecule ejected in the opposite direction of the incoming H atom, characteristic of a rebound, direct mechanism. At about 25 fs, when the backscattered products are already flying out, scattering at $\theta = 45^\circ$ starts to take place, and it is caused by large impact parameters. At longer times, forward scattering becomes neat and consolidates around $\theta = 0^\circ$. Overall, forward scattering is delayed by about 25 fs with respect to the direct backward scattering, in excellent agreement with the QCT predictions for the formation of this particular state of the reaction [106], and confirming that the ridge found in earlier calculations is caused by a delayed mechanism. In this respect, the main difference between the QCT and the rigorous QM calculations lies on the relative magnitude of the forward peak.

The time delay for $HD(v' = 3, j' = 0)$ formation has been also determined in [123] using TI calculations for specific J partial waves. According to Smith [163], the quantum time delay, $\Delta\tau_{ij}^J$, for a given $i \rightarrow j$ transition in terms of the scattering matrix element, S_{ij}^J is given by

$$\Delta\tau_{ij}^J = \mathrm{Re}\left[-i\hbar \frac{1}{S_{ij}^J} \frac{\mathrm{d}S_{ij}^J}{\mathrm{d}E}\right] \tag{4}$$

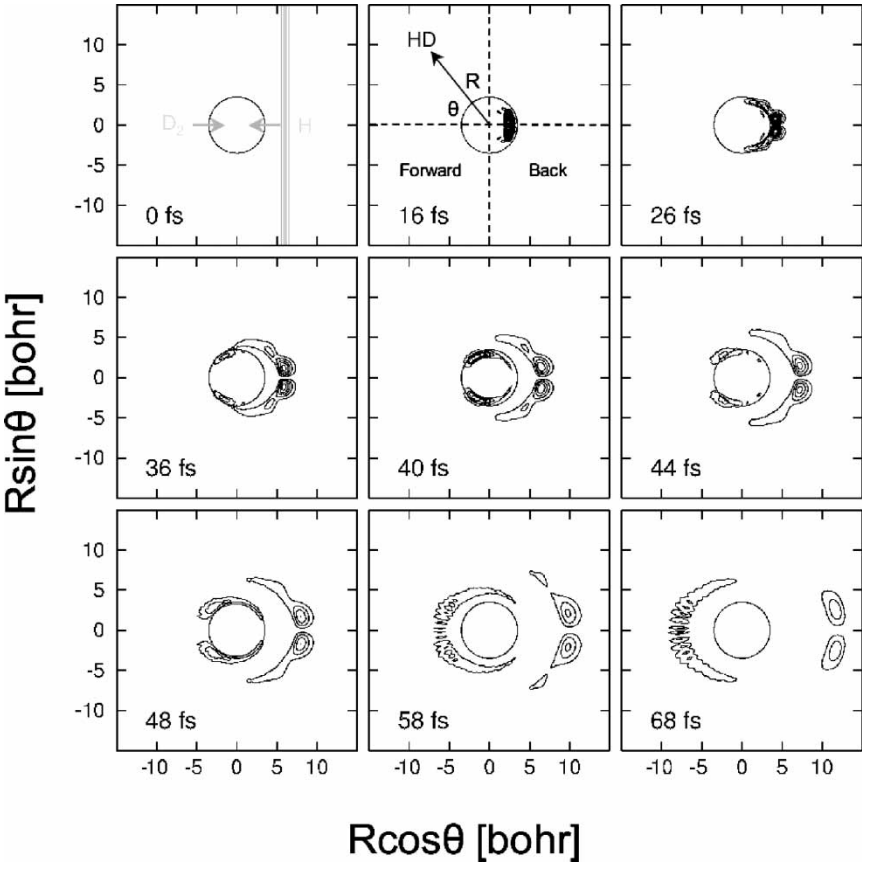

Figure 16. Snapshots from a plane wave packet description of the $H + D_2(v = 0, j = 0) \rightarrow HD(v' = 3, j' = 0) + D$ reaction. The contours at times $t > 0$ are obtained by projecting the wave packet onto the $HD(v' = 3, j' = 0)$ rovibrational wave function, taking the square modulus, and multiplying by $\sin\theta$. The contours at time $t = 0$ show the initial $H + D_2$ plane wave packet. The circles are of radius $R = 3.5$ au and give a rough indication of the extent of the transition state region. Two reaction mechanisms are visible separated by a time delay of about 25 fs. Reprinted with permission from [109]. Copyright 2002 Nature Publishing Group.

and measures the time that an outgoing wave function into channel j is delayed (positive $\Delta\tau_{ij}^J$) or advanced (negative $\Delta\tau_{ij}^J$) relative to a freely evolving wave packet at the same energy and total angular momentum. The calculation of the time delays were carried out for $J = 0$ at the total energy corresponding to the peak '1' in the $P(E; J = 0)$ (see top panel of figure 14). A value of -16 fs was obtained. The calculation for $J = 18$ corresponded to the same J-shifted peak, which appears at $E_{tot} \approx 1.85$ eV, and the time delay was found to be 12 fs. Since $J = 18$ is the J value which contributes more to the forward peak, the difference between the two time delays ($\approx$28 fs) is a measure of the time of appearance of forward scattering with respect to backward scattering. This value is in very good agreement with that reported by Althorpe *et al.* [109]. However, the advantage of the PWP method lies on the fact that it actually serves to generate pictorial albeit rigorous 'movies' of how the products are scattered in time

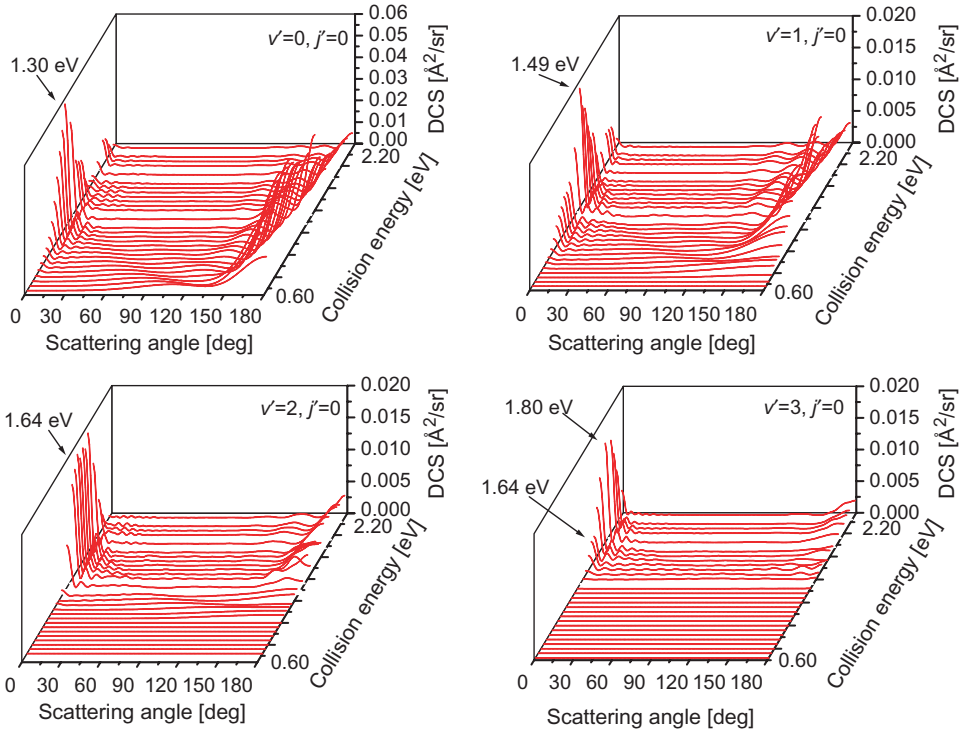

Figure 17. Three dimensional perspectives of the QM DCSs for the $H + D_2(v = 0, j = 0) \rightarrow HD(v' = 0\text{–}3, j' = 0) + D$ reactions as a function of collision energy in the range 0.60–2.20 eV calculated on the BKMP2 PES. The arrows indicate the collision energy at which the forward peak is maximum for every v' state of the product.

and space. The PWP approach constitutes a powerful method to interpret and elucidate reaction mechanisms, as it has been shown in other instances [164, 165]. Morevoer, as it will be shown in the next section, further analysis of the DCSs can be carried out by applying time and scattering filters to the scattering amplitudes.

The evolution of the DCS, and in particular of forward scattering for the different HD vibrational states ($v' = 0\text{–}3$) and $j' = 0$ is presented in figure 17, where the collision energies at which the forward peak is highest are indicated for each v' state. The similitude of the behaviour for the different vibrational states is remarkable, although there is a shift in collision energy as v' increases (see also figures 21–24 of [126]). Forward scattering seems to be transferred from one vibrational level to the following as collision energy increases. A similar effect is observed in the QCT calculations, as shown in figure 18, although the magnitude of the forward peak is considerably smaller in this case. Interestingly, at collision energies well above the maximum of the forward peak for each vibrational state, the magnitude and shape of the QM and QCT DCSs become more similar.

Shortly after the publication of the article by Althorpe *et al.* [109], Yang, Skodje and coworkers reported measurements and calculations of the state resolved DCS for the $H + HD(v = 0,\ j = 0) \rightarrow D + H_2(v', j')$ at 1.20 eV collision energy [102, 103].

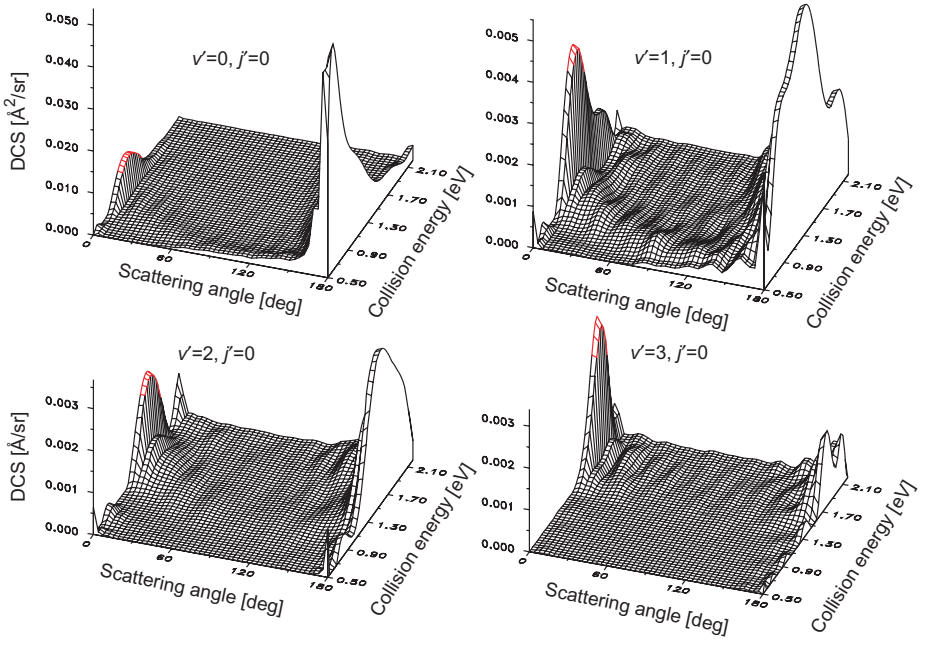

Figure 18. Same as in figure 17, but for the QCT DCSs.

The experiments were carried out in crossed molecular beams using the H-atom Rydberg 'tagging' technique developed by Welge and co-workers [92], but covering the whole angular range. The TOF spectra of the D atoms were measured at different laboratory angles and were then transformed into the CM frame. The excellent resolution achieved in this experiment allowed the clear identification of the different H_2 rovibrational states, and thus state-to-state DCS could be precisely measured. The comparison with TI QM calculations on the BKMP2 PES lead to an excellent agreement with minor differences, possibly due to experimental uncertainties at some particular angles and final states. As it could be expected, sharp forward peaks in the DCS were clearly discerned in $v' = 0$ and $j' = 0$–3. It must be remarked that no convolution with theoretical results was needed to extract the DCS in the CM frame. As in the case of the $H + D_2$ reaction, the analysis of the QM results showed that the forward peak for $v' = 0$ is dominated by few partial waves around $J = 25$. The analysis of the angle resolved time delays using the amplitude of scattering, $f_{ij}(\theta, E)$, can be expressed as [166]

$$\Delta\tau_{ij}(\theta, E) = -\hbar \frac{\mathrm{d}}{\mathrm{d}E} \mathrm{Arg}[f_{ij}(\theta, E)] \tag{5}$$

where Arg[f] is the phase of the complex function f. The results confirmed also in this case a delay of $\approx$20 fs in forward scattering with respect to backward scattering. The classical picture presented in [102] coincides essentially with that discussed above.

Basically, there is a slowing down due to the radial energy to centrifugal energy conversion associated with large impact parameters, which allows the rotation of the intermediate or short-lived complex and the ejection of the products in the forward direction. The quantal interpretation suggested in [103, 167] is based on the participation of quantized bottleneck states [167] corresponding to the stretch-bend excitations of the H–H–D complex. Using an approximate hamiltonian, centrifugally shifted in J, the spectral quantization method [168, 169] was applied and the corresponding probability density of the bottleneck wavefunction revealed that there are stretching and bending excitations. It was concluded that no clear Feshbach resonance state was present. The delay was rather due to a threshold effect, which causes a slowing down near the top of the barrier. We differ the implications and meaning of quantum bottleneck states to Section 5.

In summary, forward scattering in the $H + D_2$ reaction and the other isotopic variants of the H_3 reactive system appears only for low rotational states ($j' = 0$–2) in each vibrational manifold, and is associated with the largest impact parameters that give rise to reaction. The most interesting feature is that the mechanism that causes forward scattering is delayed with respect to the appearance of backward scattering. All these characteristics are predicted by both QM and QCT calculations, although the magnitude of forward scattering predicted by QM calculations, which is in excellent agreement with the experimental results, is considerably larger than the classical one. Whether forward scattering is or not associated to the existence of a resonance, or, at least, if there exists a genuine quantum effect which might be associated to this feature will be treated in the next section.

5. Resonances and interferences

The identification of resonances in the $H + D_2$ reaction, and in particular, the possible relationship of these resonances with the observed forward scattering has not yet been clarified in previous sections. Since the early days of development of quantum scattering theory, it was recognized that the presence of quantum bound states in the short lived complexes of the two colliding species should give rise to resonances, which would manifest as peaks in the energy dependence of cross section.

In particular, the intriguing, rather strong oscillations observed in the state resolved reaction probability as a function of the total energy have been traditionally associated with resonances without any definitive proof. These oscillations seem to survive in the specific integral cross sections, albeit for most of the final states are barely appreciable [126, 129]. Finally, oscillations have also been experimentally observed and corroborated by QM calculations in the backward scattering of the state resolved differential cross sections as a function of the collision energy and its interpretation has been the subject of several very recent works. In this section, after a short historical overview, we will discuss these findings and their possible interpretations.

As pointed out earlier [93, 129], theoretical simulations are necessary to establish if an experimental feature is in fact a manifestation of a resonance. The use of theory implies that the PES and the quantum dynamical calculations must be accurate enough to reproduce the experiment. Fortunately, for the H_3 reactive system and all its isotopic

variants, theoretical calculations have proved to be extremely accurate and able to reproduce even the finer details experimentally obtained. Calculations from various authors using different methodologies yield the same results, even for the most subtle details, and this is indeed most reassuring. Additionally, QCT calculations are always desirable to discern clearly which of the effects are purely of quantal nature or if they have a counterpart in the classical description of the dynamics.

Resonance behaviour in reaction dynamics has attracted much interest since the very beginning of the development of the field. It is out of the scope of the present review to discuss thoroughly the meaning and influence of resonances in chemical reactions. The subject has been recently discussed in [170]. Clear indications of the appearance of scattering resonances in chemical reactions came in the early 1970s with the first exact QM collinear calculations performed for the $H + H_2$ reaction by Truhlar and Kuppermann [171, 172]. In these calculations, the oscillations observed in the collision energy dependence of the total cross sections were attributed to the effect of interfering amplitudes for different semiclassical paths between reagents and products [172]. Independently, Levine and Wu [173] demonstrated the existence of resonances in reactive collisions from collinear close-coupling calculations for this same reaction. Levine and Wu showed that the resonances are due to a strong coupling between the relative motion along the reaction coordinate and the internal degrees of freedom of the triatomic complex. In subsequent works by Wu *et al.* [174–176], resonances were clearly observed when adiabatic potential wells along the reaction coordinate exist in the PES. Schatz and Kuppermann [177] analysed in detail the oscillations obtained in collinear calculations for the $H + H_2$ reaction in terms of scattering phase shifts, time delays and Argand diagrams (plots of the imaginary and real parts of the S matrix elements as a function of energy). They assigned these features to compound-state Feshbach resonances, a concept adopted from nuclear physics [178] and used for the first time in the context of reaction dynamics to denote quasibound states associated with a PES having no well but coupled to other states, such that the resulting 'adiabatic' potential may support bound levels. Later Schatz and Kuppermann [71] showed that 'resonance' peaks were reduced in magnitude but still persisted in 3D QM calculations at $J = 0, 1$.

Since the advent of exact, i.e. fully converged QM results, for the title reaction, it was found that the reaction probability for $J = 0$ as a function of the collision energy presented more or less pronounced oscillations that could not be reproduced by QCT calculations [76]. These oscillations have been generally attributed to resonance phenomena (see for instance, [75] and references therein, and more recently [126]). For the hydrogen exchange reaction, many QM calculations indicate that the possible scattering resonances are very broad (corresponding to short-lived quasibound complexes) and they were termed *elusive* for that reason [75]. It was expected that resonances would show up preferentially in state-resolved magnitudes measured as a function of energy.

As mentioned in the previous section, detailed calculations by Kendrick [126] and Chao and Skodje [129] have shown that the oscillations observed in the energy evolution of the reaction probability survive the summation over the angular momentum partial waves and appear in the converged state-to-state integral cross sections, especially at low j'. Therefore, one possible candidate for a resonance behaviour are these oscillations found in the state resolved integral cross section.

Interestingly, a small reminiscence of these oscillations seems to persist even in the initial state selected total reactive cross section, summed over all final states, for the $H + D_2(v = 0,\ j = 0, 1)$ reaction, as shown by the precise calculations of Sukiasyan and Meyer [133], and they were also attributed to transition state resonances without any further analysis. These oscillations are probably too small to be detectable in any experiment under the present state-of-the-art level of resolution.

In 2000, Kendrick *et al.* [124] reported the experimental observation of a resonance structure at the collision energy of 0.94 eV in the $H + D_2 \rightarrow HD(v' = 0, j' = 7) + D$, which show up as a broad peak of 0.1 eV width in the energy dependence of the $v' = 0, j' = 7$ state-resolved integral cross as a function of collision energy. The existence of this presumed resonance seemed to be supported by theoretical predictions based on accurate QM scattering calculations on the BKMP2 PES, including only the first seven partial waves, i.e. total angular momentum $J \leq 6$. In addition, a prominent peak near 0.94 eV was found in the backward scattering region. Even though the authors recognized that at least another 20 partial waves were needed to obtain fully converged results at collision energies up to 1.3 eV, they claimed that the qualitative shape of the pronounced resonance near 0.94 eV seemed to be independent of the number of partial waves included. This conclusion was reinforced by the apparent excellent agreement with the results of single molecular beam photon initiated experiments in which the HD products were detected state-selectively by $2 + 1$ REMPI [124]. However, the experiment had important limitations, given the rapid variation of the experimental sensitivity functions with scattering angle and its lack of sensitivity to backward scattering. Subsequent QM calculations on the BKMP2 PES performed by Aoiz *et al.* [122] at collision energies within the 0.6–1.3 eV range demonstrated, however, that no evidence of resonance structure is found once a fully converged ($J \leq 33$) calculation is carried out. This can be appreciated in the top panel of figure 19, where the QM excitation function for the $HD(v' = 0, j' = 7)$ channel of the $H + D_2$ reaction is represented for different maximum values J_{max} retained in the calculation. If only 7 partial waves are considered, the excitation function shows the narrow maximum attributed by Kendrick *et al.* to a resonance structure. However, as J_{max} increases, this feature in the excitation function washes out, and when convergence is reached, no narrow maximum is observed. The DCS (bottom panel of figure 19) also changes with growing J. For $J \leq 6$, the DCS is backward, but this character changes to a clear sideways peak for higher J. The absence of observable resonance features is reinforced by the agreement found between QM and QCT calculations as shown in figure 20, where a three dimensional representation of the QM and QCT DCS *vs.* collision energy is depicted. The same conclusion was reached by Chao and Skodje [129] and Kendrick [126] from well converged time-independent QM calculations.

In the early nineties Truhlar and co-workers introduced the concept of quantized dynamical bottlenecks [179–184] as quantized transition states associated to effective reaction barriers. These dynamical bottlenecks would control the flow of reactive flux from reactants to products and thus the chemical reactivity over the entire range of energies relevant to thermal rate constants up to a high temperature. The idea is rooted in the traditional transition state theory (TST), which considers the activated complex as an excited, activated molecule in route from reactants to products, precisely

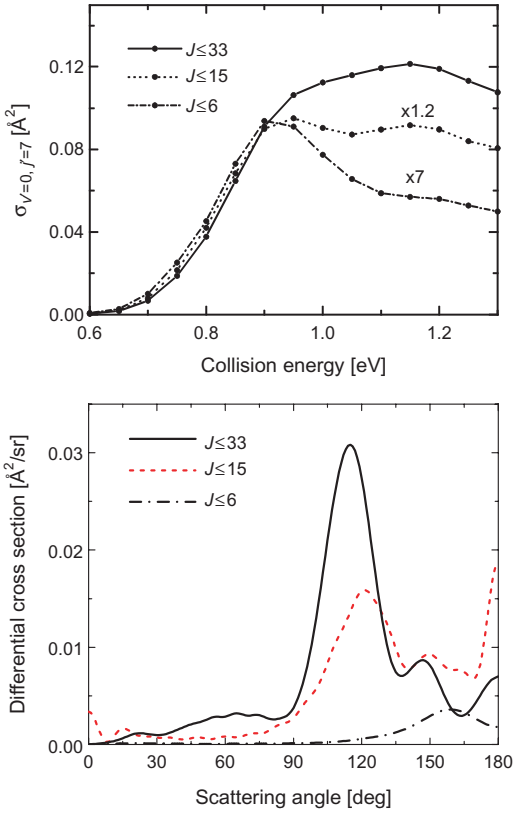

Figure 19. Top panel: QM state-resolved integral cross section as a function of collision energy in the range 0.6–1.3 eV for the $H + D_2(v = 0, j = 0) \rightarrow HD(v' = 0, j' = 7) + D$ reaction calculated on the BKMP2 PES. Solid line: fully converged QM calculation including $J \leq 33$. Dotted line: calculation including $J \leq 15$. Dot-dashed line: calculation including $J \leq 6$. Bottom panel: QM DCS for the same reaction at the collision energy of 1.3 eV. Solid line: fully converged QM calculation including the first 34 partial waves ($J \leq 33$). Dotted line: calculation including $J \leq 15$. Dot-dashed line: calculation including $J \leq 6$. Reprinted with permission from [122]. Copyright 2001 American Institute of Physics.

located at the top of the barrier. Those degrees of freedom of the activated complex orthogonal to the reaction coordinate, s, will posses a discrete spectrum of quantum levels corresponding to the bound motion of the complex at a fixed value of s, and hence the quantum states can be labelled by the quantum numbers for motion orthogonal to the reaction coordinate. In the variational version of the TST, the location of the activated complex is taken as that for which the density of states is minimal.

In the microcanonical formulation of the TST the key quantity for the determination of rate constants at a given total energy, $k(E)$, is the number of states of the activated complex $N^{\ddagger}(E)$, so that

$$k(E) = \frac{N^{\ddagger}(E)}{h\rho_R(E)} \tag{6}$$

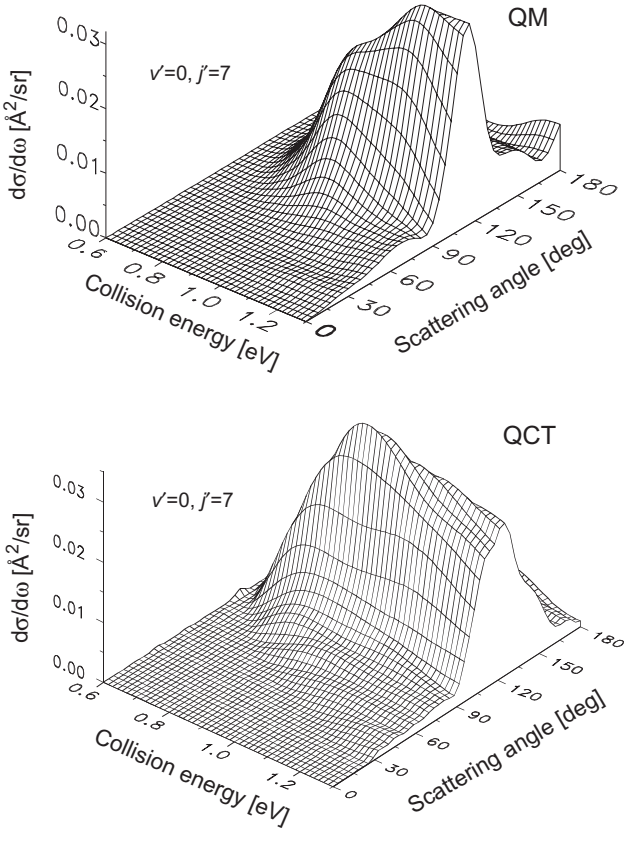

Figure 20. Three dimensional perspectives of the QM (top) and QCT (bottom) DCSs for the $H + D_2$ $(v = 0, j = 0) \rightarrow HD(v' = 0, j' = 7) + D$ reactions as a function of collision energy in the range 0.60–1.3 eV calculated on the BKMP2 PES. Top panel reprinted with permission from [122]. Copyright 2001 American Institute of Physics.

where $\rho_R(E)$ is the density of states of the reactants per unit volume per unit energy and h is Planck's constant. The total number of states can be decomposed further in the number of states of the activated complex at given total angular momentum J, $N^{\ddagger}(E; J)$, which accounts for the different values of J that participate in the reaction.

Similarly, in the exact theory of bimolecular reactions, the cumulative reaction probability at a given total energy and total angular momentum is defined as

$$N_r(E, J) = \sum_n \sum_{n'} P_{n \rightarrow n'}(E, J), \tag{7}$$

where $P_{n \rightarrow n'}(E, J)$ is the state-to-state, $v, j, K \rightarrow v', j', K'$, reaction probability at fixed values of E and J. The microcanonical rate constant is given by

$$k(E; J) = \frac{N_r(E, J)}{h\rho_R(E)} \tag{8}$$

and the total energy dependent rate is

$$k(E) = \sum_J (2J+1)k(E;J) \tag{9}$$

which is analogous to that obtained in TST. As discussed thoroughly in [184], the two formulations are equivalent and the number of states of the transition state can be directly compared with the cumulative reaction probability. In fact, if TST were an accurate description of the quantum dynamics, the $N_r(E;J)$ would increase in stepwise unit increments at the energy levels of the activated complex and the transition state would be an ideal dynamical bottleneck without recrossing. Chatfield *et al.* [184] used the exact $N_r(E;J=0)$ calculated for the $D+H_2$ reaction on the LSTH PES and fitted the results to a relatively simple model based on a inverted parabolic barrier with an adjustable transmission coefficient to account for recrossing. The density of reactive states, that is, the derivative of the cumulative reaction probability with respect to the energy, shows pronounced peaks that were assigned to quantized transition state levels, i.e. quantum bottlenecks, labelled by a set of three quantum numbers, stretching, bending and vibrational angular momentum, $[v_{ss}, v^{\Omega}_{bend}]$ for a linear molecule. Even though the peaks for the density of reactive states for higher J are progressively broader as more states become allowed, some of the states for angular momenta as high as $J=9$ could be clearly assigned. The results obtained by Skodje and Yang [167] on the BKMP2 PES for the same reaction were practically the same as those by Chatfield *et al.* [184]. The analysis can be extended to more detailed quantities as the initial state selected reaction probability and the specific reaction probabilities by summing the state-to-sate reaction probability in n' and n, respectively, and conclusions can be extracted with regard to the influence of the transition states on the state-selected and state-specific reactivity [184].

As pointed out by Skodje and Yang [167], the crucial question is whether the discrete spectrum of quantum states of an activated complex influences the detailed dynamics of a chemical reaction down to the level of state specific DCS, or in other words, which can be the experimental observables sensitive to the quantization of the activated complex. Any dynamic observable in a bimolecular reaction is necessarily subject to an average over a range of impact parameters or total angular momenta. The shorter this range the more likely the experimental observation of bottlenecks. It was shown in the previous section that the forward peak was caused mainly by a relatively small set of J, and that the time delays for these J coincide nicely with those obtained for the forward peak.

Allison *et al.* [185] in an attempt to explain some of the observations on the $H+D_2 \rightarrow HD(v'=3,\ j'=0)+D$ reaction studied by Zare and coworkers [106] at 1.64 eV, developed a locally adiabatic vibrational model. Their analysis concluded that a 'barrier resonance' was present in the DH–H exit valley at $E_{col}=1.64$ eV and $J=21$. In this terminology, a barrier resonance is associated with a barrier height and thus a quantum bottleneck of the transition state in the exit barrier of the vibrationally adiabatic potential. The classical analog of these barrier resonances would be a slow-down of the particle at the top of the barrier. As commented on in the previous

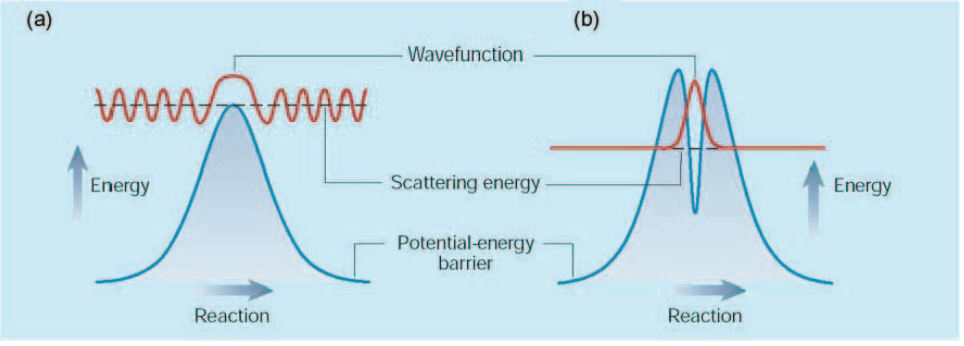

Figure 21. (a) Threshold effect: the scattering energy (dashed line) coincides with the top of a potential energy barrier; crossing this 'threshold' causes the reactants to slow down and leads to the increased amplitude in the QM wavefunction at the barrier maximum. (b) Resonance effect: a 'quasi-bound' quantum state exists in the well between the double maxima of a potential energy barrier. Reprinted with permission from [190]. Copyright 2002 Nature Publishing Group.

section, Skodje, Yang and coworkers [103, 167] reached the same conclusion with regard to the forward peak in the H + HD reaction into $v' = 0$, $j' = 0$ products. Using a more refined analysis based on spectral quantization methods, they identified a quantized bottleneck in the theoretical spectrum at 1.20 eV collision energy, and it was characterized as a mixed state corresponding to the adiabatic barrier states (v_{ss}, v_{bend}) (1, 0) and (0, 2) which appear for $J = 25$. Although the resulting wavefunction presents one node in the symmetric stretch and two nodes in the bending, it was found to be delocalized along the reaction coordinate.

At this point, it is convenient to distinguish between a Feshbach resonance and a barrier bottleneck, which in the terminology of Truhlar and coworkers is called 'barrier resonance' [186–189]. Whether the latter can be identified as 'true' resonances is a matter of debate. The subject has been treated by Manolopoulos in a enlightening note [190] prologuing the article by Harich *et al.* [103].

Feshbach resonances are associated with trapping in a well of an effective potential (see the right part of figure 21); for instance a vibrationally adiabatic potential. The existence of quasibound states causes the probability density of the wavefunction to show peaks near the turning points of the wells [185]. Obviously, the trapping causes a time delay associated to the decay of the quasibound state into reaction products, and might be very significant. The analysis of a Feshbach resonance in the energy complex plane [178, 186] is expected to show a neat and fairly isolated pole close to the real axis. It should be pointed out that there is no classical analogue of this effect. In addition, the spectral quantization should indicate a clear localization of the wavefunction not only in the transverse modes but also along the reaction coordinate. Thus far, the only case for which a clear Feshbach resonance has been found experimentally and identified theoretically in chemical reactive scattering corresponds to the F + HD → HF + D reaction at collision energies below the barrier for reaction. In this region no classical scattering takes place, and in the absence of direct scattering the identification of an isolated resonance was possible [187, 188]. The analysis carried

out by Althorpe on the F + HD reaction using PWP [164, 165] could isolate resonance scattering and determine its evolution in time, finding that the decay of the quasibound state can take as long as 1.5 ps. This does not mean that scattering resonances cannot take place in other reactions already calculated by accurate QM methods. Candidates are, for instance, Li + HF and some insertion reactions as $C(^1D) + H_2$. Unfortunately, in most of these cases, direct scattering competes with resonance scattering and the isolation of these resonances is not so clear since the dynamical observables become too blurred to be measured.

The barrier quantum bottlenecks (or threshold barriers or barrier resonances, depending on the authors) have a different nature. To begin with, no well in the effective potential is needed for the existence of these bottlenecks, as illustrated in the left part of figure 21, but they can also be associated to the barriers limiting a potential well [185]. There is a clear classical analogue in the slowing down of the reactants as they pass over the barrier. In QM this is reflected by an increase in the wavefunction amplitude, and hence an increase in the probability of finding the system in the region of the barrier. The associated time delay is likely to coincide with that found classically. However, the wave function still has a considerable amplitude away from the barrier, and is therefore not localized along the reaction coordinate. Finally, the analysis of the complex energy is likely to show a string of poles rather than a single pole [185]. In principle, the transition from a barrier bottleneck to a Feshbach resonance could take place by varying the PES shape as shown by Friedman and Truhlar [189]. However, other authors [190, 191] claim that the situation is mathematically different for the two types of 'resonances' and that they should not be considered as the same physical phenomenon.

In summary, all authors agree at this point that the forward scattering in the $H + D_2$ (or that of other isotopic variants) is not a Feshbach resonance. If we restrict the term resonances to those associated with wells (either 'shape' or 'Feshbach') [186], the forward peak for the title reaction is not a resonance. Certainly is not a pure quantum effect, since is also found in QCT calculations. Whether it is mainly a quantum effect with a classical counterpart or a classical one enhanced in QM is probably a matter of opinion.

In the calculations of Miller and Zhang [75], oscillations in the backward scattering appeared when the state resolved DCS were plotted as a function of the collision energy. Little attention was paid to this phenomenon. Successive calculations for the various isotopic variants of this reaction confirmed their presence. In particular, for the $H + D_2 \rightarrow HD(v' = 3, j' = 0) + D$ reaction these oscillations were found in the TD QM by Althorpe [136]. A first, interesting investigation of this effect was given by Althorpe [136] and its summary is portrayed in figure 22. At the top of the figure, the DCS multiplied by $\sin\theta$ is represented as a function of the collision energy for this particular final state. Apart from the evolution of forward scattering, discussed in the previous section, broad oscillations in the backward region are apparent. The $d\sigma(\theta, E)/d\omega$ was derived by the Fourier transform of the amplitude of scattering as a function of θ and t, whose square gives the $d\sigma(\theta, t)/d\omega$, represented in the middle panel of figure 22. An inspection of this figure shows two distinct regions. The first one, to the left side of the cut line, corresponds to short scattering times and is confined in the backward region. To the right of this line delayed forward scattering

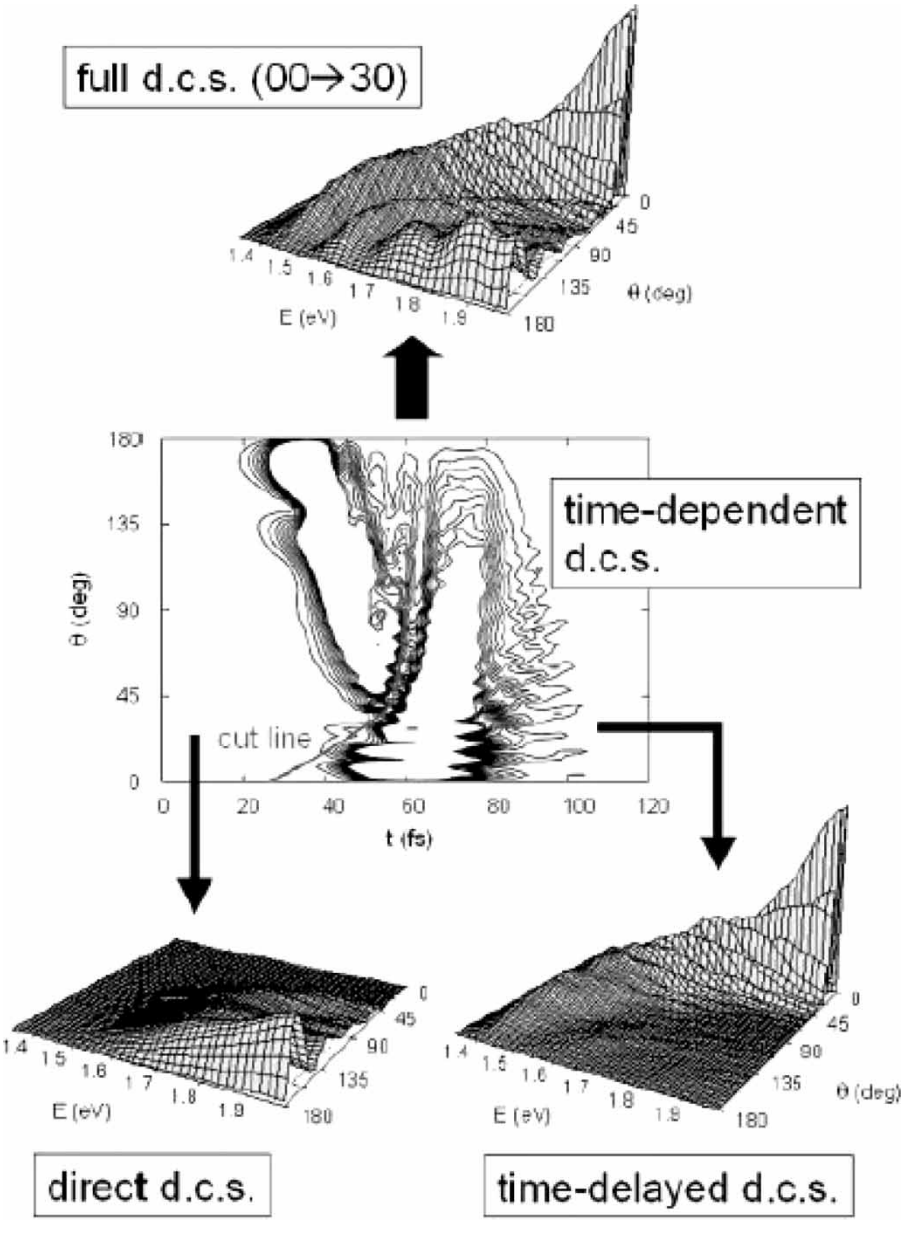

Figure 22. Illustration of the use of time filters within the PWP approach to analyze the state-to-state DCS corresponding to the $H + D_2(v = 0, j = 0) \rightarrow HD(v' = 3, j' = 0) + D$ reaction. The central plot corresponds to the time-dependent DCS multiplied by a factor of $\sin\theta$ and shows clearly the backward-scattered tail of the time-delayed mechanism. Time filters are applied to the left and right of the cut-line, to produce separate cross sections for the direct and time-delayed mechanisms (bottom panel). In the top panel, the series of humps visible in the backward direction along the energy axis come from the time-delayed mechanism and are magnified approximately sevenfold by QM interference with the direct mechanism. Reprinted with permission from [136]. Copyright 2002 American Institute of Physics.

appears, but is not entirely confined in the forward hemisphere and extends as a tail to the backward region at longer times. Then, Althorpe applied two time filters to recover from the time dependent DCS the energy dependent DCS corresponding to the left and right sides of the separating line, and the results are shown in the bottom panel of figure 22. The DCS corresponding to shorter times is purely backward without oscillations, whereas that from longer times contains the ridge and the forward scattering. There are also some humps in the backward region but they are too small to be clearly appreciated. These would be the DCSs obtained if the two mechanisms were operating independently without interfering with each other. The comparison with the full DCS, shown in the top panel of figure 22, reveals that interference between the two mechanisms produces large effects, manifested as a series of oscillations in the backward direction along the energy axis, which are completely absent in the DCS corresponding to the direct mechanism. The conclusion was that quantum interference with the direct mechanism amplifies the oscillations by an order of magnitude. Moreover, it is because of the interference that the oscillations are so pronounced as to be experimentally detectable.

Shortly afterwards, Dai *et al.* [104] carried out measurements of the state-to-state differential cross section as a function of collision energy at a particular scattering angle for $H + D_2(v=0,\ j=0) \rightarrow HD(v'=0,\ j'=2) + D$. Actually, the D atom TOF spectrum was measured at 19 energies in the range 0.4–1.0 eV at the same laboratory angle, chosen so that it corresponds to CM angles around $\theta = 160^\circ$. Clear oscillations were found as a function of the collision energy that were very well acounted for by QM calculations on the BKMP2 PES, as shown in figure 23.

Skodje, Yang and coworkers [104, 167] provided an explanation to these oscillations. They argued that measuring backward scattering products is equivalent to proba relatively reduced range of low impact parameters. The oscillations in the DCS would be the consequence of the oscillations found in the reaction probability $P_{n\rightarrow n'}(E, J)$ for low J values, whose origin can be traced back to the quantum bottleneck states (QBS), which clearly show up in the analysis of the derivative of the cumulative reaction probability by Truhlar and coworkers [179, 180, 184]. The oscillations could be explained by using a schematic picture represented in the bottom panel of figure 23. A series of adiabatic potential curves correlate initial and final rovibrational states along the reaction coordinate. Near the barrier, these curves become more widely spaced as the rotational levels correlate with bendings of the transition state. However, before and after the transition state, there may be an appreciable vibrationally non-adiabatic coupling, and the incident and outgoing flux can be redistributed among several reagent or product channels. Consequently, several quantum bottlenecks control the reactive flux as it passes the transition state. The final state-to-state reaction probability is affected by a number of QBS pathways, and will be the result of a coherent superposition of amplitudes, each from a different pathway. Since the cumulative reaction probability is an incoherent sum of scattering amplitudes, the effects of the coupling in the entrance and exit channel are averaged out, and the steps are only governed by the quantum levels of the transition state. This will not be the case in the state-to-state reaction probability or in the DCS. Within this picture, the interferences observed by Althorpe [136] giving rise to the oscillation in the backward scattering would correspond to interferences from a series of bottlenecks mixed by couplings in the reagent and exit valleys.

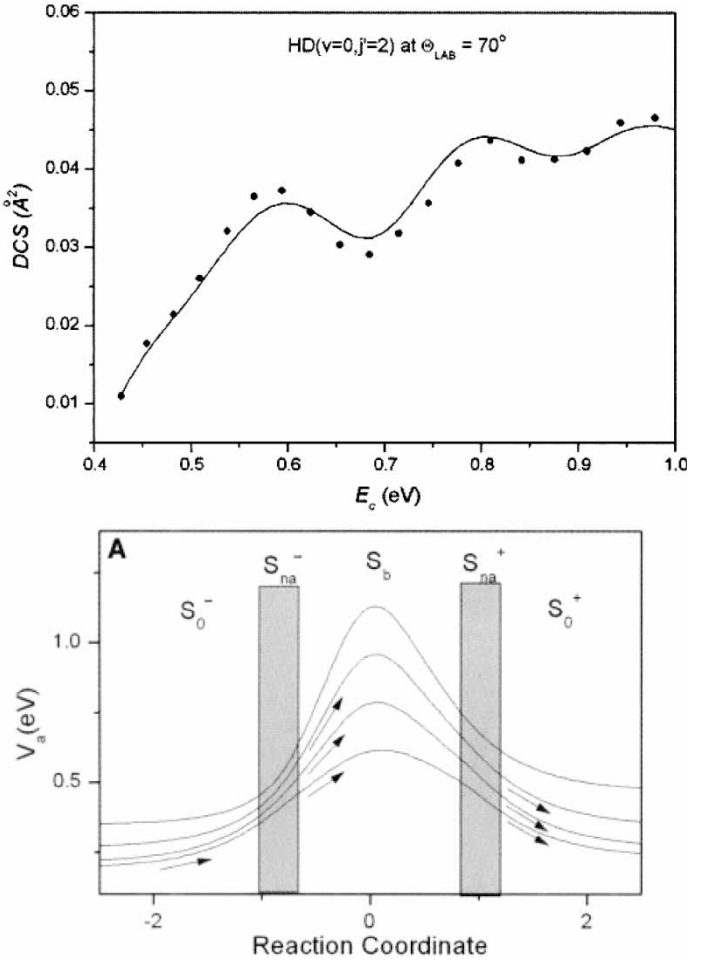

Figure 23. Top panel: Experimental (solid circles) and QM (solid line) DCS for the $H + D_2(v = 0, j = 0) \rightarrow HD(v' = 0, j' = 2) + D$ reaction measured at the laboratory angle of 70° at different center-of-mass collision energies within the range 0.4–1.0 eV. The LAB angle of 70° corresponds approximately to backward scattering in the CM frame. The transformation from LAB to CM is energy dependent. Bottom panel: Schematic correlation diagram illustrating the role of quantum bottlenecks on the reaction dynamics. Reprinted with permission from [104]. Copyright 2003 American Association for the Advancement of Science.

Skodje and Yang argued that the oscillations found in the reaction probability and the ridges in the DCS as a function of energy are not caused by Feshbach resonances but by interferences of QBS states.

This explanation is most appealing, but there are still two aspects that deserve some consideration. First of all, in contrast to forward scattering, which is caused by a limited set of J, many more partial waves with different J contribute to backward scattering. This is apparent in figure 8 of this review, and in more detail in figure 26 of [102]. In this latter figure, J values up to 15 from a total of 25 contributing to the $H + HD$

reaction at 1.20 eV, participate in the backward scattering. Secondly, QCT calculations by Persky, Kornweitz and Baer [192–194] and by Aoiz *et al.* [76] show also oscillations in the state resolved DCS in the backward region, analogous but not identical to those in QM calculations. A thorough investigation of this effect using QCT is necessary, as well as QCT calculations of cumulative reaction probabilities, which, to our knowledge have not been published for the H_3 reactive system.

6. Geometric phase and non-adiabatic effects

Most dynamical studies on the $H + H_2$ reaction have been carried out on the ground electronic PES for total energies of the colliding system below that of the minimum of the first excited potential surface ($\approx$2.70 eV with respect to the bottom of the $H_2(^1\Sigma_g^+)$ well). Under these circumstances, the reactivity of the system has been assumed to be entirely determined by the ground state Born–Oppenheimer PES, the contribution of excited electronic surfaces has been considered negligible and only recently, a slight non Born–Oppenheimer (diagonal) correction to the barrier height has been included to account for low temperature rate constants [160], as discussed in Section 2. However, a complication could arise from the fact that the ground and the first excited PESs of H_3 present a conical intersection for equilateral triangle (D_{3h}) nuclear geometries as pointed out in 1990 by Lepetit and Kuppermann [195]. When the nuclear coordinates follow a closed path encircling a conical intersection, the electronic wavefunction changes sign. The nuclear problem is solved on the PES which does not contain any information about this sign change. Since the total electronuclear wavefunction must be continuous and single valued, a sign change has to be introduced into the nuclear wave function in order to rectify the situation [196–198]. This change of sign called sometimes 'molecular Aharonov-Bohm effect' [199, 200] was shown to be a particular case of the more general 'geometric phase' or 'Berry phase' [201] found in quantum systems with parametric time dependence that undergo a cyclic adiabatic time evolution. The term 'geometric phase' (GP) is the most widely used in studies of reaction dynamics (see [127] for a recent review on the subject). The geometric phase is ignored in most theoretical studies although, in principle, GP effects could influence nuclear motion even at energies clearly below that of the conical intersection. In any case, possible GP effects are expected to increase in importance as the energy of the system approaches that of the conical intersection. In 1991, Wu *et al.* [202] performed a fully converged QM calculation of integral and differential cross sections, including the GP, for the $H + H_2$ reaction on the LSTH PES over the 0.7–1.2 eV total energy, E, range. The authors concluded that the geometric phase strongly influenced the DCSs and to a lesser extent the integral cross sections for *para* $\rightarrow$ *para* and *ortho* $\rightarrow$ *ortho* transitions even at $E = 1.2$ eV. For *ortho* $\rightarrow$ *para* and *para* $\rightarrow$ *ortho* and for isotopic variants with dissimilar hydrogen atoms, GP effects were found to be much smaller and measurable effects were not expected for $E \lesssim 2.2$ eV. These calculations were subsequently extended by Wu and Kuppermann [77] to cover the 0.3–2.6 eV total energy range and significant GP effects were observed for $E > 1.8$ eV. In 1993 Kuppermann and Wu [78] reported the results of accurate QM calculations for the $D + H_2 \rightarrow HD + H$ isotopic variant of the reaction

for E values of 0.78, 1.25 and 1.8 eV, corresponding to those of the experiments of Continetti *et al.* [49] and of Kliner *et al.* [60]. The calculations were performed with and without inclusion of the geometric phase and were termed GP and NGP, respectively. Significant differences were observed between the GP and NGP state-resolved integral cross sections for the $D + H_2(v = 1, j = 1) \rightarrow HD(v' = 1, j')$ reaction at a collision energy of 1.0 eV (total energy 1.8 eV) corresponding to the experimental conditions of [60]. As indicated in Section 1, this measurement was controversial, both because of possible experimental problems (see comments in [61]) and because of its singular discrepancy with theoretical calculations [25, 62, 64, 65]. The new GP results of Kuppermann and Wu could apparently settle the dispute. The NGP data were in good agreement with the previous QM calculations, whereas the GP data, peaking at lower j', accounted for the experimental result. This is shown in the upper panel of figure 24 and was taken as a clear manifestation of the geometric phase effect in chemical reactions. A shift of the peak of the rotational distribution toward lower j' was also observed in QCT calculations by Adhikari and Billing [203] upon introduction of a vector potential in the classical hamiltonian, but the agreement with the experimental $P(j')$ was still bad. More recent QM calculations, shown in the lower panel of figure 24, contradict however this interpretation and will be discussed at length below.

At the lowest energy investigated by Kuppermann and Wu ($E = 0.78$ eV), the agreement between GP and NGP integral and differential cross sections was very good. At $E = 1.25$ eV the accordance was very good in the integral cross sections, but some differences were found in the rovibrationally resolved DCSs. The calculations were performed for the $D + H_2(v = 0) \rightarrow HD(v = 0, j') + H$ reaction at $E_{col} = 1.01$ eV, corresponding to the higher collision energy of the experiment of Continetti *et al.* [49] and the theoretical results were compared, in an indirect way, with experimental data. In fact, the calculated v', j' resolved DCSs were compared to empirical DCSs derived from the deconvolution of the measured data. The accord with the GP DCSs was found to be somewhat better than with the NGP ones, but the direct experimental information was much less detailed, since the measurements provided only partial *vibrational* resolution of HD and no definitive conclusions could be drawn. The difference between v', j' resolved GP and NGP calculated DCSs was seen to increase appreciably for the higher energy ($E = 1.8$ eV) and Kupperman and Wu [78] predicted that GP effects would become noticeable once fully rotationally resolved DCS measurements were performed.

In 1995, Wu and Kuppermann [90] calculated GP and NGP differential cross sections for the $H + D_2 \rightarrow HD + D$ reaction on the LSTH surface at a collision energy of 1.29 eV (total energy 1.481 eV) and compared their results with the molecular beam RPI experiment of Kitsopoulos *et al.* [81]. As indicated in Section 2, this experiment was also polemical since it yielded DCSs and velocity distributions that did not agree with those of theoretical calculations [87–89], which could in turn reproduce quite well the results of a higher resolution experiment based on the Rydberg atom TOF technique at the same collision energy [79]. The GP calculations of Wu and Kuppermann [90] could reproduce the discrepant experimental peak at $\approx 160^\circ$ in the DCS of the scattered HD, as illustrated in the top panel of figure 25 (in the original works of Kitsopoulos *et al.* [81] and of Wu and Kuppermann [90], the DCS is referred to the scattering of D atoms and the peak appears at $\approx 20^\circ$. Both representations are equivalent). This conflicting feature was again explained by Wu and Kuppermann [90]

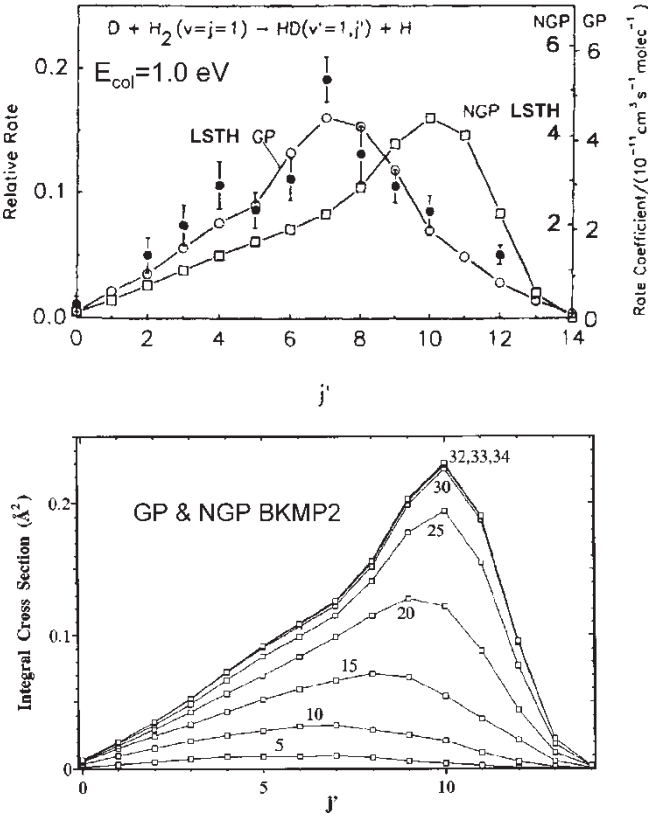

Figure 24. Upper panel: rate coefficients for the production of individual rotational states in the $D + H_2(v = 1, j = 1) \rightarrow HD(v' = 1, j') + H$ reaction at a collision energy of 1.0 eV. Solid circles with error bars: experimental data by Zare and co-workers [60]. Open symbols: GP and non GP calculations by Kuppermann and Wu [78] on the LSTH surface. Lower panel: State resolved integral cross sections for the same reaction calculated by Kendrick [127] on the BKMP2 PES. The numbers of the different graphs indicate the maximum value of J considered and demonstrate the convergence of the calculations. GP and NGP results are indistinguishable. Top panel reprinted with permission from [78]. Copyright 1993 Elsevier Science. Bottom panel reprinted with permission from [127]. Copyright 2003 American Chemical Society.

as a GP effect, but in this case a controversy started, since the observed discrepancy was not only with NGP calculations, but also with higher resolution measurements. A new Rydberg atom TOF experiment of Schnieder *et al.* [91] in 1995 increased notably the resolution of the technique providing for the first time rovibrationally state resolved DCSs in very good agreement with NGP theoretical results (see comments above and bottom panel of figure 25). The experiment was carried out at a slightly lower collision energy ($E_{col} = 1.28$ eV, $E = 1.471$ eV) and the total DCS measured was very similar to that of the previous measurements [79] and thus at variance with the DCS of the RPI experiment and with the GP calculations. Kuppermann and Wu published then a work [118] in which the observed experimental peak was interpreted as a very narrow resonance corresponding to the $H + D_2(v = 0, j = 0) \rightarrow HD(v' = 0, j' = 4, 5)$ transitions, centered at $E_{col} = 1.29$ eV and present only when the GP was taken into account.

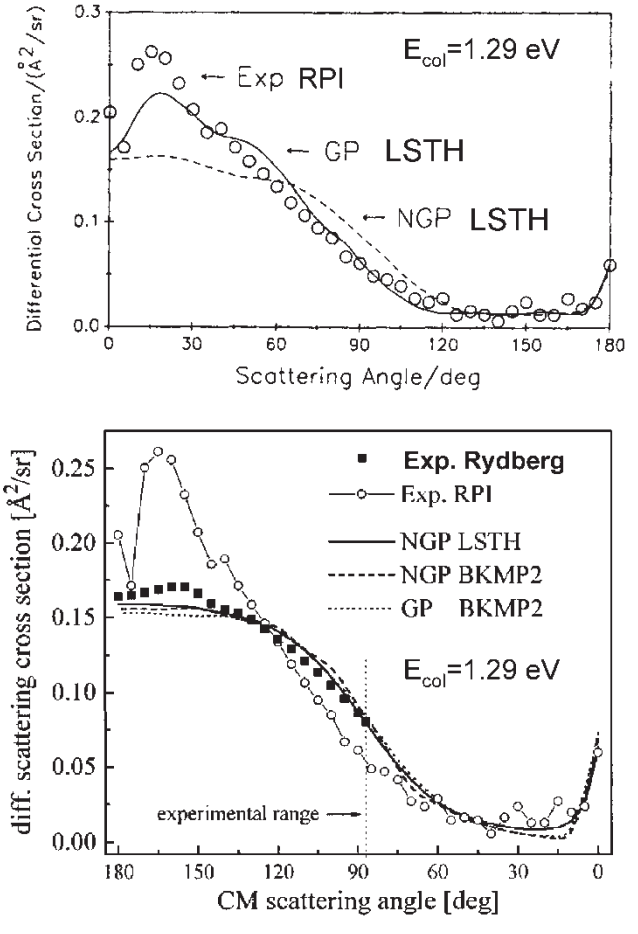

Figure 25. DCS for the reaction $H + D_2(v = 0, j = 0) \rightarrow HD(v = 0, j') + D$ at a collision energy of 1.29 eV. Upper panel: Symbols, DCS derived from the reaction product imaging data of Kitsopoulos *et al.* [81]. Solid and dashed lines GP and NGP calculations by Wu and Kuppermann [90] on the LSTH PES. Lower Panel: Open symbols and line, experimental DCS by Kitsopulos *et al.* [81]. Closed symbols, experimental data from the Rydberg tagging experiment of Wrede and Schnieder [96]. Solid line, NGP calculation by D'Mello *et al.* [89] on the LSTH PES. Dashed and dotted lines NGP and GP calculations by Kuppermann and Wu (cited in [96]) on the BKMP2 PES.

The authors concluded [118] that, given the location and width of this resonance, it should have no influence in the experiment at $E_{col} = 1.28$ eV, in accordance with the observations, but predicted marked effects, both in the total and in the state-resolved DCSs, at $E_{col} = 1.29$ eV. In an attempt to experimentally verify the predicted resonance, Wrede and Schnieder [96] carried out further Rydberg 'tagging' experiments over the 1.27–1.30 eV collision energy (1.461–1.491 eV total energy) range. The collision energy was varied within the small interval of interest by slightly changing the intersection angle of the molecular beams. The experimental data did not show any indication of the resonance and were always well reproduced with the previous NGP calculations on the LSTH PES [63, 87, 89]. Kuppermann and Wu [90, 118] had noted that the energy

of the GP resonance depended very sensitively on the accuracy of the potential surface. They performed new calculations on the BKMP2 PES (unpublished results cited in [96]), that led to very similar GP and NGP total DCS at $E_{col} = 1.29$ eV, that were now in good agreement with the experimental DCSs from the Rydberg 'tagging' experiments [79, 91, 96] and at variance with the RPI measurements of Kitsopoulos *et al.* [81] (see bottom panel in figure 25). In retrospect, the fortuitous coincidence of a dubious experimental feature with a manifestation of a narrow GP resonance calculated on an 'inaccurate' PES, is indeed remarkable. Interestingly, whereas a good agreement was found between all the NGP total DCSs [63, 87, 89, 90] around $E_{col} = 1.29$ eV, appreciable differences appear between the v', j' state-resolved NGP DCSs of Wu and Kuppermann [90] and those from experiment and from the rest of theoretical calculations (compare, for instance figure 13 of [92] and figure 2 of [90]).

In later works, Kuppermann and Wu [119, 204] have indicated that the predicted GP resonance is shifted to $E = 1.44$ eV on the BKMP2 surface, below the investigated experimental range. Kuppermann and co-workers suggested that given the extreme sensitivity of the location of the predicted resonances to the potential, the accuracy of the H_3 surface had to be further improved and constructed a new PES based on extensive quantum Monte Carlo calculations [156]. As far as we know this surface has not been used in reactive scattering calculations and, as indicated above, its accuracy has been recently questioned [157, 158].

More molecular beam experiments, based on the Rydberg atom TOF technique were conducted at higher energies [95, 99], even slightly above the conical intersection [97], and in all cases the measurements were in good agreement with the results of non GP QM or QCT calculations on the available *ab initio* PESs [14–17, 100]. Additionally, detailed QCT calculations on the BKMP2 PES at these high collision energies showed that the number of reactive trajectories surrounding the conical intersection and thus the likelihood of GP effects in a QM calculation, is indeed very small, $\approx$0.3% at 2.2 eV and 1.4% at 2.67 eV [205]. Only for trajectories at 2.3 eV collision energy and D_2 molecules excited into $v = 1$ this percentage starts to be significant (5%).

The absence of detectable GP effects in all the high resolution experiments motivated further calculations. In recent times Kendrick has carried out a thorough theoretical investigation of the role of the geometric phase on the reactivity of the $H + H_2$ system and isotopic variants [125–128]. GP calculations within the vector potential (VP) approach were applied to the $H + D_2$ reaction at $E_{col} = 1.29$ eV [125]. These calculations showed that geometric phase effects cancel out in all of the state resolved integral and differential cross sections for all energies, when the contributions of odd and even values of the total angular momentum are added together. The study was done for $J \leq 5$ and the cancellation was found for both the LSTH and BKMP2 surfaces. The author pointed out that the cancellation appears to be due to symmetry properties and should be independent of the potential energy surface and hold for all J. In a subsequent work, Kuppermann and Wu [119] contested this conclusion by presenting new calculations at the same collision energy, converged until $J = 46$, on the same two PESs. The calculations showed agreement between GP and NGP DCSs for $J \leq 5$ on both surfaces and also for higher J on the BKMP2, but appreciable differences between GP and NGP DCSs appeared for the higher J values on the LSTH in accordance with the earlier results of the authors [90]. The GP calculations used the double

boundary condition (BC) method, as did all the previous calculations by Wu and Kuppermann, but the two formulations (BC and VP) are mathematically equivalent.

However, Kendrick [128] pointed at deficiencies in the methodology of Kuppermann and Wu and stressed the previously mentioned disagreement between the NGP v', j' state resolved DCSs from Wu and Kuppermann [90] and those from experiment [92] and from calculations by other groups, including new results by himself [63, 87, 89, 126], and suggested that the calculations of Kupperman and Wu contain some errors that have to be resolved [128].

Kendrick [127] has also investigated the $D + H_2(v, j) \rightarrow HD(v', j') + H$ reaction in the 0.4–2.32 eV total energy range. GP and NGP calculations were performed on the BKMP2 PES for $J \leq 34$. For the GP calculations BC and VP approaches were used and led to the same results, as expected. Geometric phase effects were again found to cancel out when odd and even J values were added together to compute integral and differential cross sections. In particular the products' rotational distribution was calculated for the $D + H_2(v = 1, j = 1) \rightarrow HD(v' = 1, j') + H$ reaction at a total energy of 1.8 eV, corresponding to the conditions of the experiment of Kliner *et al.* [60]. The GP and NGP rotational distributions were indistinguishable and in good agreement with the results of previous NGP calculations [62, 64, 65, 78] and were at variance with the experimental data [60] and with the GP calculations of Kuppermann and Wu [78], as shown in the bottom panel of figure 24. This new results questioned both the earlier GP calculations and the experimental measurements, that were also controversial from the experimental point of view [61]. As suggested by Kendrick [128], a confirmation of this experiment is needed in order to resolve the remaining discrepancies between theory and experiment. Till now, all the higher resolution Rydberg 'tagging' experiments which have been carried out at a high number of collision energies between 0.4 and 2.67 eV (total energies $\approx$0.6–2.86 eV) are in excellent agreement with the results of NGP theoretical calculations [79, 91, 92, 95–99, 101–104].

Recently, the influence of the geometric phase on the reactive dynamics of the $H + H_2$ system has been estimated with a different approach. Juanes-Marcos and Althorpe [206] have computed wave packets in hyperspherical coordinates for the $H + H_2$ ($v = 0$, $j = 0) \rightarrow H_2 + H$ reaction over the 0.75–2.02 eV collision energy range without including the GP. For the conditions investigated, the wave packet failed to encircle the conical intersection and the authors concluded that this weakened the case for strong GP effects, but did not rule them out entirely. More recently [207], however, these authors have carried out wave packet calculations on the $H + H_2$ reaction over the 0.4–2.5 eV total energy range using the BKMP2 PES, both with and without the inclusion of the geometric phase effect. In this work they incorporated the VP approach into the Jacobi Hamiltonian. The results show very good agreement with those of Kendrick [128] predicting that GP effects show up in the state-to-state reaction probabilities but cancel exactly when partial waves are summed to obtain the integral cross section. Since the two methods are very different, it is unlikely that the coincidence between the corresponding results can be fortuitous. Therefore it can be stated that GP effects do not have any influence on the ICS, in contradiction with the conclusions of Kuppermann and Wu [119]. Juanes-Marcos and Althorpe have found that very small GP effects could be at best observable in the state-to-state DCSs above 1.8 eV, especially in the $H + H_2$ variant of the reaction, in a hypothetical high resolution experiment.

Although the presence of observable GP effects in the dynamics of the $H + H_2$ reaction cannot be entirely excluded, in the light of the present evidence, the high expectations raised from the first theoretical studies [77, 78] have not been fulfilled to date in spite of the extensive experimental work of the last decade. Instead of being frequent for energies approaching that of the conical intersection, GP effects seem to be rather elusive. At present no unquestioned experimental evidence exists and recent theoretical work [128] indicates that they should cancel out in observable integral or differential cross sections at least for isotopic variants with dissimilar atoms. The emphasis is now laid on the identification of GP resonances that depend critically on the features of the PES and that might even be too short lived to be experimentally detectable [119].

Apart from the debated geometric phase effects, non-adiabatic transitions in the region of proximity of the two electronic surfaces are also a possibility at high enough collision energies. The highest collision energy accessed till now in a Rydberg 'tagging' experiment [97] is 2.67 eV, corresponding to a total energy of 2.86 eV, slightly above that of the conical intersection (≈2.7 eV). The experimental data could be well reproduced by means of QCT calculations on the LSTH and BKMP2 ground state PESs. Mahapatra *et al.* [134] have recently reported the results of a time-dependent wave packet calculation of the dynamics of the $H + H_2$ reaction for energies extending up to the onset of the three-body dissociation (4.74 eV) considering the ground and first excited DMBE PESs. These calculations, restricted to $J = 0$, found no noticeable effect of the conical intersection on the reaction dynamics. The absence of significant non-adiabatic crossings for this system is not too surprising. At the high collision energies of these studies triangular configurations of the nuclei do contribute to reactive scattering, but the region of configuration of the three nuclei for which the two electronic states are nearly degenerate is very small and slight deviations from the D_{3h} symmetry cause a large splitting of the two electronic surfaces making non-adiabatic transitions unlikely.

7. Rotational distributions of reactive and inelastic scattering

The dynamical relevance of the rovibrational state distributions of the product molecules in the $H + H_2$ reaction has been repeatedly stressed in the previous sections. In the following we will comment on recent and sometimes controversial studies pertaining to the last five years.

In 2000, Zare and co-workers were able to measure the rotational distribution of the $H + D_2 \rightarrow HD(v' = 3, j') + D$ reaction at 1.64 eV collision energy using the *photoloc* technique [106] (see Section 3 for details). In these experiments, the expansions producing the molecular jets were not strong enough to fully relax the internal degrees of freedom of the D_2 molecules and, thus, different rotational states of the $D_2(v = 0)$ reagent molecules contributed to the reaction. The measurements were compared with the results of QCT calculations carried out on the BKMP2 PES simulating the experimental D_2 rotational population in the beam. A good agreement between theory and experiment was found, although the QCT distribution was slightly hotter than the experimental one, a feature that had been observed in many previous

comparisons with experimental and QM results and that has been attributed to the histogramatic method employed to assign quantum numbers to the product molecules in the QCT method.

In a subsequent study published in 2004, Zare and co-workers measured rotational distributions for the same $H + D_2 \rightarrow HD(v' = 3, j') + D$ reaction at eight different collision energies in the range 1.49–1.85 eV [113]. Using a previous measurement of the state-resolved excitation function for this reaction [111], it was possible to determine the relative reaction cross section as a function of both collision energy and product rotational quantum number j'. The experimental results were compared with TI and TD QM scattering calculations carried out at all the experimental collision energies on the BKMP2 PES. Surprisingly, it was found that the two QM calculations yielded significantly colder rotational distributions than experiment, specially at the highest collision energies, as shown in figure 26. The rotational distributions calculated by the TI and TD QM methods are practically indistinguishable.

The TI and TD QM calculations were performed only for the reaction with $D_2(v = 0, j = 0)$ molecules, although, as indicated in the preceding paragraph, rotationally excited D_2 molecules up to $j = 2$ were participating in the experiment. In order to account for the possible effect of reagent rotation on the measured rotational distributions, QCT calculations for the reaction with $D_2(v = 0, j = 0–2)$ molecules were performed at 1.64 and 1.85 eV collision energies. In addition, the histogramatic method usually employed in QCT calculations for the assignment of rovibrational quantum numbers to the product molecule, was replaced by a recently developed gaussian binning procedure [113]. This gaussian binning procedure has proved to be superior for the correct description of the QCT results and gives rotational distributions in better agreement with accurate QM scattering calculations, specially for thermoneutral or slightly endothermic channels of a given reaction. The implementation of the method, which is based in an original idea by Bonnet and Rayez [208], has been described in detail in several works where QCT and accurate QM calculations have been compared for a series of insertion reactions [209, 210]. In this binning method, a gaussian function centered at the quantal action and with a given width is used to weight the trajectories following the criteria that the closer the vibrational action of a given trajectory to the nearest integer, the larger the weighting coefficient for that trajectory. The good behaviour of the method for the hydrogen exchange reaction was demonstrated in [113]. In addition, it was shown that, for this reaction, reagent rotational excitation has little effect on the product rotational distributions. Thus, reagent rotational excitation in the molecular beam cannot explain the measured hotter rotational distributions in comparison with the exact QM calculations.

Careful checks were performed in the measurements to rule out any experimental artifact producing the hotter rotational distributions [113] and it was concluded that deficiencies in the adiabatic PES or the absence of non-adiabatic effects in the theoretical treatment were most probably responsible for the observed disagreement. Nevertheless, TI QM calculations on the latest, highly accurate, CCI PES [158] at 1.85 eV collision energy show, as expected, an almost perfect agreement with those performed on the BKMP2 PES (see figure 27 and discussion at the end of Section 3). Furthermore, as commented on in the previous section, the most recent calculations indicate that geometric phase or non-adiabatic effects are not expected to affect

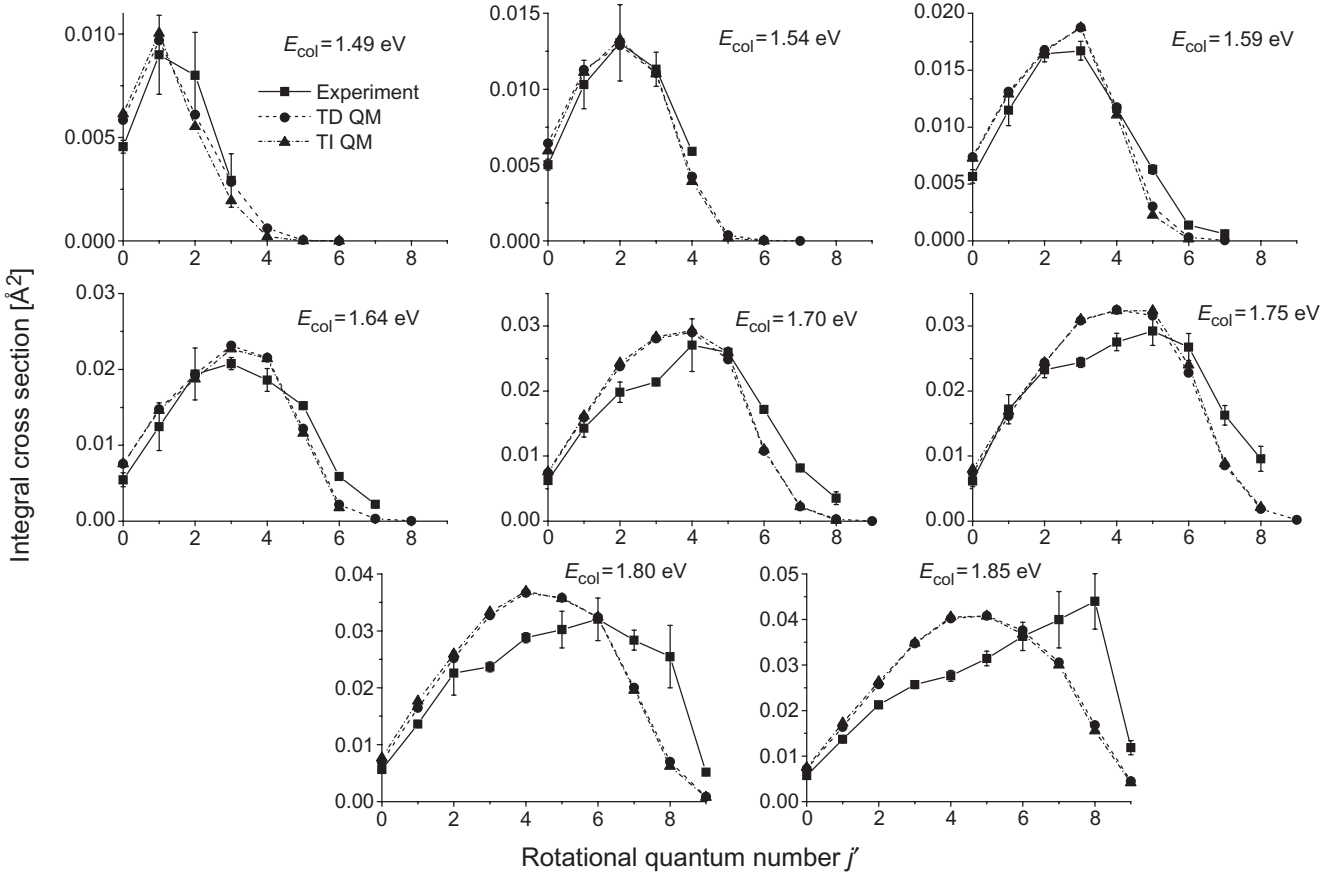

Figure 26. Experimental and TI and TD QM rotational distributions for the $H + D_2(v = 0, j = 0) \rightarrow HD(v' = 3) + D$ reaction over the 1.49–1.85 eV range of collision energies [113]. Both QM calculations were performed on the BKMP2 PES. Black squares with error bars: experimental results. Blues squares: TI QM results. Red circles: TD QM results. For most collision energies, TI and TD rotational distributions are indistinguishable. The experimental distributions have been scaled to the theoretical ones. Adapted from figure 4 of [113].

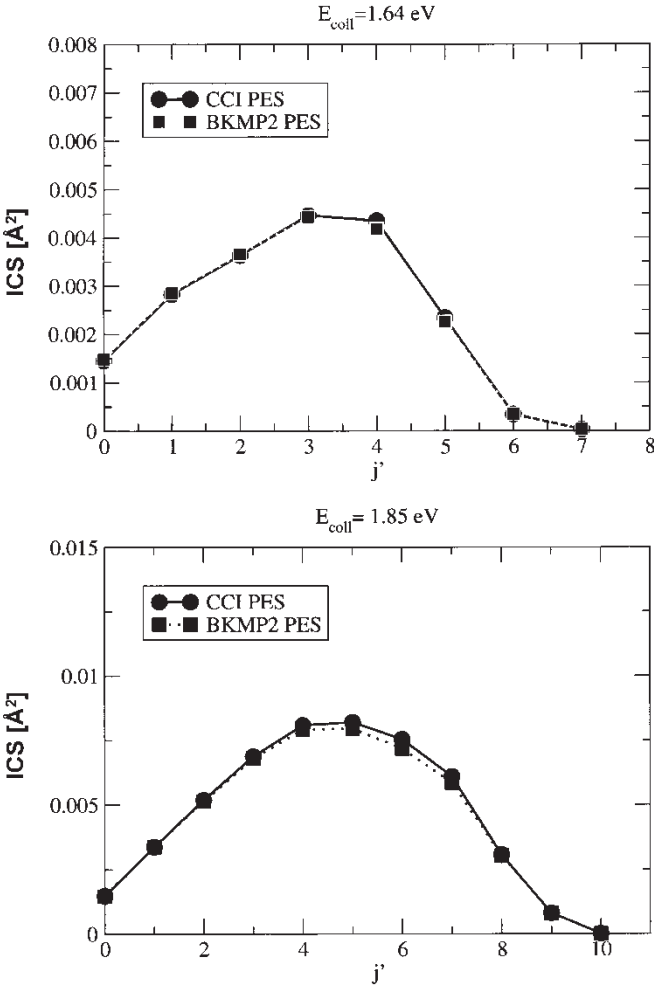

Figure 27. TI QM rotational distributions for the $H + D_2(v = 0, j = 0) \rightarrow HD(v' = 3) + D$ reaction calculated on the BKMP2 and CCI PESs at 1.64 eV and 1.85 eV collision energies. The results obtained on both versions of the PES are practically indistinguishable.

substantially the dynamics of the hydrogen exchange reaction, even at the highest collision energies investigated thus far.

The disagreement found between theory and experiment for the $v' = 3$ rotational distributions becomes even more intriguing considering the results of a subsequent work, in which the rotational distributions for the $H + D_2 \rightarrow HD(v' = 2, j') + D$ reaction were measured at nine collision energies in the 1.30–1.85 eV range, using exactly the same experimental methodology [112]. As can be seen in figure 28, a very good agreement was found, in this case, between the experimental data and TI and TD QM scattering calculations. No clear explanation for the observed disagreement is available up to date and more experimental and theoretical work would be necessary to disentangle this paradox.

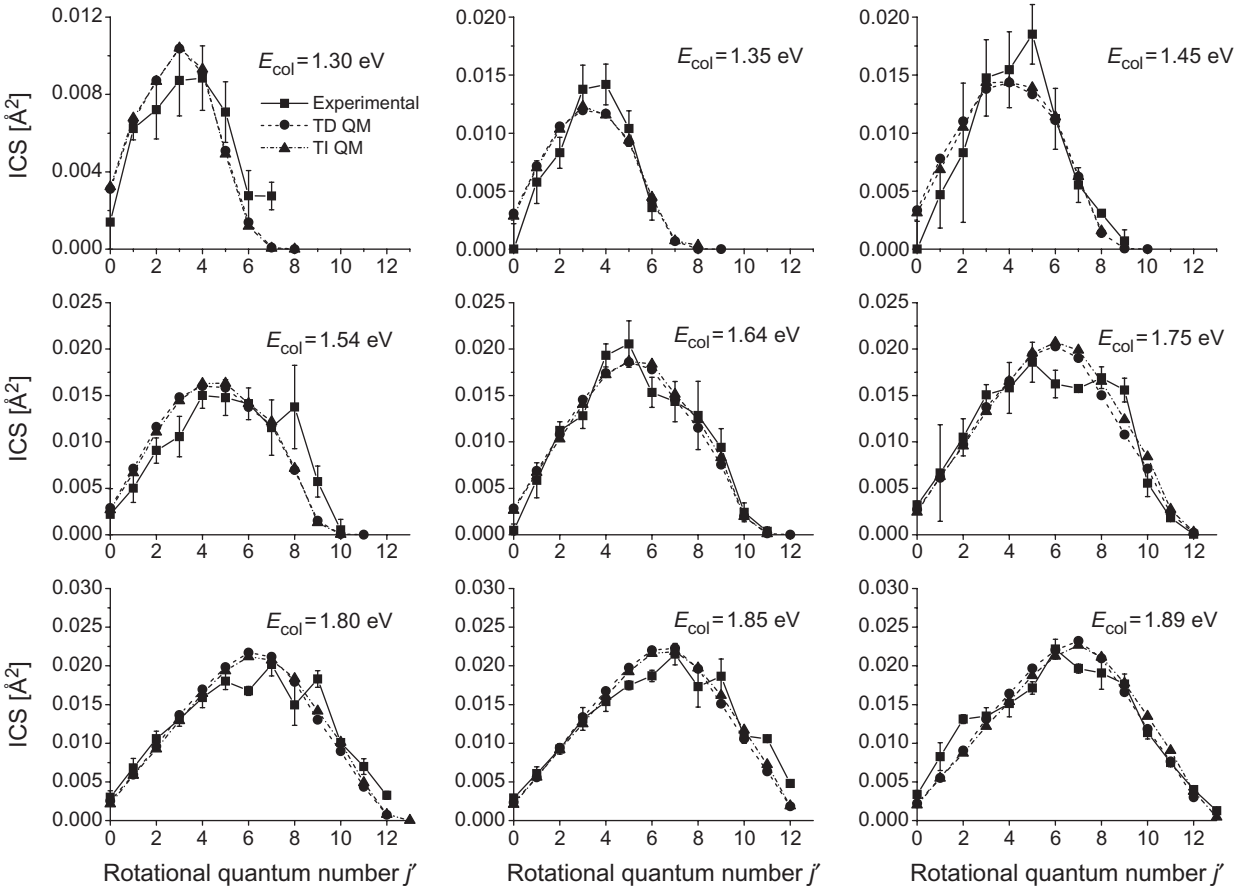

Figure 28. Same as in figure 26 but for the $H + D_2(v = 0, j = 0) \rightarrow HD(v' = 2) + D$ reaction over the 1.30–1.89 eV range of collision energies [112]. The experimental distributions have been scaled to the theoretical ones. Adapted from figure 6 of [112].

Inelastic scattering in $H + H_2$ collision has received comparatively little attention. Only relatively scarce studies [54, 56, 57, 67] have been devoted to this process. However, it is very relevant for the general understanding of the molecular interactions involved in reactivity. At low collision energies, inelastic scattering can yield important information about the van der Waals well and the long range forces in the entrance channel. At collision energies above 1.2 eV, at which the reactive cross section levels off for most of the isotopic variants of the reaction, recrossing collisions may play an important role, especially for the production of vibrational excitation.

Recent experiments by Zare and co-workers [211] have determined the rovibrational product state distribution for $H + D_2$ inelastic scattering at 1.55 eV and 1.85 eV collision energies using the same *photoloc* technique described already in Section 3 for the measurement of reactive collisions. In this case, the D_2 molecules inelastically scattered into a given v', j' state are detected. The experimental results were compared with TI and TD QM scattering and QCT calculations carried out on the BKMP2 PES.

As a result of the homonuclear character of the target molecule, inelastic transitions with Δj odd have a null probability. Thus, inelastic collisions have a negligible probability of interconversion between *ortho* and *para* D_2. To account for the Δj even parity rule in the QCT calculations, the assignment of final rovibrational states of the D_2 molecule was made determining first v' and j' in the standard way, rounding to the nearest integer the real semiclassical values of v' and j'. If the resulting integer j' corresponded to a $\Delta j = j' - j$ even, the rotational number was taken to be j', if Δj was odd, the final rotational number was taken to be $j' + 1$. The cross sections resolved in final vibrational states for inelastic collisions are the same for *ortho* and *para* D_2, that is, starting in $j = 0$ or $j = 1$. Accordingly, the experiment yielded a *ortho*:*para* ratio of 2:1 within each vibrational manifold, just reflecting the statistical distribution of these species in the reagents. All the theoretical calculations confirmed this experimental finding [211].

The rotational distributions for the process $H + D_2 \rightarrow H + D_2(v' = 1, 2, j')$ are shown in figure 29, where the experimental (relative) cross sections have been scaled to the TI QM results. As can be seen, the agreement of the experimental data with the theoretical results is very good, except for few minor details. As in the reactive case, both TD (not shown) and TI QM methodologies yield practically identical results [211]. The QCT cross sections are almost in quantitative agreement with the experimental and QM data. It should be noticed that if the experimental rotational distributions would have been scaled to the QCT data, the agreement with the latter would be almost as good as with the QM cross sections.

One of the discrepancies between the experimental rotational distributions and the theoretical ones is that the former are slightly hotter than the latter. This is due to the fact that the theoretical calculations represented in figure 29 are for D_2 in $j = 0$, whereas, as in the reactive experiments (see above), higher rotational states are present in the molecular beam. Figure 30 shows the comparison between the experimental data and the QCT calculations assuming a D_2 rotational temperature of 150 K, at which the $j = 0$ and $j = 2$ rotational states have a similar contribution while that from higher j states is negligible. In this case, the experimental cross sections have been scaled to the QCT data. As can be seen, the agreement between the two sets of results is very good and improves slightly with respect to those shown in figure 29.

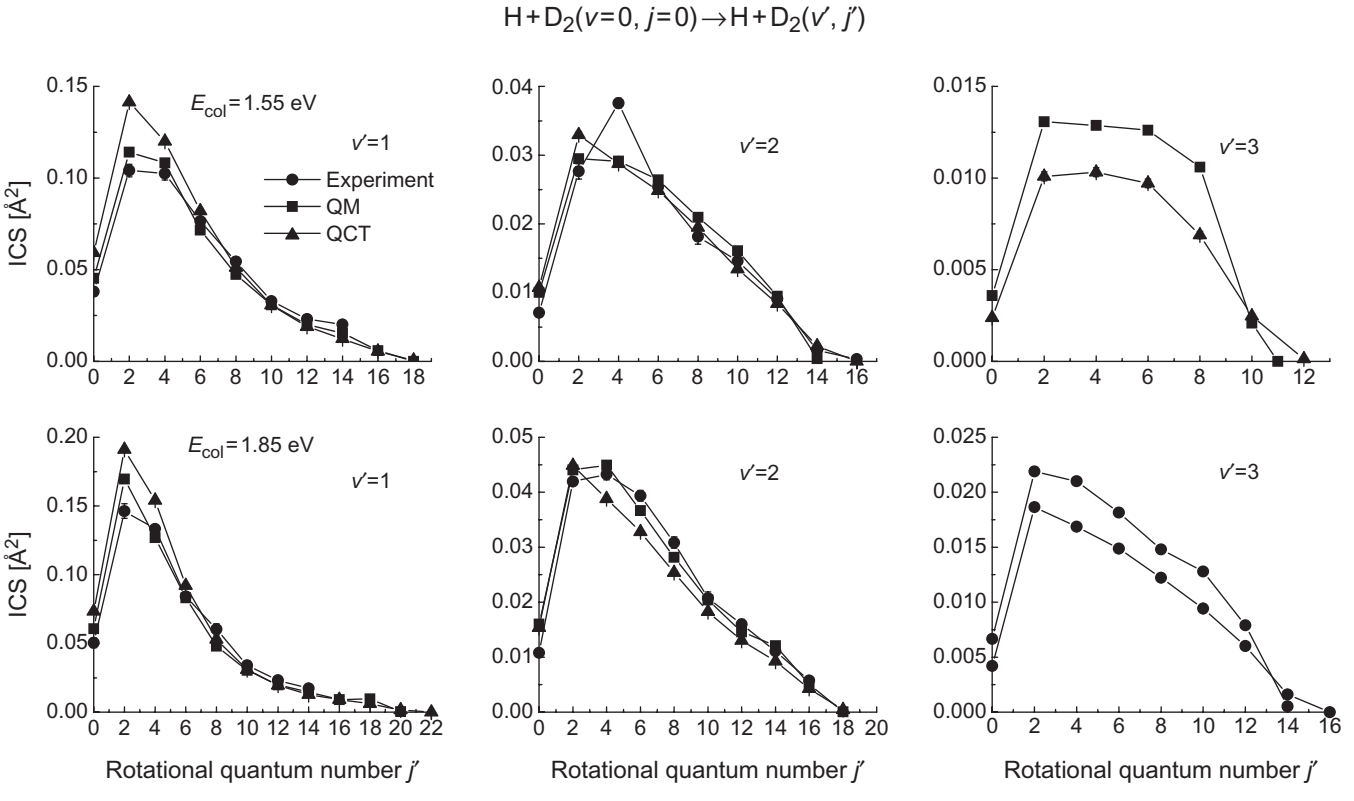

Figure 29. Rotational distributions at the indicated collision energies and vibrational manifolds for $H + D_2(v = 0, j = 0)$ inelastic scattering. Black circles: experimental measurements. Red squares: TI QM calculations on the BKMP2 PES. Blue triangles: QCT calculations on the BKMP2 PES. The experimental distributions have been scaled to the QM results. For the $v' = 3$ manifold only theoretical results are available.

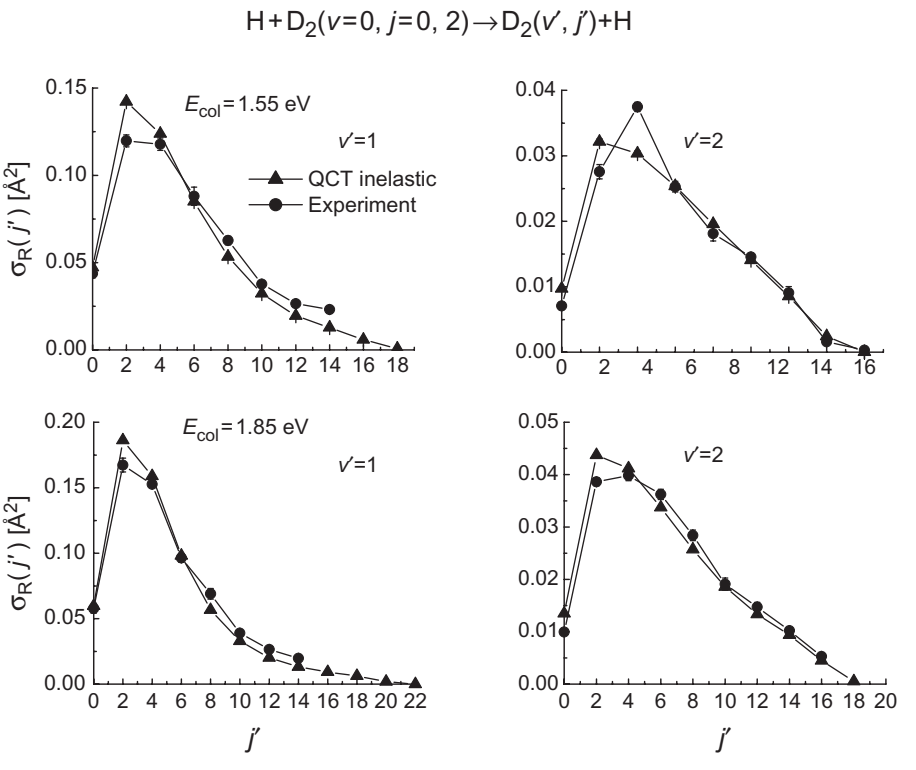

Figure 30. Rotational distributions at the indicated collision energies and vibrational manifolds for $H + D_2(v = 0, j = 0, 2)$ inelastic scattering. Black circles: experimental measurements. Red triangles: QCT results obtained on the BKMP2 PES considering the contribution from collision with $D_2(v = 0, j = 0, 2)$. The experimental distributions have been scaled to the theoretical ones.

When the rotational distributions of inelastic and reactive scattering are compared for the same final vibrational quantum number of D_2 and HD, two main features are observed. First, the absolute values of the cross sections are considerably larger for inelastic scattering, clearly indicating that inelastic scattering competes favourably with reactive scattering. Second, the rotational distributions for reactive scattering are much hotter than those corresponding to inelastic scattering. As a general trend, for inelastic scattering, the fraction of the total energy going into rotation at a given v' state, decreases slightly as collision energy increases. In addition, as v' grows, the fraction of energy going into rotation increases slightly, in contrast with the results obtained for reactive scattering.

One of the main differences between inelastic and reactive scattering is the maximum impact parameter implied. A value of $b_{max} = 1.3$ Å is sufficient to encompass all reactive scattering, and this value does not change from $E_{col} \approx 1.2$ eV up to 2.67 eV. In contrast, b_{max} becomes 1.8 Å for inelastic scattering at 1.85 eV collision energy. Figure 31 shows the TI QM and QCT inelastic and reactive probability as a function of total angular momentum, i.e. the opacity functions, for production of D_2 and HD in $v' = 1$–3 from $H + D_2(v = 0, j = 0)$ collisions. It is apparent that reactive scattering

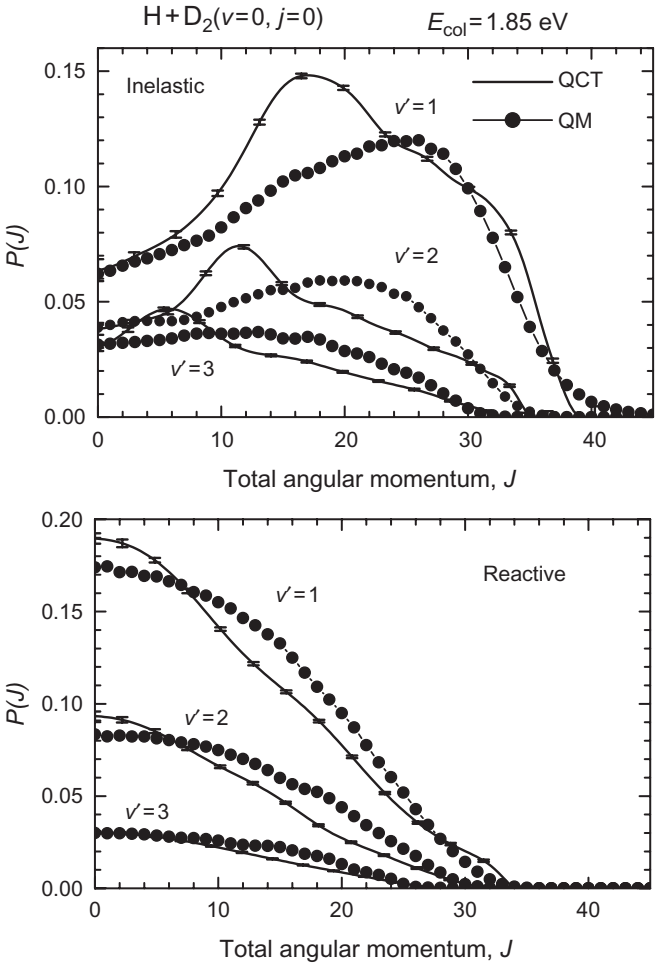

Figure 31. Vibrationally state resolved QCT and QM opacity functions, $P(J)$, for inelastic (top panel) and reactive (bottom panel) $H + D_2(v = 0, j = 0)$ collisions at 1.85 eV collision energy.

takes place at lower orbital angular momenta than inelastic scattering for a given v' state of the D_2 or HD products. As an example, for the formation of $HD(v' = 1)$, one finds $J_{max} = l_{max} = 33$ ($b_{max} = 1.28$ Å), whereas J_{max} extends to 40 ($b_{max} = 1.5$ Å) for the excitation of D_2 to $v' = 1$ in inelastic collisions. In addition, the reaction probability is higher at low J for reactive collisions leading to a given $HD(v')$ state than for the production of the corresponding vibrationally excited $D_2(v')$ in inelastic collisions. The exception is $v' = 3$, the highest HD state accessible at this collision energy, were both probabilities are similar. Therefore, low impact parameters (low J) tend to promote reaction, whereas, high impact parameters (high J) promote inelastic transitions with vibrational excitation.

The agreement between QCT and QM vibrationally state resolved opacity functions is somewhat better for reactive scattering than for inelastic scattering, where the

accordance is only qualitative. In the case of reactive scattering, the QCT reaction probability at low J is slightly larger than the QM one, whereas the opposite is true at intermediate J (10–25). For inelastic scattering, although the values of $P(J = 0)$ are in very good coincidence for the various v' states, the QCT calculations predict a quicker rise of $P(J)$ with J giving rise to a bump at intermediate values of J, which is absent in the QM calculations. At higher J values, the QCT inelastic probabilities decrease more rapidly than the QM ones, whose maxima appear at higher J values. In addition, the range of J values that give rise to excitation into $v' = 1$ is larger in the QM calculations.

Although the opacity functions provide a valuable clue for the understanding of the mechanism that produces either inelastic excitation or reaction, it does not contain all the necessary information. The higher impact parameters and thus higher orbital angular momenta involved in the inelastic vibrational excitation would seem to lead to a larger rotational excitation than that produced in the reactive collisions. However, just the opposite is observed in both the theoretical and experimental results. A further point is the investigation of the role played by the recrossing mechanism in the vibrational excitation of the D_2 molecule [212]. In classical mechanical terms, recrossing takes place when a given trajectory goes over the barrier into the product valley but returns to the reagent valley without reacting. A 'recrossing trajectory' in a $A + BC$ collision can be defined as that for which the incoming R_{AB} (or R_{AC}) internuclear distance becomes smaller than the corresponding value at the transition state, whereas that of the initial diatom, R_{BC} becomes larger. For a symmetric system as H_3, a recrossing trajectory occurs when at least once R_{AB} (or R_{AC}) is smaller than R_{BC} and the trajectory is not reactive. At the collision energies commented on in this section, it is expected that recrossing would play an important role, and this is indeed what is observed, as shown in figure 32. The general trend is that low impact parameters are more prone to produce recrossing trajectories than higher b. For $v' = 1$, direct scattering, i.e. without recrossing, has a larger contribution to the total yield than that from recrossed trajectories. For $v' = 2$, and especially for $v' = 3$, recrossing becomes the predominant mechanism. It is clear from these data that the bumps observed in the different v' state resolved $P(J)$s are due, almost exclusively, to recrossing trajectories. The more direct scattering is confined at high values of J.

By comparing the QM and QCT $P(J)$s shown in figure 32, it can be concluded that recrossing is overestimated in the classical calculations. In the QM case, part of this scattering probably becomes reactive. Additionally, direct, non-recrossing, scattering seems to be more important in promoting the vibrational excitation. A clear cut quantal definition for this effect as that used in the classical context, does not exist. In this sense, it would be necessary to define which fraction of the wavefunction has already traversed the dividing surface between reagents and products in order to define the QM counterpart of the classical recrossing. Nonetheless, it is clear that recrossing plays an important role in the vibrational excitation of the D_2 molecule in inelastic collisions.

Another variable which can be also examined in the classical trajectories is the angle of attack. It has been found that the initial angle of attack, at sufficiently large distances, is essentially uncorrelated with the tendency to produce vibrational excitation in inelastic collisions [212]. This is not surprising, since, at the collision energies considered, large impact parameters are involved in the inelastic vibrational excitation, and the centrifugal forces in the region of close approach are very important.

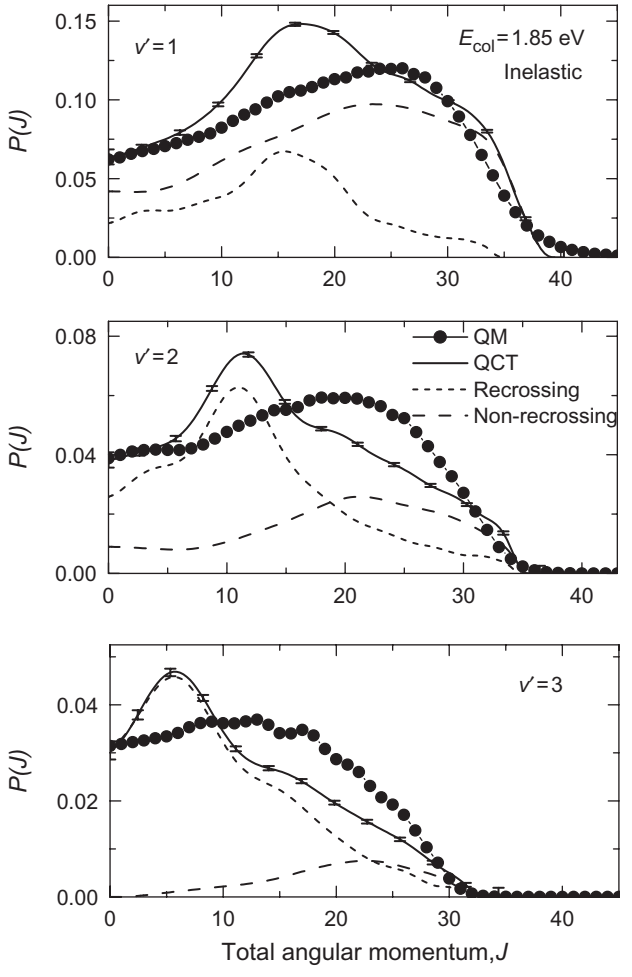

Figure 32. Vibrationally state resolved QCT and QM opacity functions, $P(J)$, for inelastic $H + D_2$ ($v = 0, j = 0$) collisions at 1.85 eV collision energy. The contribution from recrossing (dotted lines) and non-recrossing (dashed lines) trajectories in the QCT calculations are depicted.

The examination of the inelastic trajectories indicates that orientation by the PES and long range forces do not play an important role at these high collision energies. Trajectories run without any potential are practically indistinguishable from those with the actual potential almost to the point of closest approach, i.e. when the repulsive forces of the potential are experienced by the incoming atom. However, the angle at the closest approach distance reveals that the more collinear is the collision, the greater becomes the vibrational excitation. Head-on collisions lead preferentially to inelastic scattering. This is especially the case at low impact parameters. The centrifugal forces provide a kinematical orientation, and, if the collision takes place with a collinear configuration, the system, with a large radial energy, overcomes the transition state, hits the inner repulsive wall and recrosses back to the reagent valley. At sufficiently high

impact parameters, however, the trajectories can be more glancing. In the course of the approach the system looses most of the radial energy and there is not enough energy along the line-of-the-centers to overcome the barrier to reaction.

Undoubtedly, more experiments and further calculations are needed to understand the mechanism of inelastic scattering leading to vibrational excitation of the molecule. The use of the plane wave technique [131], so successfully employed in revealing the details of reactive scattering from a QM point of view, may also shed light into the mechanism of vibrational excitation and the actual role of the recrossing process.

8. Conclusions and outlook

Cumulative investigations over decades have produced a very large body of data about the hydrogen-atom exchange reaction. Thermal rate constants derived from bulk measurements are available between roughly 200 and 2000 K, and the results of dynamical (single collision) experiments span now the approximate 0.4–2.7 eV collision energy range. From a theoretical point of view various PESs, based on *ab initio* calculations of high accuracy, have been constructed and thorough QM and QCT calculations of the reaction dynamics have been performed on these surfaces. As a result of these combined efforts the essential characteristics are now very well known.

The hydrogen nuclei can be considered to move on an adiabatic, repulsive PES with a high barrier even in the most favourable orientation, which corresponds to a collinear arrangement. Consequently, the reaction has a large threshold and a small cross section and proceeds via a direct recoil mechanism, without formation of long lived complexes. Close to threshold the center-of-mass scattering of the product molecules is restricted to a narrow angular range around the backward direction with respect to that of the incoming atom, but as the collision energy increases, non-collinear configurations participate also in the reaction and the range of scattering angles becomes broader. Vibrational excitation of the reagent molecule lowers appreciably the reaction threshold and leads to a great enhancement of the thermal rate constants. In contrast, rotational excitation has a dual role. In the post threshold region, it can either reduce or enhance reactivity by influencing the relative orientation of the collision partners en route to reaction. The effects of rotation depend on the actual degree of excitation, the collision energy and the mass combination of the reagents.

Whereas these results were already obtained in theoretical calculations between the sixties and eighties, the experimental verification took much longer and many of the details have only been confirmed during the last ten years. Even now, some of the mentioned features, like the interesting role of rotational excitation, have not been investigated experimentally. Good agreement between experimentally and calculated thermal rate constants over the whole temperature range investigated was reported only in 2003. A slight non-adiabatic correction had to be applied to the barrier height in order to account theoretically for the lowest temperature measurements, and the earlier experimental rate constants had to be replaced by new and more precise data at high temperatures.

The overwhelming majority of the dynamical experimental data, and in particular those with higher resolution yielding, since 1995, ro-vibrationally state resolved

DCSs, can be well reproduced with QM calculations on the various versions of the ground state Born–Oppenheimer PES. The good general behaviour of the QCT method for the description of the experimental results further shows, that the dynamics of the nuclear motion is to a great extent classical. Isolated discrepancies between experiment and theory are still to be solved, but it is unlikely that they will change appreciably the global picture of the dynamics already available.

With the improvement in the theoretical methodology and the increase in the experimental resolution, an intensive search for QM effects started about fifteen years ago. However, except for tunnelling in the low temperature rate constants of some of the isotopic variants, purely QM effects seem to play a very small role in the global dynamics. Attempts to identify scattering resonances in the energy evolution of the integral cross sections have failed repeatedly. Forward peaks in the experimental state-resolved DCSs were associated with delayed scattering and tentatively attributed to Feshbach resonances. However, delayed scattering leading to forward peaks was also obtained in classical calculations and a more thorough analysis of the QM results established that they corresponded rather to a threshold effect. Oscillations in the collision-energy dependence of state-resolved backward scattering have been also experimentally observed and explained in terms of interferences of different quantized transition-state pathways. Nevertheless, similar oscillations were also obtained in QCT calculations. Finally, after more than a decade of debate, there is still no clear undisputed evidence of observed geometric phase effects related to the existence of a conical intersection between the two first potential energy surfaces of H_3.

In spite of the intensive studies of the last decades, there are many prospects for future work on the title reaction. In the first place, all methodological developments in the field of reaction dynamics continue to use $H + H_2$ as a benchmark (see for instance [213, 214]). Besides, the just mentioned discrepancies and doubts of interpretation should be clarified, especially those concerning the possible identification of geometric phase effects and the characteristics of quantum bottleneck states. In this respect, the QCT oscillations in backward scattering should be investigated more deeply. In addition, the influence of the internal (ro-vibrational) energy of the reagents in the reactivity and, in particular, that of rotational excitation, deserves a more thorough experimental study.

There are other aspects of the reactivity of the H_3 system, addressed by different groups, though in general not so thoroughly studied as those discussed in the previous sections. They involve usually more extreme temperatures or energies than those considered till now. Before closing the review some of these studies will be briefly mentioned.

The transition state of the $H + H_2$ reaction can also be accessed from the higher electronic levels of H_3. The lowest potential energy surface of H_3 is repulsive, as discussed throughout this review, and has thus a dissociative character, but the molecule has a series of bound excited states consisting of a core formed by the stable H_3^+ ion and an outer Rydberg electron that contributes only weakly to the bond. Work on the H_3 molecule until 1990 is reviewed in [11]. The two lower PESs of H_3 are degenerate for D_{3h}, where they correlate with the $(2p)1E'$ electronic state [215]. An atomic displacement leading to a symmetry lowering lifts the degeneracy and gives rise to the already mentioned conical intersection. The two lower potential surfaces are often referred to as the two sheets of the ground electronic state. The lower sheet correlates asymptotically

to $H + H_2(X^1\Sigma_g^+)$ and is the one relevant for the chemical reactivity discussed in the previous sections, and the upper sheet correlates to $H + H_2(b^3\Sigma_u^+)$, which leads to dissociation into three hydrogen atoms.

The Rydberg states of H_3, which correspond to equilateral triangle nuclear geometries, decay by UV emission and can provide valuable information about the properties of the ground state in the vicinity of the conical intersection. In 1994, Bruckmeier *et al.* [216] identified two broad maxima in the emission spectrum, that were attributed to decay into the two sheets of the ground state. Subsequent theoretical work by Köppel and co-workers [217, 218] using a time dependent wavepacket formalism could reproduce the spectra very well and lead to an extremely fast ($\approx$5 fs) decay from the upper to the lower sheet, indicating a very effective non-adiabatic coupling between them. This coupling corresponds to the D_{3h} nuclear symmetry obtained directly in Frank-Condon transitions from the excited state. As indicated previously, non-adiabatic processes between the two lower surfaces (sheets) are unimportant for other geometries. Further studies on the decay from different Rydberg states, including an analysis of the different dissociation pathways, are providing much insight about the dynamics of internal conversion and non-adiabatic coupling mechanisms in H_3 (see for instance [219, 220] and the references cited therein and in [170]).

Reactive and inelastic collisions for $H + H_2$ at very low temperatures have been investigated theoretically by means of transition state theory and QM calculations [221–223]. The calculations stressed the crucial role of the attractive van der Waals interactions in the calculated cross sections. Below a few K, the theoretical rate coefficients tended to vary slowly or to remain nearly constant in approximate accordance with Wigner's threshold law [224]. Some of these results were compared in a rough way to experimental measurements of hydrogen atom exchange processes in the solid phase [225] and qualitative agreement was found. The recent developements in the trapping of ultracold atoms and molecules [226, 227] open, at least in principle, new possibilities for a rigorous comparison between theory and gas-phase experiments in this very low temperature range, of great interest for the interstellar medium.

Pioneering experimental work on the reactive scattering of highly excited hydrogen Rydberg atoms with D_2 molecules has also been reported [228]. These first results, which open an interesting new field, show that the dynamics of the process is similar to that of the $H^+ + D_2$ ion molecule reaction, which suggests that the Rydberg electron behaves practically as a spectator during the reactive encounter.

We have not covered the subject of vector correlations for the H_3 system, which deserves to be treated at length. The information provided by the study of the spatial direction of the reactant rotational angular momentum on the reactivity and the resulting polarization of the rotational angular momentum of the products can be of crucial importance for the understanding of the dynamics of a given reaction. There have been some studies on the so called **k**-**k**′-**j**′ correlations [120, 121], where **k**, **k**′ and **j**′ are the directions of the initial and final relative velocities and of the products' angular momentum, respectively. It was shown there, that the HD emerging from the reaction is not only strongly aligned but also oriented. Similarly, present theoretical studies on the role of the polarization of the initial rotation [229] indicate that the various dynamical observables are strongly affected and, to a large extent, controlled by the polarization of **j**. More work is guaranteed on this subject in the near future.

All the open issues and less explored paths mentioned in the previous paragraphs warrant further theoretical and experimental studies on the dynamics of the simplest chemical reaction.

Acknowledgements

We would like to express our gratitude to Dick Zare, V. Sáez Rábanos, J. F. Castillo and J. Aldegunde for their longstanding collaboration with us and for providing with some unpublished material. This work has been financed by the DGES of Spain under the grants BQU2002-04627-C02-02, FTN2003-0828-C03-03, FIS2004-00456. The research was performed within the Unidad Asociada 'Qumica Fsica Molecular' between the Universidad Complutense and the CSIC.

References

[1] F. London, Z. Elektrochem. **35,** 552 (1929).
[2] H. Eyring, J. Chem. Phys. **3,** 107 (1935).
[3] M. G. Evans and M. Polanyi, Tans. Faraday Soc. **31,** 875 (1935).
[4] M. Karplus, R. N. Porter, and R. D. Sharma, J. Chem. Phys. **43,** 3259 (1965).
[5] A. Kuppermann, G. C. Schatz, and M. Baer, J. Chem. Phys. **65,** 4596 (1976).
[6] G. C. Schatz and A. Kuppermann, J. Chem. Phys. **65,** 4668 (1976).
[7] D. G. Truhlar and R. E. Wyatt, Annu. Rev. Phys. Chem. **27,** 1 (1976).
[8] R. D. Levine, Int. J. Chem. Kinet. **18,** 1023 (1986).
[9] G. C. Schatz, Annu. Rev. Phys. Chem. **39,** 317 (1988).
[10] J. J. Valentini and L. Phillips, in *Advances in Gas Phase Photochemistry and Kinetics*, edited by M. N. R. Ashfold and E. Baggott, Vol. 2 (Royal Society of Chemistry, London, 1989).
[11] H. Buchenau, J. P. Toennies, J. Arnold, and J. Wolfrum, Ber. Bunsenges. Phys. Chem. **94,** 1231 (1990).
[12] R. N. Porter and M. Karplus, J. Chem. Phys. **40,** 1105 (1964).
[13] M. Baer (Editor), *Theory of Chemical Reaction Dynamics* (Boca Raton, CRC Press, 1985).
[14] P. Siegbahn and B. Liu, Chem. Phys. **68,** 2457 (1978).
[15] D. G. Truhlar and C. J. Horowitz, J. Chem. Phys. **68,** 2466 (1978); ibid, J. Chem. Phys. **71,** 1514(E) (1979).
[16] A. J. C. Varandas, F. B. Brown, C. A. Mead, D. G. Truhlar, and N. C. Blais, J. Chem. Phys. **86,** 6258 (1987).
[17] A. I. Boothroyd, W. J. Keogh, P. G. Martin, and M. R. Peterson, J. Chem. Phys. **95,** 4343 (1991).
[18] M. Mladenovic, M. Zhao, D. G. Truhlar, D. W. Schwenke, Y. Sun, and D. J. Kouri, Chem. Phys. Lett. **146,** 358 (1988).
[19] M. Mladenovic, M. Zhao, D. G. Truhlar, D. W. Schwenke, Y. Sun, and D. J. Kouri, J. Phys. Chem. **92,** 7035 (1988).
[20] J. Z. H. Zhang and W. H. Miller, Chem. Phys. Lett. **153,** 465 (1988).
[21] J. Z. H. Zhang and W. H. Miller, Chem. Phys. Lett. **159,** 130 (1989).
[22] J. Z. H. Zhang and W. H. Miller, J. Chem. Phys. **91,** 1528 (1989).
[23] D. E. Manolopoulos and R. E. Wyatt, Chem. Phys. Lett. **159,** 123 (1989).
[24] J. M. Launay and M. Le Dourneuf, Chem. Phys. Lett. **163,** 178 (1989).
[25] N. C. Blais, M. Zhao, D. G. Truhlar, D. W. Schwenke, and D. J. Kouri, Chem. Phys. Lett. **166,** 11 (1990); ibid, **81,** 368E (1992).
[26] W. H. Miller, Annu. Rev. Phys. Chem. **41,** 245 (1990).
[27] B. A. Ridley, W. R. Schulz, and D. J. Le Roy, J. Chem. Phys. **44,** 3344 (1966).
[28] A. A. Westenberg and N. J. de Haas, J. Chem. Phys. **47**, 1393 (1967).
[29] H. R. Mayne and J. P. Toennies, J. Chem. Phys. **75,** 1794 (1981).
[30] B. C. Garrett and D. G. Truhlar, Proc. Nat. Acad. Sci. USA **76,** 4755 (1979).
[31] B. C. Garrett and D. G. Truhlar, J. Chem. Phys. **72,** 3460 (1980).
[32] B. C. Garrett, D. G. Truhlar, A. J. C. Varandas, and N. C. Blais, Int. J. Chem. Kinet. **18,** 1065 (1986).

[33] I. S. Jayaweera and P. D. Pacey, J. Phys. Chem. **94,** 3614 (1990).
[34] J. V. Michael, J. Chem. Phys. **92,** 3394 (1990).
[35] J. V. Michael and J. R. Fisher, J. Phys. Chem. **94,** 3318 (1990).
[36] T. J. Park and J. C. Light, J. Chem. Phys. **94,** 2946 (1991); ibid, **96,** 8853 (1992).
[37] J. V. Michael, J. R. Fischer, J. M. Bowman, and Q. Sun, Science. **249,** 269 (1990).
[38] G. C. Schatz, Chem. Rev. **87,** 81 (1987).
[39] N. C. Blais, D. G. Truhlar, and B. C. Garrett, J. Chem. Phys. **78,** 2363 (1983).
[40] I. D. Reid, D. M. Garner, L. Y. Lee, M. Senba, D. J. Arseneau, and D. G. Fleming, J. Chem. Phys. **86,** 5578 (1987).
[41] G. C. Schatz, J. Chem. Phys. **83,** 3441 (1985).
[42] M. E. Mandy and P. G. Martin, J. Phys. Chem. **95,** 8726 (1991).
[43] T. Dreier and J. Wolfrum, Int. J. Chem. Kinet. **18,** 919 (1986).
[44] R. Götting, V. Herrero, J. P. Toennies, and M. Vodegel, Chem. Phys. Lett. **137,** 524 (1987).
[45] J. Geddes, H. F. Krause, and W. L. Fite, J. Chem. Phys. **56,** 3298 (1972).
[46] G. H. Kwei and V. W. S. Lo, J. Chem. Phys. **72,** 6265 (1980).
[47] R. Götting, H. Mayne, and J. P. Toennies, J. Chem. Phys. **85,** 6396 (1986).
[48] S. A. Buntin, C. F. Giese, and W. R. Gentry, Chem. Phys. Lett. **168,** 513 (1990).
[49] R. E. Continetti, B. A. Balko, and Y. T. Lee, J. Chem. Phys. **93,** 5719 (1990).
[50] V. J. Herrero and I. Tanarro, Vacuum **52,** 3 (1999).
[51] M. Zhao, D. G. Truhlar, D. W. Schwenke, and D. J. Kouri, J. Phys. Chem. **94,** 7074 (1990).
[52] G. W. Johnston, B. Katz, K. Tsukiyama, and R. Bersohn, J. Phys. Chem. **91,** 5445 (1987).
[53] U. Gerlach-Meyer, K. Kleinermans, E. Linnebach, and J. Wolfrum, J. Chem. Phys. **86,** 3047 (1987).
[54] D. F. Gerrity and J. J. Valentini, J. Chem. Phys. **81,** 1298 (1984); ibid, J. Chem. Phys. **83,** 2207 (1985).
[55] J.-C. Nieh and J. J. Valentini, Phys. Rev. Lett. **60,** 519 (1988).
[56] D. L. Phillips, H. B. Levene, and J. J. Valentini, J. Chem. Phys. **90,** 1600 (1989).
[57] J.-C. Nieh and J. J. Valentini, J. Chem. Phys. **92,** 1083 (1990).
[58] E. E. Marinero, C. T. Rettner, and R. N. Zare, J. Chem. Phys. **80,** 4142 (1984).
[59] D. A. V. Kliner, D. E. Adelman, and R. N. Zare, J. Chem. Phys. **94,** 1069 (1991).
[60] D. A. V. Kliner, D. E. Adelman, and R. N. Zare, J. Chem. Phys. **95,** 1648 (1991).
[61] D. E. Adelman, N. E. Shafer, D. A. V. Kliner, and R. N. Zare, J. Chem. Phys. **97,** 7323 (1992).
[62] D. Neuhauser, R. S. Judson, D. J. Kouri, D. E. Adelman, N. E. Shafer, D. A. V. Kliner, and R. E. Zare, Science **257,** 519 (1992).
[63] M. D'Mello, D. E. Manolopoulos, and R. E. Wyatt, J. Chem. Phys. **94,** 5985 (1991).
[64] S. L. Mielke, R. S. Friedman, D. G. Truhlar, and D. W. Schwenke, Chem. Phys. Lett. **188,** 359 (1992).
[65] W. J. Keogh, A. I. Boothroyd, P. G. Martin, S. L. Mielke, D. G. Truhlar, and D. W. Schwenke, Chem. Phys. Lett. **195,** 144 (1992).
[66] N. C. Blais and D. G. Truhlar, Chem. Phys. Lett. **102,** 120 (1983); ibid, **162,** 503 (1989).
[67] N. C. Blais and D. G. Truhlar, J. Chem. Phys. **83,** 2201 (1985).
[68] I. Schechter and R. D. Levine, Int. J. Chem. Kinet. **18,** 1023 (1986).
[69] F. J. Aoiz, V. Candela, V. J. Herrero, and V. Sáez Rábanos, Chem. Phys. Lett. **161,** 270 (1989).
[70] F. J. Aoiz, O. Puentedura, V. J. Herrero and V. Sáez Rábanos, Chem. Phys. Lett. **198,** 321 (1992).
[71] G. C. Schatz and A. Kuppermann, Phys. Rev. Lett. **35,** 1266 (1975).
[72] D. E. Manolopoulos and R. E. Wyatt, J. Chem. Phys. **92,** 810 (1990).
[73] S. M. Auerbach, J. Z. H. Zhang, and W. H. Miller, J. Chem. Soc. Faraday Trans. **86,** 1701 (1990).
[74] R. E. Continetti, J. Z. H. Zhang, and W. H. Miller, J. Chem. Phys. **93,** 5356 (1990).
[75] W. H. Miller and J. Z. H. Zhang, J. Phys. Chem. **95,** 12 (1991).
[76] F. J. Aoiz, V. J. Herrero, and V. Sáez Rábanos, J. Chem. Phys. **97,** 7423 (1992).
[77] Y.-S. M. Wu and A. Kuppermann, Chem. Phys. Lett. **201,** 178 (1993).
[78] A. Kuppermann and Y.-S. M. Wu, Chem. Phys. Lett. **205,** 577 (1993).
[79] L. Schnieder, K. Seekamp-Rahn, F. Liedeker, H. Steuwe, and K. H. Welge, Faraday Discuss. Chem. Soc. **91,** 259 (1991).
[80] L. Schnieder, W. Meier, K. H. Welge, M. N. R. Ashfold, and C. M. Western, J. Chem. Phys. **92,** 7027 (1990).
[81] T. N. Kitsopoulos, M. A. Buntine, D. P. Baldwin, R. N. Zare, and D. W. Chandler, Science **260,** 1605 (1993).
[82] A. T. J. B. Eppink and D. H. Parker, Rev. Sci. Instrum. **68,** 3477 (1997).
[83] C. R. Gebhardt, T. P. Rakitzis, P. C. Samartzis, V. Ladopoulos, and K. N. Kitsopoulos, Rev. Sci. Instrum. **72,** 3848 (2001).
[84] J. J. Lin, J. Zhou, W. Shin, and K. Liu, Rev. Sci. Instrum. **74,** 2495 (2003).
[85] D. Townsend, M. P. Minitti, M.P, and A. G. Suits, Rev. Sci. Instrum. **74,** 2530 (2003).
[86] F. J. Aoiz, V. J. Herrero, O. Puentedura, and V. Sáez Rábanos, J. Chem. Phys. **100,** 758 (1994).

[87] F. J. Aoiz, L. Bañares, M. J. D'Mello, V. J. Herrero, V. Sáez Rábanos, L. Schnieder, and R. E. Wyatt, J. Chem. Phys. **101,** 5781 (1994).
[88] S. L. Mielke, D. G. Truhlar, and D. W. Schwenke, J. Phys. Chem. **98,** 1053 (1994).
[89] M. J. D'Mello, D. E. Manolopoulos, and R. E. Wyatt, Science **263,** 102 (1994).
[90] Y.-S. M. Wu and A. Kuppermann, Chem. Phys. Lett. **235,** 105 (1995).
[91] L. Schnieder, K. Seekamp-Rahn, J. Borkowski, E. Wrede, K. H. Welge, F. J. Aoiz, L. Bañares, M. J. D'Mello, V. J. Herrero, V. Sáez Rábanos, and R. E. Wyatt, Science **269,** 207 (1995).
[92] L. Schnieder, K. Seekamp-Rahn, E. Wrede, and K. H. Welge, J. Chem. Phys. **107,** 6175 (1997).
[93] F. J. Aoiz, L. Bañares, and V. J. Herrero, in *Advances in Classical Trajectory Methods*, edited by W. L. Hase, Vol. 3, p. 121 (JAI Press Inc., Stanford, CT, 1998).
[94] F. J. Aoiz, L. Bañares, and V. J. Herrero, J. Chem. Soc., Faraday Trans. **94,** 2483 (1998).
[95] E. Wrede, L. Schnieder, K. H. Welge, F. J. Aoiz, L. Bañares, and V. J. Herrero, Chem. Phys. Lett. **265,** 129 (1997).
[96] E. Wrede and L. Schnieder, J. Chem. Phys. **107,** 786 (1997).
[97] E. Wrede, L. Schnieder, K. H. Welge, F. J. Aoiz, L. Bañares, V. J. Herrero, B. Martínez-Haya, and V. Sáez Rábanos, J. Chem. Phys. **106,** 7862 (1997).
[98] L. Bañares, F. J. Aoiz, V. J. Herrero, M. J. D'Mello, B. Niederjohann, K. Seekamp-Rahn, E. Wrede, and L. Schnieder, J. Chem. Phys. **108,** 6160 (1998).
[99] E. Wrede, L. Schnieder, K. H. Welge, F. J. Aoiz, L. Bañares, J. F. Castillo, B. Martínez-Haya, and V. J. Herrero, J. Chem. Phys. **110,** 9971 (1999).
[100] A. I. Boothroyd, W. J. Keogh, P. G. Martin, and M. R. Peterson, J. Chem. Phys. **104,** 7139 (1996).
[101] S. A. Harich, D. Dai, X. Yang, S. D. Chao, and R. T. Skodje, J. Chem. Phys. **116,** 4769 (2002).
[102] S. D. Chao, S. A. Harich, D. Dai, C. C. Wang, X. Yang, and R. T. Skodje, J. Chem. Phys. **117,** 8341 (2002).
[103] S. A. Harich, D. Dai, C. C. Wang, X. Yang, S. D. Chao, and R. Skodje, Nature **419,** 281 (2002).
[104] D. Dai, C. C. Wang, S. A. Harich, X. Wang, X. Yang, S. D. Chao, and R. T. Skodje, Science **300,** 1730 (2003).
[105] F. Fernández-Alonso, B. D. Bean, and R. N. Zare, J. Chem. Phys. **111,** 1022 (1999); ibid, **111,** 1035; ibid, **111,** 2490.
[106] F. Fernández-Alonso, B. D. Bean, J. D. Ayers, A. E. Pomerantz, R. N. Zare, L. Bañares, and F. J. Aoiz, Angew. Chem. Int. Ed., **39,** 2748 (2000).
[107] B. D. Bean, F. Fernández-Alonso, and R. N. Zare, J. Phys. Chem. A **105,** 2228 (2001).
[108] F. Fernández-Alonso, B. D. Bean, R. N. Zare, F. J. Aoiz, L. Bañares, and J. F. Castillo, J. Chem. Phys. **115,** 4534 (2001).
[109] S. C. Althorpe, F. Fernández-Alonso, B. D. Bean, J. D. Ayers, A. E. Pomerantz, and R. N. Zare, and E. Wrede, Nature **416,** 67 (2002).
[110] B. D. Bean, J. D. Ayers, F. Fernández-Alonso, and R. N. Zare, J. Chem. Phys. **116,** 6634 (2002).
[111] J. D. Ayers, A. E. Pomerantz, F. Fernández-Alonso, F. Ausfelder, B. D. Bean, and R. N. Zare, J. Chem. Phys. **119,** 4662 (2003).
[112] F. Ausfelder, A. E. Pomerantz, R. N. Zare, S. C. Althorpe, F. J. Aoiz, L. Bañares, and J. F. Castillo, J. Chem. Phys. **120,** 3255 (2004).
[113] A. E. Pomerantz, F. Ausfelder, R. N. Zare, S. C. Althorpe, F. J. Aoiz, L. Bañares, and J. F. Castillo, J. Chem. Phys. **120,** 3244 (2004).
[114] N. E. Shafer, A. J. Orr-Ewing, W. R. Simpson, H. Xu, and R. N. Zare, Chem. Phys. Lett. **212,** 155 (1993).
[115] E. Shafer-Ray, A. J. Orr-Ewing, and R. N. Zare, J. Phys. Chem. **99,** 7591 (1995).
[116] W. R. Simpson, A. J. Orr-Ewing, T. P. Rakitzis, S. A. Kandel, and R. N. Zare, J. Chem. Phys. **103,** 7299 (1995).
[117] G. C. Schatz, J. Chem. Phys. **100,** 12839 (1996).
[118] A. Kuppermann and Y.-S. M. Wu, Chem. Phys. Lett. **241,** 229 (1995).
[119] A. Kuppermann and Y.-S. M. Wu, Chem. Phys. Lett. **349,** 537 (2001).
[120] M. P. de Miranda, D. C. Clary, J. F. Castillo, and D. E. Manolopoulos, J. Chem. Phys. **108,** 3142 (1998).
[121] M. P. de Miranda, F. J. Aoiz, L. Bañares, and V. Sáez Rábanos, J. Chem. Phys. **111,** 5368 (1999).
[122] F. J. Aoiz, L. Bañares, and J. F. Castillo, J. Chem. Phys. **114,** 8237 (2001).
[123] F. J. Aoiz, L. Bañares, J. F. Castillo, and D. Sokolovski, J. Chem. Phys. **117,** 2546 (2002).
[124] B. K. Kendrick, L. Jayasinghe, S. Moser, M. Auzinsh, N. Shafer-Ray, Phys. Rev. Lett. **84,** 4325 (2000); ibid, **86,** 2482-(E) (2001).
[125] B. K. Kendrick, J. Chem. Phys. **112,** 5679; ibid, **114,** 4335-(E) (2001).
[126] B. K. Kendrick J. Chem. Phys. **114,** 8796 (2001).

[127] B. K. Kendrick, J. Chem. Phys. **118,** 10502 (2003).
[128] B. K. Kendrick, J. Phys. Chem. A **107,** 6739 (2003).
[129] S. D. Chao and R. T. Skodje, Chem. Phys. Lett. **336,** 364 (2001).
[130] D. Skouteris, J. F. Castillo, and D. E. Manolopoulos, Comput. Phys. Commun. **133,** 128 (2000).
[131] S. C. Althorpe, Int. Rev. Phys. Chem. **23,** 219 (2004).
[132] A. Jäckle, M.-C. Heitz, and H.-D. Meyer, J. Chem. Phys. **110,** 241 (1999).
[133] S. Sukiasyan and H.-D. Meyer, J. Phys. Chem. A **105,** 2604 (2001).
[134] S. Mahapatra, H. Köppel, and L. S. Cederbaum, J. Phys. Chem. A **105,** 2321 (2001).
[135] S. C. Althorpe, J. Chem. Phys. **114,** 1601 (2001).
[136] S. C. Althorpe, J. Chem. Phys. **117,** 4623 (2002).
[137] S. C. Althorpe and D. C. Clary, Annu. Rev. Chem. Phys. **54,** 493 (2003).
[138] S. L. Mielke, G. C. Lynch, D. G. Truhlar, and D. W. Schwenke, J. Phys. Chem. **98,** 8000 (1994).
[139] K.-I. Tsuda, K. Moribayashi, and H. Nakamura, Chem. Phys. Lett. **231,** 439 (1994).
[140] K.-I. Tsuda, K. Moribayashi, and H. Nakamura, J. Chem. Phys. **103,** 5512 (1995).
[141] F. J. Aoiz, L. Bañares, T. Díez-Rojo, V. J. Herrero, and V. Sáez Rábanos, J. Phys. Chem. **100,** 4071 (1996).
[142] F. J. Aoiz, L. Bañares, V. J. Herrero, V. Sáez Rábanos, and I. Tanarro, J. Phys. Chem. **101,** 6165 (1997).
[143] D.-G. Barg, H. R. Mayne, and J. P. Toennies, J. Chem. Phys. **74,** 1017 (1981).
[144] C. A. Boonenberg and H. R. Mayne, Chem. Phys. Lett. **67,** 108 (1984).
[145] N. Sathyamurthy and J. P. Toennies, Chem. Phys. Lett. **143,** 323 (1988).
[146] H. Kornweiz, A. Persky, I. Schechter, and R. D. Levine, Chem. Phys. **169,** 489 (1990).
[147] F. J. Aoiz, V. J. Herrero, and V. Sáez Rábanos, J. Chem. Phys. **94,** 7991 (1991).
[148] S. Hochman-Kowal and S. Persky, Chem. Phys. **222,** 29 (1997).
[149] S. M. Auerbach and W. H. Miller, J. Chem. Phys. **100,** 1103 (1994).
[150] F. J. Aoiz, L. Bañares, J. F. Castillo, and V. J. Herrero, J. Chem. Phys. **111,** 9891 (1999).
[151] H. Partridge, C. W. Bauschlicher, J. R. Stallcop, and E. Levin, J. Chem. Phys. **99,** 5961 (1993).
[152] D. L. Diedrich and J. B. Anderson, Science **258,** 786 (1992).
[153] D. L. Diedrich and J. B. Anderson, J. Chem. Phys. **100,** 8089 (1994).
[154] A. Aguado and M. Paniagua, J. Chem. Phys. **96,** 1265 (1992).
[155] L. Bañares and M. J. D'Mello, Chem. Phys. Lett. **277,** 465 (1997).
[156] Y.-S. M. Wu, A. Kuppermann, and B. Anderson, Phys. Chem. Chem. Phys. **1,** 929 (1999).
[157] S. L. Mielke, B. C. Garrett, and K. A. Peterson, J. Chem. Phys. **111,** 3806 (1999).
[158] S. L. Mielke, B. C. Garrett, and K. A. Peterson, J. Chem. Phys. **116,** 4142 (2002).
[159] B. C. Garrett and D. G. Truhlar, J. Chem. Phys. **82,** 4543 (1985).
[160] S. L. Mielke, K. A. Peterson, D. W. Schwenke, B. C. Garrett, D. G. Truhlar, J. V. Michael, M.-C. Su, and J. W. Sutherland, Phys. Rev. Lett. **91,** 063201 (2003).
[161] J. V. Michael, M.-C. Su, and J. W. Sutherland, J. Phys. Chem. A **108,** 432 (2004).
[162] J. G. Muga and R. D. Levine, Chem. Phys. Lett. **162,** 7 (1989).
[163] F. T. Smith, Phys. Rev. **118,** 349 (1960).
[164] S. C. Althorpe, Chem. Phys. Lett. **370,** 443 (2003).
[165] S. C. Althorpe, J. Phys. Chem. A **107,** 7152 (2003).
[166] M. L. Goldberger and K. M. Watson, *Collision Theory* (Wiley, New York, 1964).
[167] R. T. Skodje and X. Yang, Int. Rev. Phys. Chem. **23,** 253 (2004).
[168] R. T. Skodje, R. Sadeghi, H. Köppel, and J. L. Krause, J. Chem. Phys. **101,** 1725 (1994).
[169] R. Sadeghi and R. T. Skodje, J. Chem. Phys. **102,** 193 (1995).
[170] F. Fernández-Alonso and R. N. Zare, Ann. Rev. Phys. Chem. **53,** 67 (2002).
[171] D. G. Truhlar and A. Kuppermann, J. Chem. Phys. **52,** 3841 (1970).
[172] D. G. Truhlar and A. Kuppermann, Chem. Phys. **56,** 2232 (1972).
[173] R. D. Levine and S.-F. Wu, Chem. Phys. Lett. **11,** 557 (1971).
[174] S.-F. Wu and R. D. Levine, Mol. Phys. **22,** 881 (1971).
[175] S.-F. Wu, B. R. Johnson, and R. D. Levine, Mol. Phys. **25,** 609 (1973).
[176] S.-F. Wu, B. R. Johnson, and R. D. Levine, Mol. Phys. **25,** 839 (1973).
[177] G. C. Schatz and A. Kuppermann, J. Chem. Phys. **59,** 964 (1973).
[178] J. R. Taylor, *Scattering Theory* (John Wiley & Sons, New York, 1972).
[179] D. C. Chatfield, R. S. Friedman, D. G. Truhlar, B. C. Garrett, and D. W. Schwenke, J. Am. Chem. Soc. **113,** 486 (1991).
[180] D. C. Chatfield, R. S. Friedman, D. G. Truhlar, and D. W. Schwenke, Faraday Discuss, Chem. Soc. **91,** 289 (1991).
[181] D. C. Chatfield, R. S. Friedman, D. W. Schwenke, and D. G. Truhlar, J. Phys. Chem. **96,** 2414 (1992).

[182] D. C. Chatfield, R. S. Friedman, G. C. Lynch, D. G. Truhlar, and D. W. Schwenke, J. Chem. Phys. **98,** 342 (1991).
[183] D. C. Chatfield, R. S. Friedman, S. L. Mielke, D. W. Schwenke, G. C. Lynch, T. C. Allison, and D. G. Truhlar, in *Dynamics of Molecules and Chemical Reactions*, edited by R. E. Wyatt and J. Z. Zhang (Marcel Dekker, New York, 1995).
[184] D. C. Chatfield, S. L. Mielke, T. C. Allison, and D. G. Truhlar, J. Chem. Phys. **112,** 8387 (2000).
[185] T. C. Allison, R. S. Friedman, D. J. Kaufman, and D. G. Truhlar, Chem. Phys. Lett. **327,** 439 (2000).
[186] M. S. Child, *Molecular Collision Theory* (Academic Press, London, 1974).
[187] R. T. Skodje, D. Skouteris, D. E. Manolopoulos, S.-H. Lee, F. Dong, and K. Liu, Phys. Rev. Lett. **85,** 1206 (2000).
[188] R. T. Skodje, D. Skouteris, D. E. Manolopoulos, S.-H. Lee, F. Dong, and K. Liu, J. Chem. Phys. **112,** 4536 (2000).
[189] R. S. Friedman and D. G. Truhlar, Chem. Phys. Lett. **183,** 539 (1991).
[190] D. E. Manolopoulos, Nature **419,** 266 (2002).
[191] T. Seideman and W. H. Miller, J. Chem. Phys. **95,** 1768 (1991).
[192] M. Baer, H. Kornweitz, and A. Persky, J. Chem. Phys. **92,** 6335 (1990).
[193] H. Kornweitz, A. Persky, and M. Baer, J. Chem. Phys. **94,** 5524 (1991).
[194] A. Persky and H. Kornweitz, Chem. Phys. Lett. **184,** 479 (1991).
[195] B. Lepetit and A. Kuppermann, Chem. Phys. Lett. **166,** 581 (1990).
[196] C. A. Mead and D. G. Truhlar, J. Chem. Phys. **70,** 2284 (1979).
[197] C. A. Mead, J. Chem. Phys. **72,** 3839 (1980).
[198] C. A. Mead, Rev. Mod. Phys. **64,** 51 (1992).
[199] C. A. Mead, Chem. Phys. **49,** 23 (1980).
[200] Y. Aharonov and D. Bohm, Phys. Rev. **115,** 485 (1959).
[201] M. V. Berry, Proc. R. Soc. London, Ser. A **392,** 45 (1984).
[202] Y.-S. M. Wu, A. Kuppermann, and B. Lepetit, Chem. Phys. Lett. **186,** 319 (1991).
[203] S. Adhikari and G. D. Billing, J. Chem. Phys. **107,** 6213 (1997).
[204] A. Kuppermann, in *Dynamics of Molecules and Chemical Reactions* edited by R. E. Wyatt and J. Z. H. Zhang (Marcel Dekker, New York, 1996).
[205] E. Wrede, Energieabhängige Untersuchung der Wasserstoffaustauschreaktion, PhD thesis, Bielefeld, 1998.
[206] J. C. Juanes-Marcos and S. C. Althorpe, Chem. Phys. Lett. **381,** 743 (2003).
[207] J. C. Juanes-Marcos and S. C. Althorpe, J. Chem. Phys., **122**, 20434 (2005).
[208] L. Bonnet and J. C. Rayez, Chem. Phys. Lett. **277,** 183 (1997).
[209] L. Bañares, F. J. Aoiz, P. Honvault, and J.-M. Launay, J. Chem. Phys. **118,** 565 (2003).
[210] L. Bañares, F. J. Aoiz, P. Honvault, and J.-M. Launay, J. Phys. Chem. A **108,** 1616 (2004).
[211] A. E. Pomerantz, F. Ausfelder, R. N. Zare, J. C. Juanes-Marcos, S. C. Althorpe, V. Sáez Rábanos, F. J. Aoiz, L. Bañares, and J. F. Castillo, J. Chem. Phys. **121,** 6587 (2004).
[212] F. J. Aoiz, *et al*., unpublished results.
[213] W. H. Miller, Y. Zhao, M. Ceotto, and S. Yang, J. Chem. Phys. **127,** 337 (2003).
[214] M. Baer, T. Ve'rtesi, G. J. Halasz, A. Vibok, and S. Suhai, Faraday Disc. Chem. Soc. **119,** 1329 (2004).
[215] H. F. King and K. Morokuma, J. Chem. Phys. **71,** 3213 (1979).
[216] R. Bruckmeier, C. Wunderlich, and H. Figger, Phys. Rev. Lett. **72,** 2550 (1994).
[217] S. Mahapatra and H. Köppel, Phys. Rev. Lett. **81,** 3116 (1998).
[218] H. Köppel, M. Döscher, and S. Mahapatra, Int. J. Quantum Chem. **80,** 942 (2000).
[219] U. Müller and P. C. Cosby, Phys. Rev. **59,** 3632 (1999).
[220] I. Mistrik, R. Reichle, H. Helm, and U. Müller, Phys. Rev. A **63,** 042711 (2001).
[221] T. Takayanagi, N. Masaki, K. Nakamura, M. Okamoto, S. Sato, and G. C. Schatz, J. Chem. Phys. **86,** 6133 (1987).
[222] T. Takayanagi and N. Masaki, J. Chem. Phys. **95,** 4154 (1991).
[223] N. Balakrishnan, R. C. Forrey, and A. Dalgarno, Chem. Phys. Lett. **280,** 1 (1997).
[224] E. P. Wigner, Phys. Rev. **73,** 1002 (1948).
[225] T. Miyazaki, T. Hiraku, K. Fueki, and Y. Tsuchihashi, J. Phys. Chem. **95,** 26 (1991).
[226] J. M. Doyle, B. Friedrich, J. Kim, and D. Patterson, Phys. Rev. A. **52,** R2515 (1995).
[227] H. L. Bethlem and G. Meijer, Int. Rev. Phys. Chem. **22,** 73 (2003).
[228] E. Wrede, L. Schnieder, K. Seekamp-Schnieder, B. Niederjohann, and K. Welge, Phys. Chem. Chem. Phys. **7,** 1577 (2005).
[229] J. Aldegunde, M. P. de Miranda, J. M. Haigh, B. K. Kendrick, V. Sáez Rábanos, and F. J. Aoiz, J. Phys. Chem. A **109**, 6200 (2005).